IRON-CATALYZED BELOUSOV-ZHABOTINSKY HYDROGELS AND LIQUID

CRYSTALS

A Dissertation

by

ILSE BELEN NAVA MEDINA

Submitted to the Office of Graduate and Professional Studies of
Texas A&M University
in partial fulfillment of the requirements for the degree of

DOCTOR OF PHILOSOPHY

Chair of Committee,	Zhengdong Cheng
Committee Members,	Tahir Cagin
	Akhilesh K. Gaharwar
	Jodie L. Lutkenhaus
Head of Department,	Ibrahim Karaman

August 2020

Major Subject: Materials Science and Engineering

ABSTRACT

The Belousov-Zhabotinsky (BZ) reaction is one of the most studied nonlinear dynamic chemical systems due to its autonomous periodic oscillations. It represents a suitable model for various oscillatory phenomena in Nature such as neuron synapsis, cardiac muscle beating and/or tachycardia, cellular formation cycle in molds, and other types of live-organism morphogenesis. The complexity of the BZ reaction chemical mechanism led to the creation of the Fields-Koros-Noyes model (FKN) that allows for studies via theoretical and mathematical models. Thus, experimental studies of this reaction are necessary to create 3D and life-like models. To bring these models into a more naturalistic setting, we researched the BZ reaction through hydrogels containing iron because of its natural occurrence and relevance. Chemically, the BZ reaction requires a catalyst based on iron (Fe), ruthenium (Ru) or cerium (Ce), and most of the current reports employ Ru. Alternatively, we employed Fe complexes as the catalyst due to their lower toxicity compared to Ru. The Fe-based catalyst was incorporated into polymer matrices (PNIPAM-co-PAAm, gelatin + kappa-carrageenan, and gelatin) to obtain hydrogels that exhibited pattern-rich, self-oscillatory response. Hence, the hydrogels served as models to investigate the effect of liquid crystalline structures on oscillations, the effect of geometry on the wave pattern of 3D-printed hydrogels, and the autonomous motion of hydrogels. Overall, these results open the door for future research on BZ reaction systems with low-toxicity. Furthermore, they contribute to the creation of new 3D locomotive hydrogels and to the development of realistic 3D models that could mimic Nature more efficiently.

DEDICATION

To my parents, for their infinite love and for all the sacrifices and dedication they have

given towards my education.

To my brother, for his patience, solidarity and joyful companionship.

ACKNOWLEDGEMENTS

CONTRIBUTORS AND FUNDING SOURCES

NOMENCLATURE

ϕ	Volume fraction
τ	Extent of the reaction
AAm	Acrylamide
BZ	Belousov-Zhabotinsky
CHD	1,4-cyclohexanedione
f	Stoichiometric factor
FKN	Fields-Koros-Noyes model
GA	Glutaraldehyde
KC, Kappa	Kappa-carrageenan
KCl	Potassium chloride
MA	Malonic acid
NIPAM	N-isopropylacrylamide
Phen	Phenanthroline
PAAm	Polyacrylamide
PNIPAM	Poly(N-isopropylacrylamide)

TABLE OF CONTENTS

LIST OF FIGURES

LIST OF TABLES

CHAPTER I

INTRODUCTION

1.1 Belousov-Zhabotinsky reaction

The earliest steps in the discovery of the Belousov Zhabotinsky reaction were

done in the 1950s[1] by the Soviet scientist Boris Belousov while he was trying to

reproduce the Krebs Cycle by mixing inorganic compounds in a test tube. He discovered

that an aqueous solution of citric acid (in the presence of bromate and cerium) presented

interchangeable colors between colorless and pale yellow every minute and,

simultaneously, this mixture produced carbon dioxide bubbles. These first findings were

later enhanced by Anatol M. Zhabotinsky and they prompted for the creation of the

Belousov-Zhabotinsky (BZ) reaction. This reaction motivated for further studies on

other oscillating reactions such as Briggs-Rauscher[2] and Old-Nassau[3] reactions.

The BZ reaction is a chemical system with nonlinear kinetic behavior and it is

characterized by reaction-diffusion conditions[4-6] . The chemicals in the reaction diffuse

throughout the solution and generate concentration gradients, which are responsible for

spatio-temporal phenomena. Considered as a chemical clock too[7], the BZ reaction

requires that certain chemicals react and cause a physical change (color being the most

known) after a specific amount of time (induction period). These color changes are

oscillatory as they happen at predictable time intervals. Physically, those color changes

in the BZ reaction generate spatio-temporal patterns in the form of various observable

waves. The generated waves can be planar waves[8-10], spiral waves[11-12] and target

waves[13]. The planar waves refer to line waves propagating from one direction to another;

1

and among the bidimensional wave patterns (which frequently occur in Nature), target

waves and spiral waves are the most common ones. Target waves comprise repeated

waves that self-organize as concentric circles whereas spiral waves show the geometrical

shape of a spiral.

The production of such patterns occurs from the interaction of four types of chemicals in

the reaction: an organic substrate (OS), an oxidizing agent ($NaBrO_3$), an acid (nitric

acid) and a metal catalyst (M), while present in an aqueous solution. The reactivity of

these chemicals is complex[14] and includes several steps as detailed by the FKN model[15];

however, we can recognize three characteristic processes as shown below[16]:

Process A: $BrO_3^- + 2Br^- + 3H^+ \rightarrow 3HOBr$

Process B: $BrO_3^- + HBrO_2 + 2M_{red} + 3H^+ \rightarrow 2HBrO_2 + 2M_{ox} + H_2O$

Process C: $2M_{ox} + OS + BrOS \rightarrow f\, Br^- + 2M_{red} + OS_{ox} +$ other products
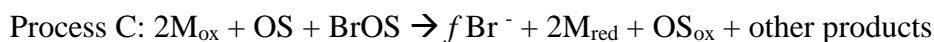
Table 1. Shortened Version for the Mechanism of the BZ Reaction

Metal ions (M) with redox potentials in the range of 1-1.4V, such as ruthenium, iron and

cerium, are known to exhibit the oscillatory BZ reaction[17]. Correspondingly, complexes

based on any of these metals facilitate the reaction as well[18].

It is important to note that in process B, $HBrO_2$ oxidizes the metal and instantaneously

regenerates its stock, allowing for a continuous loop of autocatalysis that triggers the

reaction back and forth for several cycles. This is, in other words, considered as the

positive feedback to the overall reaction. For Process C, the metal is reduced due to the

oxidation of the organic substrate. This redox process in the metal happens in both

Process B and Process C; and given the positive feedback of the overall reaction, the

changes in reduction and oxidation states of the metal are cyclic. These periodic changes in the metal valence are responsible for the visible color changes in the BZ reaction system. For the case of iron-catalyzed BZ systems, the reduced state of Fe ($^{2+}$) produces red-colored waves whereas the colorless (or light blue) waves correspond to the oxidized state (Fe^{3+}). Variations in the concentration of metal catalyst, organic substrate, acid and oxidizing agent affect the oscillations presented by the BZ reaction system[19], and those changes could compromise the wave pattern and even the oscillatory property. Nonetheless, the period and frequency at which the oscillations occur can be tuned through modifications of the chemical composition of the system.

1.2 Oscillators in Nature

Spatial pattern phenomena in Nature can be found as dynamic travelling waves or as stationary spatial patterns. Alan Turing, who was an English mathematician, started to study stationary spatial patterns in the 1950s. He dedicated part of his discoveries to recognize repetitive patterns in Nature and he considered such observations as the chemical basis of morphogenesis[20-21]. As examples of structures with Turing patterns, we can find spiral patterns in sunflowers[22-23], stripes and circles on zebras or other mammals[24-25], color pattern on sea shells[26], ring structures in tumor tissue [27-29], fingerprints[30-31], angelfish stripes[32-34], and the labyrinthine morphology of the brain cerebral cortex[35].

Turing discoveries, shortly after, motivated for studies on patterns but only through theoretical or mechanistic terms, there was no experimental evidence for such patterns in real systems[36]. Part of the reason for this limitation was, and still is, that biological systems have activator and inhibitor species that are difficult to isolate and identify. To overcome that limitation, scientists started to apply the BZ reaction as a chemical system for modeling of such phenomena[37]. Nearly forty years after the discovery of the BZ reaction and Turing's theory, chemists employed gel-based experiments to carry out the BZ reaction under stationary conditions[38]. This modification boosted the use of the BZ reaction chemical system as a tangible model to study Turing patterns.

On the other hand, dynamical travelling waves occur in numerous phenomena in Nature. Cephalopods, for example, present dynamic skin pattern[39] and other skin behavior such as camouflage[40] that serve for survival modes. The cellular cycle of a type of slime

mold, *Dictyostelium*, presents a dynamical pattern caused by waves of cyclic adenosine monophosphate (cAMP) in the aggregation stage; these waves in the form of spirals and concentric waves serve as signals between cells, thus triggering their growth and multiplication[41-42]. Similarly, spiral waves of release of free Ca^{2+} in developing oocytes (*Xenopus laevis*) have been reported[43]. The cardiac muscle has shown stationary and drifting spiral waves of excitation[44]; as a result, the initiation of those spiral waves are considered to trigger cardiac arrest and dangerous arrhythmias[45-46]. Studies on the retinas of Leghorn chickens demonstrated waves during the neurohumoral process called spreading depression; these waves are known to generate due to extracellular accumulation of K^+ ions[47]. Finally, to cite macroscale examples, forest fires propagate as spreading waves[48] and the rotating galactic disks arrange into spiral patterns[49-51]. Likewise, biological oscillators present dynamical travelling waves. At the cellular level, metabolic waves have been observed and they are believed to govern the cellular energetic activity[52]. In addition, active waves appear in glycolytic oscillations[53-54] and striped microtubule waves develop during the embryogenesis of fruit flies (*Drosophila*)[55]. More importantly, studies in monkeys and humans demonstrated that the neuronal activity is perceived as waves, and the width and pattern for mentioned waves are dictated by the self-organization of the dendrites within the cortex[56-57].

Yet, advances on studies of dynamical wave activity may not be extensive since each organism has different and complex biochemical pathways that regulate their oscillatory responses[58]. The period of such oscillations can vary from milliseconds to years among different species[59]. The firing of cold receptor in cats, for example, has a frequency of 10

Hz, the mice heart beats at an average frequency of 1.8 Hz[60], the human heart at 1.00-1.67 Hz[61] and the beating frequency of snails is approximately 0.2Hz[62]. Given the variety of the frequencies (or periods) in biological oscillators, the BZ reaction is a suitable model for further experimental studies since it allows for tuning of the oscillations as described in Section 1.1.

1.3 Design of Self-Oscillating Polymer Gels Based on the BZ Reaction

Since its creation in 1950s, advances for the Belousov-Zhabotinsky reaction have gradually progressed. Predominantly, there are discoveries that served as groundbreaking contributions: the conception of the FKN mechanism, the Oregonator computational model, the use of a gel matrix to carry out the reaction (as opposed to liquid conditions), and the confinement of the BZ reaction waves on gels. Mathematical calculations for the BZ reaction led to the creation of the FKN mechanism and the Oregonator model, in 1972 and 1974 respectively[63-64]. The Oregonator model accounted for the chemical dynamics of the system and simplified the complexity of the chemical mechanism. This realistic model allowed for later simulations that analyzed the effect of the bromide ion on oscillations[65], the temperature dependence of the reaction[66], and the occurrence of travelling waves along with their speed[67]. Simultaneously, in 1988, scientists first used a polyacrylamide gel matrix to analyze the stability of chemical patterns and transition between the different states of the reaction[38]. Lastly, the approach for the attachment of the metal catalyst in polymer matrices was innovative. The combination of these and many other theoretical and experimental approaches inspired the creation of self-oscillating polymers, a new type of responsive polymers based on the BZ reaction that arose in late 1990s[68]. Typical responsive polymers react to temperature, pH, magnetic field, and light, and reach an equilibrium upon showing of such response; in contrast, self-oscillating polymers mediated by the BZ reaction show autonomous and periodical responses since the changes are reversible. In a self-oscillating polymer, the catalyst needed for the BZ reaction is confined in a polymer gel

and once immersed in the solution with the remaining chemicals, the polymer gel

exhibits oscillatory response without the need for external stimuli. This response is

driven by the chemical cyclic change of oxidation state of the metal as described earlier.

The computational modeling has been remarkably a crucial factor in the development of

self-oscillating polymers. Balazs and coworkers first researched the pattern formation

and shape changes of gels through simulations[69]; they created a model for 2D shape

deformations and wave patterns in the gel, which are dependent on the gel's dimensions.

They improved this model by counting the polymer-solvent interactions through a gel

lattice spring model (gLSM)[70] and a year later they applied the gLSM model to 3D

computational studies of the dynamical behavior of self-oscillating gels[71]. They found

that oscillations in size and shape occur do to the chemical oscillations happening in the

BZ reaction; thus, oscillating mechanical deformation in gels was theoretically

conceivable by means of coupling of the BZ reaction to polymer matrices. Since then,

computational models continued encouraging the design and fabrication of self-

oscillating polymers.

Experimentally, the design of self-oscillating polymers originated in 1995 with the

contributions from a Japanese group[72-73]. They reported a poly N-isopropylacrylamide

(PNIPAM) gel that exhibited periodic swelling-deswelling changes in its size. Yet, these

changes occurred by a continuously stirred tank reactor. To enhance this gel system, a

polymerizable BZ catalyst based on ruthenium was synthesized and coupled to the

PNIPAM matrix[74-75]. They found that the BZ oscillating chemical reaction occurred

autonomously in the polymer network and this result led to several reports on the

incorporation of metal catalysts to polymer matrices for the creation of novel functional materials. Yoshida et.al. have developed diverse functional materials by varying the morphology and chemical composition of the self-oscillating polymers[76]. The morphology variants of the self-oscillating polymers initiated with linear polymer chains that contained the ruthenium catalyst[77]. From this report, other architectures were achieved: porous microstructures [78] (double network with crosslinked polymers), microgels presenting viscosity fluctuations due to the oscillations[79-85], comb-type gels[86], polyrotaxanes[87], polymer brushes[88] and micelles that self-assembled[89]. Furthermore, the force generated by the chemical energy in the self-oscillating polymers have proved to be a propulsive system[90-91]: tubular-shaped gels performing the BZ reaction showed peristaltic motion such as the one occurring in the intestines[92-94]; ciliary motion was present in arrays of PMMA gels made by X-ray lithography[95-96]; active surfaces transported microbodies[97-100]; and a cylinder-shaped gel self-walked (due to bending and stretching) when placed on a ratchet base[101]. In terms of chemical structure of self-oscillating polymers, the selection of polymer matrices has been explored to some extent. As described earlier, the BZ reaction needs an organic acid, a strong acid and an oxidizing agent dissolved in solution. Typically, the self-oscillating polymers begin the oscillations once immersed in such solution; however, this procedure was condensed by the creation of a quaternary polymer[102]. The quaternary polymer contained a pH control unit and an oxidant supplying site inserted into the polymer chain; thus, the gel only required to be immersed in a solution of the organic acid. Additional polymer matrices include polyethylene glycol (PEG) linear chains for changes in solubility of the

9

polymer[103-104], N,N-ethylmethylacrylamide (EMAAm) polymer for an increase in the temperature sensitivity of the system[105], poly(vinylpyrrolidone) (PVP) for studies of the temperature effect on oscillations[106], and gelatin as a biopolymer[107].

In order to create new self-oscillating polymers, the modular design can be manipulated through different parameters: the concentration of reactants in solution, the chemical structure of the polymer matrix, and the choice of metal catalyst (metal ion and ligand)[68]. The majority of self-oscillating gels described so far are based on PNIPAM polymer structures solely or copolymerized with other polymers. Similarly, the selection of metal catalyst has been restricted to ruthenium-based compounds[108]. Given the varying redox potential of the metal ions (ruthenium, iron or cerium), the library of self-oscillating polymers, along with their corresponding performance, application and frequency of oscillations, can be expanded by exploring other metal catalysts.

We decided to create new self-oscillating polymers by using metal catalysts based on iron exclusively, and we incorporated them into different polymer matrices to test their chemo-mechanical and oscillatory activity. The employment of iron was motivated by the high abundance in Earth, low toxicity and, more importantly, the key role that it plays in several biological oscillators in Nature[109-111]. Thus, self-oscillating polymers based on iron would propose materials that simulate bio-oscillations or bio-motion in a more lifelike system.

1.4 Organization of the Dissertation

The dissertation is organized as follows. In chapter II, a new catalyst based on iron was developed in order to be applied for studies on the BZ reaction. This catalyst served to create new hydrogels based on gelatin, a natural occurring polymer. The oscillating response of these hydrogels needed to be found at a new concentration of reactants due to the different catalyst employed. Additionally, a set of software and imaging tools were coupled for the correct monitoring and analysis of the reaction. This analyzing technique was established and used for any subsequent experiments of the BZ reaction performed in the following chapters.

Chapter III provides the model to explore the effect of liquid crystals on the oscillations of hydrogels based on iron. For this, the synthesis of zirconium phosphate nanoplates, serving as the liquid crystals, along with their exfoliation is reported. The exfoliated nanoplates were incorporated in the hydrogels containing the iron catalyst and tested for their oscillatory behavior. The self-arrangement of the nanoplates caused a phase transition that was monitored through the oscillatory response and wave patterns of the BZ reaction.

The employment of 3D printing was useful for the fabrication of star-shaped hydrogels based on iron as explained in Chapter IV. This chapter details the preparation of a 3D-printable polymer matrix and upon printing, we studied the effects that the geometrical shape has on the oscillations and frequencies of the reaction as well as the waves' morphology.

Chapter V investigates the motion of gelatin-based hydrogels. The design of the gelatin-based hydrogels follows the synthetic route developed in Chapter II. Different surfaces and lighting conditions were tested in order to understand and improve the motion of hydrogels. Finally, conclusions are presented in Chapter VI, together with future research directions.

CHAPTER II

SELF-OSCILLATING GELATIN CATALYZED BY IRON

2.1 Introduction

The self-oscillating polymer that we focused on for this chapter was an iron-based

gelatin created by inserting an iron catalyst into a gelatin matrix. We synthesized an iron

catalyst, as the driving force for the oscillatory reactions and we chose to attach it to a

gelatin matrix, as the natural occurring polymer.

2.1.1. Background

The most widely exploited self-oscillating polymers are catalyzed by the structure

labeled as Ru $(bpy)_3{}^{2+}$ in figure 1a[112]. The green oval is indicating the position of the the

polymer matrix, which can vary accordingly to the functional groups that serve as the

connecting site. Other structural variations include substituting the bipyridine (bpy)

ligands for pyridine (py) or terpyridine (tpy) (figure 1b)[113]. All of these variations

maintain the metal coordination number of six, given that each nitrogen in the structure

of the ligand binds to the metal.
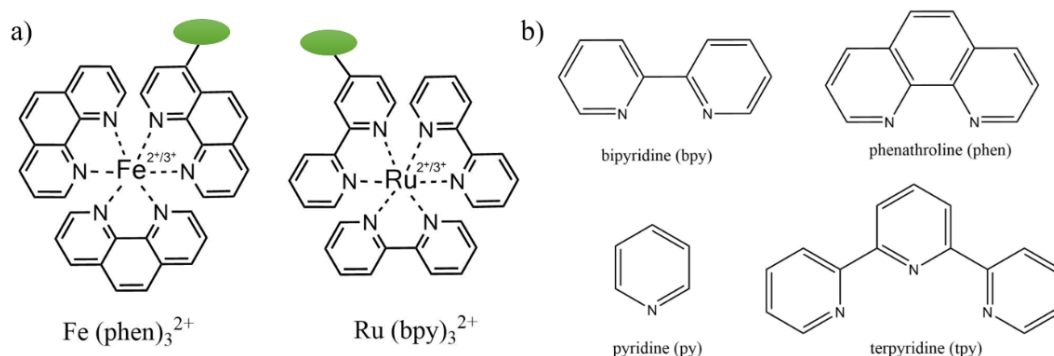
Figure 1. Chemical Structures of the Common Catalysts (a) and Ligands (b) Used for the BZ Reaction

Additional catalyst structures have been previously reported for iron-catalyzed reactions[114], but the ferroin moeity (abbreviated as Fe (phen)$_3$$^{2+}$ in figure 1a) has been marked as the most common one[115]. The employment of phenanthroline ligands in iron complexes instead of bipyridyl ones (used for ruthenium complexes) is made possible by an increased feasibility for electron transfer in phenanthroline structures[116-117]. Hence, the iron catalyst that we selected is an analogue of ferroin; a functional group was developed on the phenanthroline (phen) ligands to allow for the chemical linkage between the catalyst and the polymer matrix.

Interestingly, ferroin-based systems for BZ reaction studies include the use of few polymer matrices: PNIPAM microgels[118-120], Polyacrylamide membranes[121-123], and acryloyl morpholine (ACMO) gels[124]. Gelatin as a polymer matrix, on the other side, has been only used for the creation of self-oscillating polymers based on ruthenium given its ability to be post-functionalizated[107, 125]. In addition to this advantage, gelatin is economic, stable, easy to handle, and requires short preparation times. Moreover, the biological occurrence of gelatin makes it a suitable polymer matrix for a naturalistic setting. Thus, we were motivated to explore the linking of an iron-catalyst and gelatin matrix for the fabrication of our self-oscillating polymers as centimeter-sized, gel shapes as shown in figure 2.

Figure 2. Graphic Design of the Iron-based Gelatin

2.2 Experimental

In order to obtain the iron catalyst and to incorporate it into the polymer matrix, the following chemical synthesis route was taken (figure 3). The route comprises the bromination of a phenanthroline-like compound, which serves as the ligand, followed by the complex formation when reacted with the iron salt. This catalyst is linked to the gelatin matrix through a molecular substitution between the bromine-functional groups and the amino-residues contained in the gelatin matrix. Ultimately, unreacted amino-residues in the gelatin are crosslinked with glutaraldehyde; this crosslinking technique helps to increase the stability of the gels under acidic conditions.

Figure 3. Chemical Scheme for the Synthesis of Iron-based Gelatin

2.2.1. Catalyst Synthesis

All chemicals were purchased from Sigma Aldrich excluding 4-methyl-1,10-phenanthroline, which was purchased from Fischer Scientific. The chemicals were used as received and the water was ultra-pure, distilled, and deionized. The bromination reaction of 4-methyl-1,10-phenanthroline (**1**) was achieved based on a previous procedure[126]. 4-methyl-1,10-phenanthroline, N-bromosuccinimide (NBS) and 2,2′-Azobis(2-methylpropionitrile) (AIBN) were dissolved in 50 mL of carbon tetrachloride (CCl_4) in a 1:1:0.2 molar ratio. The mixture was stirred under UV light for four hours. The suspension was filtered and washed several times with water to isolate the 4-(bromomethyl)-1,10-phenanthroline (**2**). This brominated phenanthroline and $FeSO_4•7H_2O$ were combined in a 3:1 molar ratio (phen: iron sulfate ratio) in a small volume of water. A red suspension appeared immediately as an indication of the complex formation between the phenanthroline ligands and iron. To aid precipitation of the suspension, a saturated solution of ammonium hexafluorophosphate (NH_4PF_6) was added. The red precipitate (**3**) was isolated by filtration and dried in air to yield the iron catalyst (appendix A).

2.2.2. Gelatin Samples Preparation

A solution of gelatin was prepared by dissolving 1g of type-A gelatin (100 bloom) in 10 mL of phosphate-buffered saline solution (PBS, pH= 7.4). To prepare the iron-based gelatin (**4**), the Fe-catalyst (**3**) and the gelatin stock solution were mixed in an approximate ratio of 1.6:98.4 by weight. First, the gelatin stock was melted in a vial at

50 °C in the oven until all gelatin was dissolved and formed a homogeneous solution.

Then, Fe-catalyst (**3**) was added in small portions at 10-minute intervals, while

continuously being stirred. The vial was returned to the oven for additional 60 min to

ensure full dissolution. The final BZ gelatin solution was casted in containers and cooled

at 0 °C. To avoid degradation of unreacted gelatin residues, the BZ-gelatine shapes were

further crosslinked via reaction with glutaraldehyde. The gelatin blocks were soaked in

20 mL of 5mM glutaraldehyde solution for 24 h at room temperature. Finally, the gelatin

block was cut with a razor to obtain the desired dimensions and shapes. The gelatin

composites of assorted dimensions were placed in 20 mL of the BZ media solution. The

concentration of reactants (malonic acid or cyclohexanedione, sodium bromate and nitric

acid) for the BZ media solution were varied accordingly.

2.2.3. Monitoring of the BZ Reaction

Different techniques have been used for the monitoring of the self-oscillating polymers

including: UV-Vis spectroscopy[77], rheology[127], DLS[89], fluorescence signals[128], confocal

microscopy[129], SPM[130], QCM-D[131], microforce sensing[132], and calorimetry[133]. However,

we chose microscopy[87] as a direct way to observe the chemical wave propagation and

color changes given the long reaction times and the centimeter-sized hydrogels that we

employ.

The performance of the iron-based gelatin samples was monitored for the course of the

reaction by following the procedure shown in Figure 4.

Figure 4. Experimental Setup for the BZ Reaction and Corresponding Analysis

Given that the cross-linked gelatin samples hold the iron catalyst, they need to be immersed in a solution containing the remaining chemicals to carry out the BZ reaction (organic substrate, oxidizing agent and inorganic acid). Once they are in the solution, the reaction was monitored with a digital camera (Logitech webcam), and a software automatically captured images every 5 seconds throughout the course of the reaction (up to 10 hours). The images were compiled into a video with the use of ImageJ (National Institutes of Health, USA) software. Separately, the cyclic changes in color (interchangeable between red and transparent, corresponding to Fe^{2+} and Fe^{3+} respectively) were seen and analyzed with a code, developed in-house, for IDL software (Harris Geospatial Solutions, USA). The code was set for extraction of the red, green and blue (RGB) values from each picture. The values corresponded to the position of three (or more) fixed points evenly distributed along the sample. These color indexes were converted to hue and grey values depending on the contrast of the images. To calculate the grey (GV) and hue values, the employed formulas were:

$$GV = 0.30\,(R) + 0.59\,(G) + 0.11\,(B)$$

$$\alpha = R - 0.5(G + B);\ \beta = \frac{\sqrt{3}}{2}\,(G - B)$$

$$Hue = \frac{180}{\pi}\,Atan^2(\beta, \alpha)$$

Figure 5. Formulas to Calculate Cyclic Color Changes by IDL analysis

Oscillatory graphs were obtained when these values were plotted versus time, Fast

Fourier Transforms (FFT) were applied to the oscillatory signals via OriginLab software,

and the predominant frequency was fitted with a GaussianAmp model.

This monitoring technique was used for all subsequent experiments described in the

following chapters.

2.3 Results and Discussion for Iron-based Gelatin Samples

To first test the new iron-based gelatin samples, we employed the conditions previously

reported for ruthenium-based gelatin hydrogels[107]. The reported conditions required

malonic acid as the organic substrate. The effect of increasing concentrations of sodium

bromate, malonic acid and nitric acid were tested, and it was found that as the

concentrations were increased, the induction time (amount of time for the oscillations to

begin) and reaction time (amount of time that the oscillations last for) were decreased

(appendix A). Similarly, the concentration of chemicals was fixed and the shape of the

gels along with their dimensions was varied (Figure 6 and appendix A). Overall, the

occurrence of chemical waves was low, the wave pattern was mainly composed of

planar waves, and the frequency of oscillations did not present a significant trend.

Figure 6. Geometrical Shapes Tested for the BZ Reaction Utilizing Malonic Acid as the Organic Substrate

The rectangular shape was used as the representative of BZ reactions with malonic acid. The employed concentrations for the BZ solution were 0.08 M sodium bromate ($NaBrO_3$), 0.02 M malonic acid (MA) and 0.70 M nitric acid (HNO_3). As happened with the majority of the experiments with malonic acid, the hydrogel was able to produce planar waves; however, the obtained oscillations were irregular (Figure 7a) and showed a wide distribution of frequencies (Figure 7c).
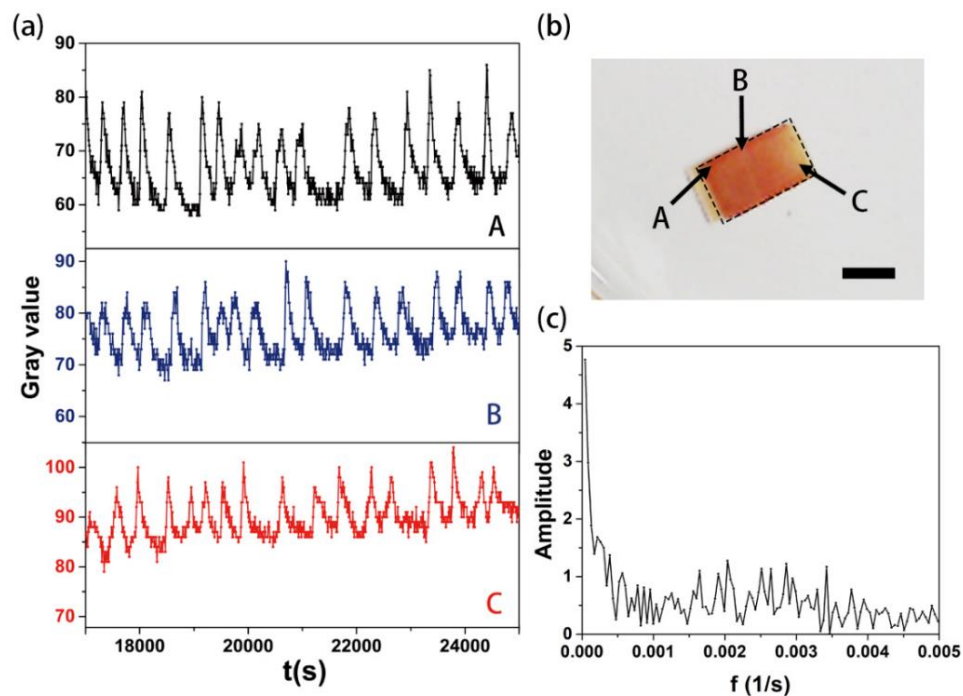
Figure 7. Rectangle-shaped Gelatin Sample with Oscillatory Behavior, Single Wave Pattern and Wide Range of Frequencies

Graphs A, B and C for part 10a) show the oscillatory signals detected on the gel at the fixed positions labelled as A, B and C, respectively. The dimensions of the rectangular prism were 0.5 x 1.0 x 0.7 cm. The scale bar in figure 7b) is 0.5 cm. Part 7c) shows the FFT of the oscillations of the black graph, which resulted in many frequencies. The FFT for the blue and red graphs presented a similar behavior, given that the period of oscillations was not constant. Nonetheless, the self-oscillatory ability of the hydrogels was present.

These irregularities in the oscillations could be hypothesized due to the low activity of iron catalysts, as it has been reported[124]. PNIPAM-based oscillating polymers have been previously tested with ruthenium and iron catalysts ($Ru(bpy)_3^{2+}$ and $Fe(bpy)_3^{2+}$). The energy of activation for the iron-catalyzed polymers proved to be higher than the one for ruthenium-catalyzed polymers (60 kJ/mol vs. 78 kJ/mol); thus, the reaction requires longer time to begin. Correspondingly, iron and ruthenium have different redox potentials; this causes variation in the feasibility for the electron transfer, which are responsible for the oscillatory color changes in the polymers. Moreover, malonic acid is identified as prone to decomposition in acidic conditions[134-135]. This decomposition produces carbon dioxide bubbles as it breaks its molecular structure. Consequently, the poor wave pattern and delayed periods observed for the rectangle-shape hydrogels suggests that the rest of the chemicals are possibly unreacted and the system is not able to produce appropriate oscillations.

To overcome the high activation energy and to improve the obtained wave patterns, the amount of reactants in the BZ media solution were modified and the organic substrate,

malonic acid (MA), was substituted with cyclohexanedione (CHD) along with an increase in its concentration[136]. It has been reported that the carbon dioxide formation disturbs the wave pattern evolution, therefore the use of CHD incites a stable oscillatory behavior of the BZ reaction[137]. By changing the oxidizing agent, we obtained an extensive sequence of target and front waves with steady and regular oscillatory signals, as presented in figure 8.
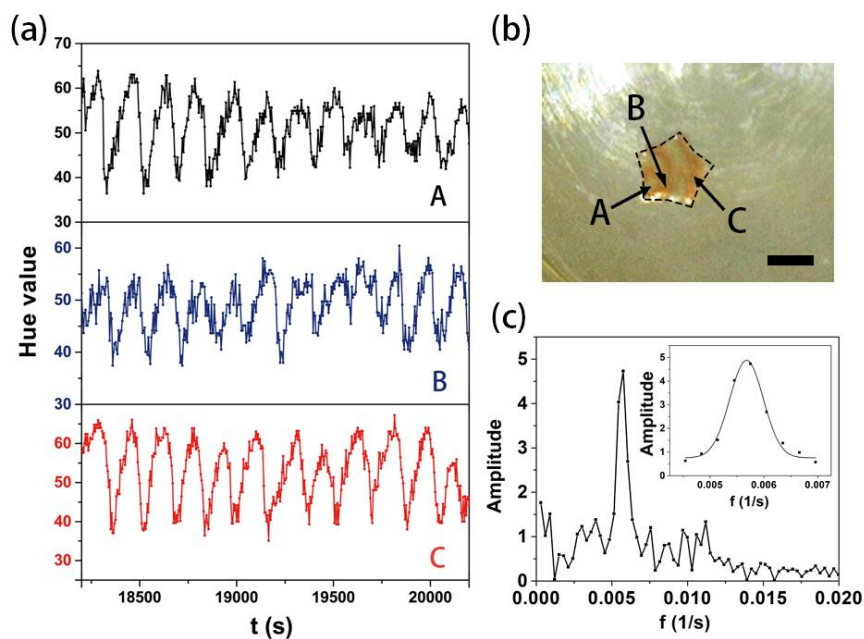
Figure 8. Star-shaped Gelatin Sample with Oscillatory Behavior, Target Waves and a Predominant Frequency of Oscillations

The concentration of reactants employed for this star-shaped gelatin were 0.10 M sodium bromate ($NaBrO_3$), 0.125 M cyclohexanedione (CHD), and 0.90 M nitric acid (HNO_3). In the same way as with the rectangular-shaped gelatin, the wave dynamics were tested at three different positions (labelled as A, B, and C in part 8b), which

correspond to the black, blue and red graphs in figure 8a, respectively. The longest

diagonal on the star had a length of 0.9 cm and the thickness was 0.3 cm (Scale bar: 0.5

cm). The FFT analysis of the black graph generated a single sharp peak for the

oscillatory frequency which yielded a value of $(5.7 \pm 0.3) \times 10^{-3}$ s^{-1}. The inset of the graph

shows the frequency peak fitted with GaussAmp model. Similarly, other gels were tested

under similar concentration of reactants and the frequencies remained defined given the

regular oscillations (appendix A).

Moreover, the self-oscillating hydrogels were tested for shape effects because of

previous computational reports on shape- and size- dependent patterns[121]. A circle-

shaped gelatin sample of the same thickness as the star-shaped sample was immersed in

a BZ reaction media solution with equal concentrations.
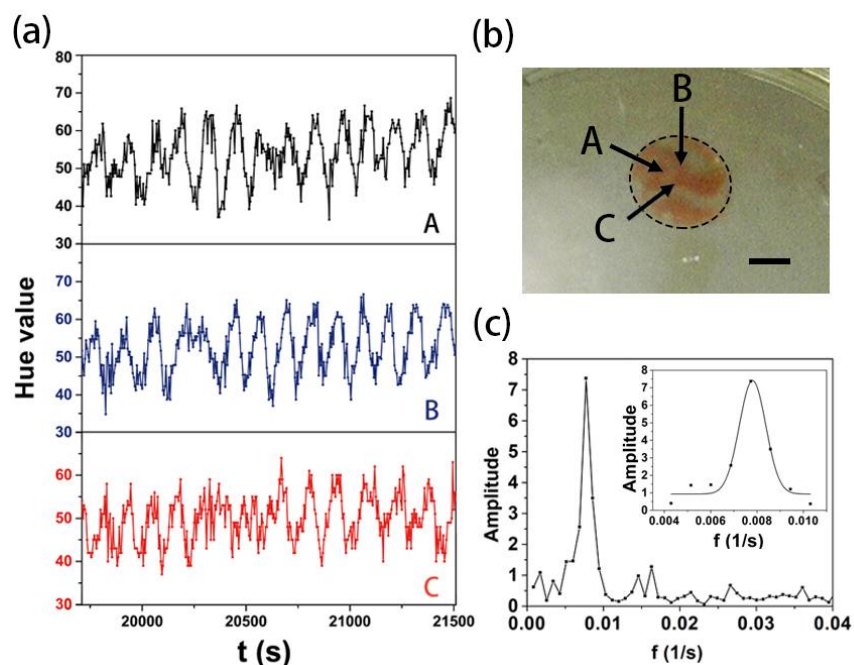
Figure 9. Circle-shaped Gelatin sample with Oscillatory Behavior, Wave Patterns and a Predominant Frequency of Oscillations

The diameter of the circle-shaped gelatin was 1.2 cm as shown in Figure 9b (scale bar is 0.5cm), and the thickness was 0.3 cm. Three oscillatory graphs were obtained based on the three locations on the gel. The FFT analysis for the oscillations (9a) yielded a single frequency of $(7.8 \pm 0.6) \times 10^{-3}$ s^{-1}, and the inset of the graph 9c presents the fitting for the frequency peak through GaussAmp model.

The circle-shaped gelatin sample presented a higher frequency than the star-shaped sample, indicating that the shape of the hydrogel influences the oscillatory frequency. The arms on the star-shaped gelatin initiated wave formation, whereas the circle-shaped gelatin showed wave diffusion originating at the center; both of these factors would affect the diffusion of chemicals, and consequently, the frequency of oscillatory color changes. The circle-shaped gelatin achieved a high frequency and it merits further exploring for the creation of self-moving materials as will be discussed in Chapter V.

2.4 Conclusions

The present chapter provided advances on the creation of self-oscillating polymers based on iron catalysts. The iron catalyst was synthesized as a non-toxic alternative to the commonly used ruthenium-based catalysts (the LD$_{50}$ for iron compounds is reported to be up to 100 times higher than that of the LD$_{50}$ for ruthenium[138]). The chemical attachment of this catalyst to the gelatin matrix (biopolymer) allows a cheap, appropriate model for nature-related research on BZ reactions. In contrast to majority of the reports for self-oscillating hydrogels that involve small-dimension microgels (micrometer to

millimeter scale), the size employed for these gelatin samples is in the centimeter-scale; which offers the ability to mimic oscillatory phenomena in large dimensions.

The use of iron as a catalyst for the BZ reaction in these hydrogels caused them to have a different reactivity than ruthenium-based hydrogels. When first evaluated for oscillatory response, the concentration of reactants used for the ruthenium-catalyzed systems was not appropriate for defined wave patterns due to a lower redox potential of iron (in contrast to ruthenium) and due to the production of bubbles caused by the decomposition of the oxidizing agent. Despite this difference in the catalytic activity of iron, using a different oxidizing agent and manipulating the concentration of the reactants proved to tune the BZ system that led to pattern-rich, regular oscillations.

An effect on oscillations and the diffusion of chemical waves due to the shape of the polymer sample was observed. However, additional experiments involving size and shape variations would further support the observation. In chapter IV, a more systematic assessment on such effect was carried out, where a 3D printing technique was employed to achieve precise sizes and to better control the shape of hydrogels. Through that approach, stars with different sizes, number of arms and the angle between the arms, altogether, proved to influence the oscillatory frequency of the hydrogels.

The monitoring technique employed for the reaction analysis proved to be efficient, as it allowed for the cyclic color detection over time, regardless of the duration of the reaction and the number of captured images. The development of this technique was crucial as it was implemented for any posterior experiments described in the next chapters.

CHAPTER III

EFFECT OF LIQUID CRYSTALS ON SELF-OSCILLATING HYDROGELS

3.1 Introduction

The self-oscillating polymers that we focused on for this chapter were hydrogels

(PNIPAM-co-PAA network) that contained ferroin as well as zirconium phosphate

nanoplates. Such nanoplates, which normally self-assemble in suspension, were

incorporated in the hydrogels in order to analyze their effect on the wave pattern and

oscillatory behavior of the BZ reaction.

3.1.1. Background

The behavior of the BZ reaction varies depending on the external conditions as well as

the reaction media. External stimuli such as electric field[139-140], magnetic field[141] and

light[142] have proved to alter the cyclic nature of the system. Alternatively, changing the

type of solvent or manipulating the reaction media by introducing soft matter structures

are other surrounding conditions that affect the dynamics of the BZ reaction. The use of

ionic protic liquids, for example, as the BZ reaction medium propitiated the oscillatory

phenomena without the need for strong acids[143]. Likewise, the velocity of wave

propagation decreases when the reaction occurs in a glassy, mesoporous media[144].

However, the options for bulk, single-phased reaction media, especially solvents, are

limited since the interacting species need to be dispersed in water-based systems. Thus,

exploiting the BZ reaction within diverse soft matter structures (biological membranes,

emulsions, liquid crystals and polymers) evaluates the oscillatory behavior under

structured media. Microemulsions have served to test how wave patterns and duration of

26

oscillations change in response to variations in the biphasic system, surfactant type and droplet size. For example, viscosity of the oil phase affects the wave patterns[145]; hexane and octane were employed as the hydrophobic phases and octane demonstrated to facilitate new excitation fronts and Turing patterns. Similarly, increasing the size of the water droplets is known to change the type of waves since it facilitates new dissipative patterns[146]. Moreover, the type of surfactant used for the microemulsion impacts the oscillatory time and frequency[147]; cationic and zwitterionic surfactants greatly affected the dynamics of the BZ reaction whereas anionic and neutral ones let the oscillations occur similarly to the ordinary BZ reaction in solution. The oscillatory property of the BZ reaction is also affected when the critical micellar concentration (CMC) is reached for such systems, and simultaneously, the wave speed decreases due to this transition[148]. On the other hand, testing the BZ reaction within phospholipid bilayers is valuable since they create membrane-like structures that aid to elucidate the kinetics of the oscillations under a biological, cellular setting. One of the first studies for this setting was introduced by Magnani et. al.[149]; they discovered that some patterns persisted for twenty minutes and did not change position when the BZ system contained 1,2-dipalmitoyl-sn-glycero-3-phosphocholine (DPPC). Other phospholipids with a chemical structure similar to the DPPC one were used to create lipid bilayers[150]; the lipid concentration acted as a control parameter for the spatial organization of patterns, causing changes in between spiral and stripped standing waves. Similarly, the diffusivity of the reactive species was affected with increasing concentration of the lipids and provoked an increase in the width of the waves. Interestingly, one of the membranes, formed with non-saturated phospholipids,

27

inhibited the overall oscillatory behavior, and it is theorized that the double bonds reacted with other species present in the BZ system. Conversely, later research reported that if cholesterol was added to lipid membranes with DMPC, the oscillatory frequency of the BZ system increased[151].

Liquid crystals are another type of soft matter that deserves attention since they portray structures found in Nature[152]. For instance, nematic ordering can be found in human cells such as melanocytes, fibroblasts, osteoblasts and adipocytes[153-154]. Similarly, actin filaments self-arrange to present an isotropic to nematic transition[155-156]. Remarkably, neuroblasts organize in a similar fashion[157], and such organization is relevant to self-oscillating polymers since the BZ reaction system is often employed to understand neural pulses and oscillations. Studies of the BZ reaction with liquid crystals have been only focused on electrically-arranging clay particles into the nematic phase[158]. Therefore, we decided to synthesize zirconium phosphate liquid crystals (α-ZrP) and incorporated them into self-oscillating hydrogels; thus, it was possible to analyze the kinetics and wave pattern of the BZ reaction under the effect of nanoparticles self-organizing from isotropic to nematic arrays.

α-Zirconium phosphate, ($Zr(HPO_4)_2$-H_2O, abbreviated as α-ZrP), is an inorganic layered material that is widely used in different applications such as catalysis[159], fuel cells[160], polymer nanocomposites[161], Janus nanosurfactants[162] and even drug delivery devices given their non-toxicity[163]. ZrP crystals are hexagonal shaped disks that can be engineered for different size and thickness (number of layers), and they can form monolayers post-exfoliation with intercalating ions[164-165]. Water suspensions of these

monolayers create liquid crystals that undergo a transition from isotropic to nematic phases by increasing their concentration. Through the incorporation of ZrP monolayers in self-oscillating hydrogels catalyzed by iron, we created a new model to gain insight on the oscillation behavior under the influence of active matter. Therefore, the model potentially mimics oscillations at cellular level environments more efficiently.

3.2 Experimental

3.2.1. ZrP Monolayers

While attempting to obtain self-oscillating gels linked to ZrP liquid crystals, an initial approach was to grow a polymer (copolymerized with the iron catalyst) from the surface of ZrP crystals. With modifications from previous literature[166], the ZrP nanoplates were synthesized in a microwave reactor via a one-pot synthesis, where the chemical precursors for the ZrP nanocrystals and a surface modifier were placed in the same chemical reactor. The surface modifier would serve as the anchoring point of the self-oscillating polymer to the ZrP disks. The ZrP crystals successfully formed (single layers with an average diameter of 50-70nm) with the surface modifier simultaneously attached. Unfortunately, the obtained crystals did not have a suitable size for stable suspensions of liquid crystals that would allow the creation of hydrogels with proper macroscale visualization and monitoring of the BZ reaction. Still, the simultaneous surface modification of the synthesized nanoplates facilitated their post-functionalization and salt and temperature resistance properties were found when they were used as nanosurfactants, thus giving it a different application. More details about the design and development of such nanoparticles can be found in appendix B.

29

3.2.2. Synthesis and Exfoliation of ZrP Nanoplates

Due to the size constraint expressed above, the appropriate α-ZrP crystals were synthesized through the hydrothermal method since it has been largely used to produce particles of bigger sizes than the microwave ones[167]. A highly concentrated solution of phosphoric acid (H_3PO_4, 15M, Sigma Aldrich) was mixed with zirconyl chloride octahydrate powder ($ZrOCl_2 \cdot 8H_2O$, Acros Organic) while vigorously stirring. The obtained suspension was placed in an autoclave reactor and left to react at 200°C for 6 h. The synthesis and isolation of the particles was performed as reported in previous literature. The obtained non-exfoliated crystals were characterized with scanning electron microscopy (SEM) as seen in Figure 10a. The Figure 10b depicts the exfoliation performed on the ZrP crystals through the addition of tetrabutylammonium hydroxide (TBA^+OH^-, Sigma Aldrich, 40wt.% in water) at a molar ratio of 1:1 in deionized water. The resulting suspension was sonicated for 10 min and left for 24h to ensure full intercalation of the ions. The dynamic light scattering (DLS) analysis of the exfoliated hexagonal crystals indicated a size of 879 ± 265 nm upon transformation from sphere to plate shape (Appendix B). The suspensions of exfoliated ZrP disks at increasing
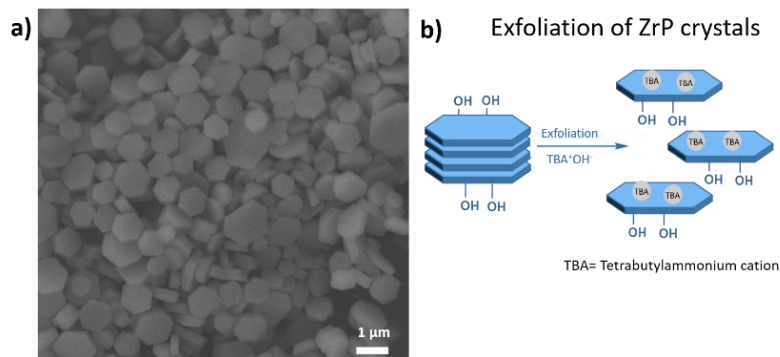
Figure 10. SEM Picture of ZrP Crystals (a) and Illustration of Their Exfoliation (b)

concentrations formed liquid crystals, as shown when they were placed under polarized light conditions (figure 11a). The volume fraction values (ϕ) were calculated as previously reported[168]. For Figure 11b, the nematic ratio was calculated for each of the suspensions and a sigmoidal fitting was done to obtain the curve.
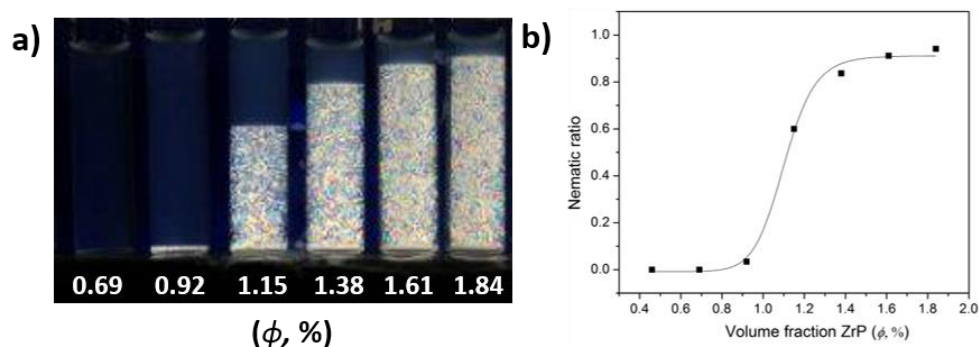
Figure 11. Liquid Crystals of ZrP Suspensions under Cross Polarized Light and I-N Transition Curve

3.2.3. Preparation of ZrP Self-Oscillating Hydrogels

Suspensions of the exfoliated liquid crystals at five different volume ratios (ϕ, in %=0.034, 0.085, 0.170, 0.260, 0.340) were used to make five hydrogels. In a 1-mL rounded glass cylinder vial (Fisher Scientific, Pittsburgh, PA), acrylamide (AAm, Alfa Aesar, 0.0235 g/mL), N-isopropylacrylamide (NIPAm, Sigma Aldrich, 0.0942 g/mL), N,N'-methylenebisacrylamide (cross-linker agent, 0.0015 g/mL, Sigma Aldrich), and urea (0.348 g/mL, MP biomedicals) were added along with 10 μL Ferroin (0.025M, Sigma Aldrich). The ZrP suspension with the corresponding ϕ was added and the vial was vortexed. Lastly, 10 μL of solution of ammonium persulfate (APS, initiator, 0.100 g/mL, Sigma Aldrich) and N,N,N',N''tetramethylethylenediamine (TEMED, catalyst, 10 μL, Fisher Scientific) were added to the 1mL vial. Immediately after, the vial was sonicated

for a few minutes to homogenize the mixture, and left to complete the radical polymerization for 24h at room temperature. The obtained hydrogels are shown in figure 12, the volume fraction of ZrP was increased from left to right while the amount of ferroin was constant. Bright spots on the polarized conditions (figure 12b) indicated the presence of liquid crystals formation.
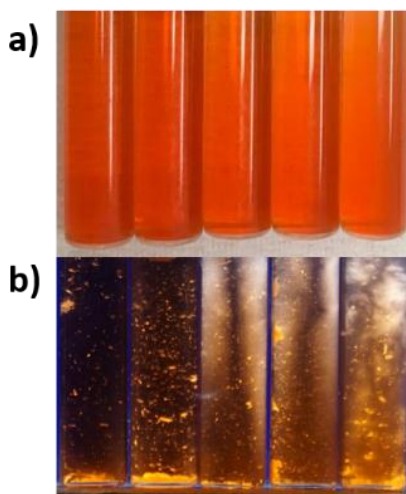
Figure 12. ZrP-Fe Hydrogels under Normal Light (a) and Polarized (b) Conditions

3.2.4. BZ Reaction Conditions

After the hydrogels formed, the glass cylinders were shattered and the hydrogels were retrieved. The oscillatory activity of the ZrP-Fe hydrogels was tested by immersing them in a solution with $NaBrO_3$ (0.10M, Sigma Aldrich), HNO_3 (0.95M, VWR), and 1,4-cyclohexanedione (0.125M, Sigma Aldrich). The monitoring of the reactions was performed with the technique described in section 2.2 by obtaining pictures from the top of the reaction every 5 seconds.

3.3 Results and Discussion

The hydrogels successfully presented diverse wave patterns and oscillatory color
changes as shown in figure 13. The analysis of the wave pattern was performed with
ImageJ and IDL analysis.
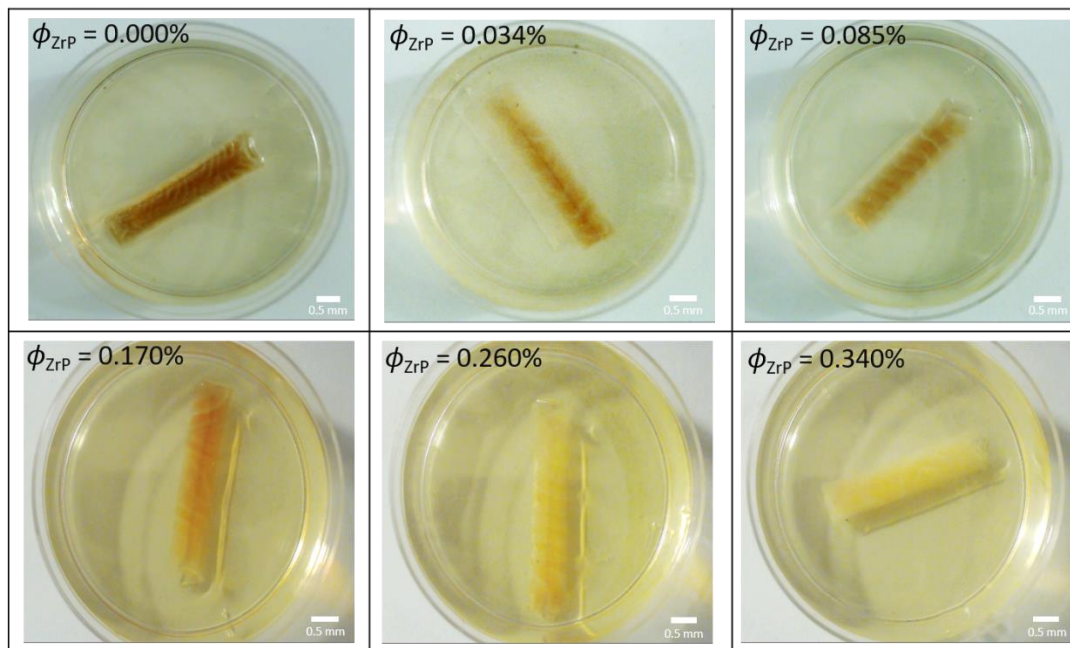
Figure 13. Oscillations in ZrP-Fe Hydrogels at Varying ZrP Concentrations

3.3.1. Image Analysis

The parameters analyzed with ImageJ software were induction time, reaction time,
wavelength and wave-pattern formation. The induction time (figure 14a) is the first point
in time where waves and color changes are seen, and the reaction time is set as the
period of time during which oscillations happen. Hydrogels required more time to
present oscillations as the amount of ZrP platelets (volume fraction, ϕ) was higher with
the exception of the range for hydrogels with $\phi = 0.085\%$ and $\phi = 0.170\%$, where a

decrease in induction time occurred. For figure 14b, the reaction time is defined as the

amount of time for which oscillatory behavior is present, in other words, it is the time

between the first oscillations and the time when all oscillatory reactions cease within the

hydrogel (end point). According to the fitting model, oscillations would last for longer

time as the
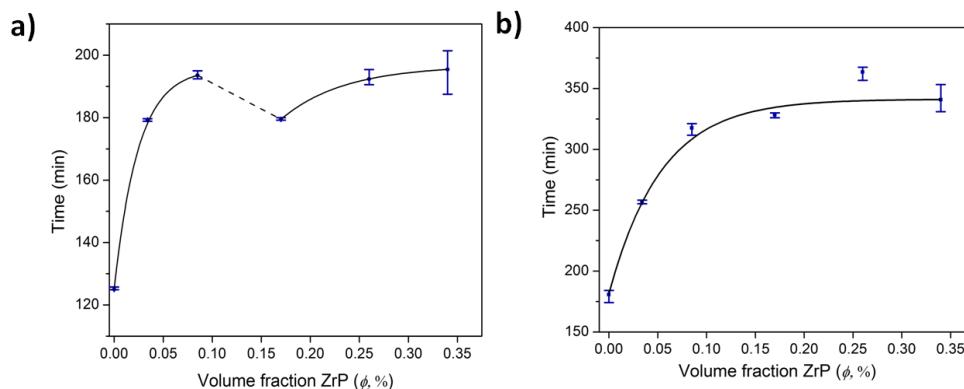
Figure 14. Induction (a) and Reaction (b) times for ZrP-Fe Hydrogels

amount of ZrP platelets was increased, such observation can be linked to an increase in

the volume of materials and chemicals reacting. Overall, inserting ZrP nanoplates delays

the starting point for the oscillations while prolonging their lifetime.

As part of the wave analysis, the term wavelength was established as the width in

between two waves of the oxidized states (Fe^{3+}, colorless) or as the width of the wave

for the reduced state (Fe^{2+}, red) as indicated by the white line in the reacting hydrogel in

Figure 15a. The wavelength was measured parallel to the direction of the travelling

oscillations and three different extents of the reactions (τ) were chosen. These extents

were ⅓ τ, ½ τ, and ¾ τ.
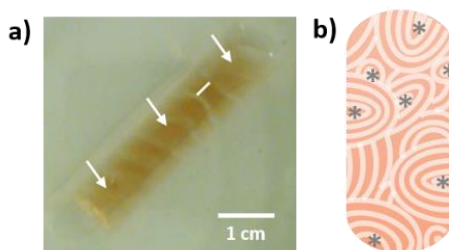
Figure 15. Graphics for Wavelength (a) and Wave Pattern (b) Analysis

For the graphs corresponding to ⅓ τ, ½ τ, figure 16a and 16b respectively, the

wavelength increased as the volume fraction of ZrP (ϕ) was increased except for a

decrease in wavelength between volume fractions ϕ =0.085 to 0.170%. Additionally, the

width of the red wave reached a local minimum at ϕ =0.170%. However, for the analysis

at ¾ τ (figure 16c), the decrease in wavelength occurred at a smaller volume fraction

(ϕ= 0.034%) which suggests that analyzing the waves at later stages is not representative

of the reaction since the chemicals begin to run out.
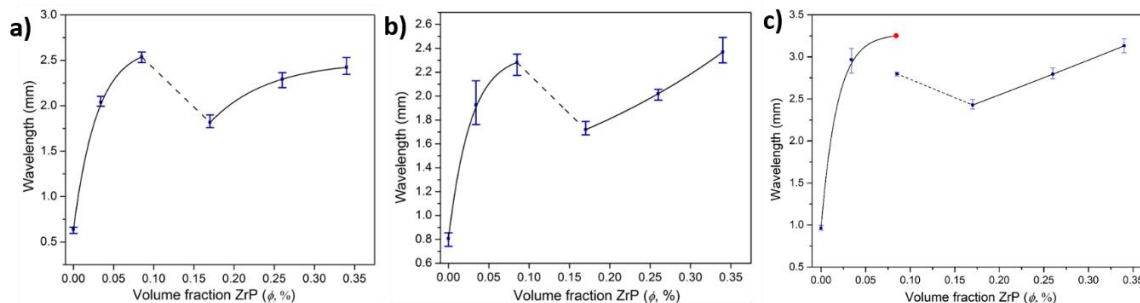
Figure 16. Analysis to the Wavelength on ZrP-Fe Hydrogels at ⅓ τ, ½ τ, and ¾ τ

Conjunctively, the behavior observed for the wavelength analysis at ⅓ τ and ½ τ agrees

with the behavior observed for induction time, since they all indicated a transition

occurring in between ϕ=0.085 to 0.170%.

For the wave pattern analysis, the number of nodes and the number of fully developed spirals and/or target waves were considered. These two parameters were analyzed at five different stages of the reaction: 30%, 40%, 50%, 60% and 70% (with a ±2.5% confidence interval). The number of nodes (labeled as # of origin points in graphs) are marked with an asterisk in figure 15b, and they represent the cores for wave pattern initiation. The hydrogels with a $\phi \leq 0.085$ % (figure 17a) presented a trend, in which the number of nodes decreased as the amount of ZrP liquid crystals was increased. Alternatively, the hydrogels with a $\phi \geq 0.170$ % (figure 17b) presented less variability in the number of nodes as the amount of liquid crystals was increased.
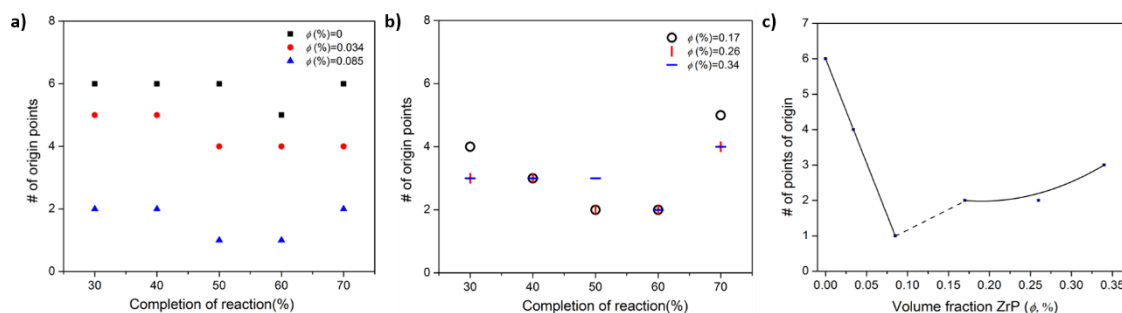
Figure 17. Number of Wave Nodes for ZrP-Fe Hydrogels. Hydrogels with $\phi \leq 0.085\%$ (a), Hydrogels with $\phi \geq 0.170\%$ (b), and all Hydrogels at ½ τ (c)

The combined graph representing all hydrogels at 50% extent of the reaction (figure 17c) showed that increasing the amount of ZrP platelets restricted the formation of nodes ($\phi \leq$ 0.085 %), but the number of nodes slightly increased after reaching ϕ=0.170%. As a result, lower volume fractions interfered with the formation of wave patterns and higher volume fractions gradually promoted them. On the other hand, the amount of fully developed spirals and/or target waves were quantified. They were identified among the

36

hydrogels as the pattern marked with an arrow in Figure 18a. The resulting data was

plotted in figure 18b and it showed that hydrogels with ϕ= 0.034% and ϕ=0.085% did

not form any full patterns, suggesting that isotropic and nematic phases coexisted in the

region. However, the number of patterns raised after reaching the volume fraction of ϕ=

0.170%.
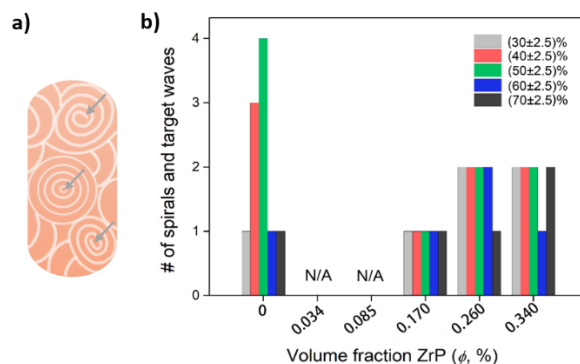
Figure 18. Spiral and Target Waves Analysis for ZrP-Fe Hydrogels

Altogether, introducing ZrP liquid crystals limited the creation of various nodes while

converting them into more localized pattern structures. Hence, analyzing the visual

characteristics of the wave patterns with ImageJ software allowed proposing an I-N

transition in the range ϕ= 0.085-0.170%, according to induction time, wavelength and

wave patterns. In order to confirm the proposed transition, a comparison of the

oscillatory frequency for each hydrogel was performed with the IDL software.

3.3.2. IDL Analysis

As established in the monitoring technique described in section 2.3, the IDL analysis

was performed at three different locations distributed uniformly in the hydrogel (arrows

in Figure 15a).

Grey values were obtained and plotted versus time to yield the graphs for all the

hydrogels (ϕ= 0, 0.034, 0.085, 0.170, 0.260 and 0.340%, appendix B). Upon applying

the Fast Fourier Transform (FFT) to the cyclic color changes, the dominant frequency

was determined. The resulting frequencies as a function of the volume fraction of ZrP

platelets are shown in figure 19b.
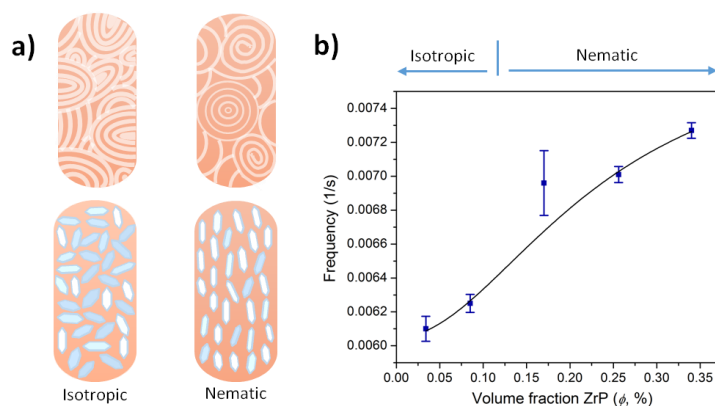
Figure 19. Illustration of Observed Wave Patterns and Platelets Ordering (a) and Oscillatory Frequencies (b) on ZrP-Fe Hydrogels

The BZ reaction performed in hydrogels without ZrP disks (ϕ= 0) had an oscillatory

frequency of $(1.98 \pm 0.2) \times 10^{-2}$ s^{-1}. The initial incorporation of disks caused a large

decrease in the frequency $(6.10 \pm 0.7) \times 10^{-3}$ s^{-1}. Thus, the cyclic color changes (or

changes of oxidation state of iron) occurred at a slower pace. Yet, as the volume fraction

of ZrP platelets was increased, the frequency of oscillations augmented. Interestingly, a

large increase in frequency was seen in between the ϕ= 0.085% and ϕ= 0.170%. This

suggests a change in the ordering of the liquid crystals for such range. Therefore, by

combining the visual characteristics obtained with ImageJ analysis and the frequencies

calculated by the IDL software, a proposed location of the transition from isotropic to

nematic ordering is depicted in the graph in figure 19b. Similarly, a graphic

representation of the observed wave patterns for hydrogels in the proposed isotropic and

nematic phases, including the ordering of the liquid crystals, is shown in figure 19a. The

BZ reactions in the hydrogels were prone to form target and spiral waves that were more

organized as the liquid crystals became nematic.

Finally, the phase transition for the ZrP-Fe hydrogels was compared with the phase

transition for the suspensions of ZrP liquid crystals. Through ImageJ analysis, the grey

values for the hydrogels under polarized light conditions (figure 12b) were extracted and

transformed into nematic ratios. The resulting graph is shown in figure 20. The phase

transition for the hydrogels (blue line) occurred at a lower volume fraction than the

phase transition for suspensions (black line). The embedment of liquid crystals into a

polymeric network along with a chromatic effect caused by the ferroin structure are

responsible for such shift[169-170].
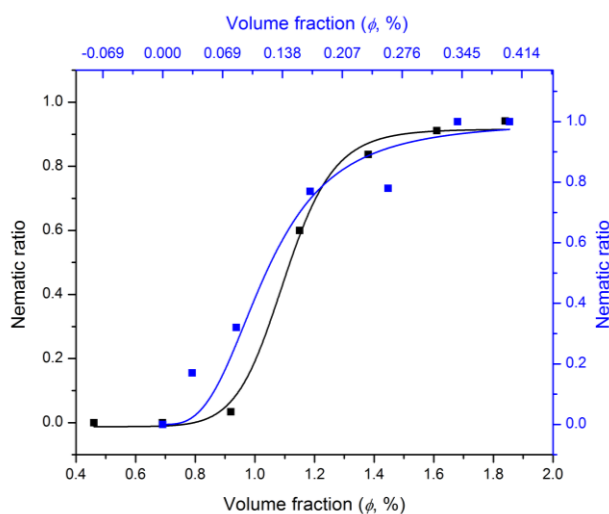
**Figure 20. Phase Diagram Curves for ZrP Suspensions (black) and ZrP-Fe
Hydrogels (blue)**

The self-assembly of the ZrP liquid crystals still occurred as when they are suspended in water. Yet, incorporating the ZrP liquid crystals into the hydrogels changed the behavior of the BZ reaction. Specifically, the wave pattern became more organized as the disks became more nematic and, in response, the frequency for oscillations was increased.

3.4 Conclusions

The effect of ZrP liquid crystals into the dynamics and wave pattern of the BZ reaction was successfully examined. The BZ reactions of the synthesized hydrogels created spiral and target waves, which were more prone to develop and stay as the liquid crystals self-arranged into the nematic phase. Once in the nematic phase, the chemical waves propagated more easily and, consequently, the frequency of oscillations was increased. Hence, the self-organization of the liquid crystals represents another method to tune the frequency of oscillations. However, the tuning of the BZ reaction with these specific hydrogels was restricted to achieve frequencies in the order of a solution-based BZ reaction. Graphene, for example, has been reported to tune the oscillatory dynamics of the BZ reaction by changing the frequency with a 4-fold increase[171]. Similarly, graphene oxide allowed to prepare an electrically conductive, mechanically tough and self-oscillating graphene nanocomposite[172]. Thus, further exploration of the tuning through higher concentrations of ZrP liquid crystals, differently-sized ZrP liquid crystals, other layered materials or liquid crystals with tubular-like or circular structures is necessary; examining these parameters could open the possibility to achieve higher ordering and

new phases, such as the smectic phase, which is present in the DNA structure or lipid domains[173-174].

The type of polymer network used for the hydrogels is not biologically-friendly due to the employment of acrylamide. However, its use for thermo-responsive hydrogels with nematic phases is supported by previous reports[175]. Additionally, one of the initial approaches suggested the incorporation of white-colored ZrP disks into biopolymeric, gelatin matrices which caused the gel to turn opaque, and the color changes and waves were not accurately visible.

The self-oscillating hydrogels described in these chapter allowed the BZ reaction to occur under isotropic and nematic phases as well as in the coexistence region (isotropic and nematic coexisiting). The synthesized hydrogels required low concentration of particles, the size of the particles was uniform and controlled and the anisotropy was obtained without an external stimuli, which is valuable when compared to previous reports because their liquid crystals required an electric field to align into the nematic phase[158]. Overall, these conditions can serve as model for oscillatory phenomena under disorganized and organized muscle or cardiac tissue. It has been reported that spiral waves in cardiac tissue are responsible for cardiac arrest[176]; therefore, obtaining conditions under which the presence of spirals is decreased is advantageous for health-related research[177].

CHAPTER IV

GEOMETRICAL SHAPE EFFECTS ON THE OSCILLATIONS OF 3D- PRINTED

HYDROGELS

4.1 Introduction

This chapter presents the employment of 3D printing technique for the fabrication of

additional self-oscillating polymers. The polymer matrix was composed of gelatin and κ-

carrageenan, two biopolymers. 3D-printed polymers were manufactured in different

shapes and sizes to assess how morphology variations changed oscillatory behavior and

wave pattern.

4.1.1. Background

The design and construction of self-oscillating polymers can be adjusted by tuning the

chemical oscillating reaction, by altering the responsive components of the polymer

matrices or by creating new processing techniques. Manipulation of the chemical

oscillation reaction and the type of responsive components within the polymer are

parameters that have been widely tested[68]. In contrast, engineering techniques for the

production of self-oscillating materials, besides flask-mediated polymerizations, are

limited. A microfluidics system, for example, was used to analyze the effect of the

continuous flow of reactants on the gel oscillations while placed inside a capillary

chamber[178]. Not only did the microfluidics devices allowed for reproduction of

oscillatory phenomena in a capillary setting at different flow rates, but they also

demonstrated an increase in the gel volume of about 500%. Other reports involving the

use of microfluidic devices allowed to study the communication between chemical

oscillators[179] and the phenomena under double emulsions environments[180]. Similarly, a microliter scale fluid dispenser equipped with a needle was used to fabricate complex patterns such as lines, spots, shape outlines and letters[181]. The micro dispenser deposited 400 µm-thick films onto a laminate substrate but a limiting factor appeared in terms of the z-direction growth. The samples were not efficiently constructed in the z-direction because the ink containing the catalyst did not penetrate fully into the patterned sample. Lastly, photolithography has been reported to aid in the photo-polymerization of diverse shapes[182]. The photo-polymerization of polyacrylamide gels was initiated and controlled by UV energy. Different exposure times for the polymerization resulted in gels with gradients in thickness. Such gradients showed to alter the way the chemical waves were formed. However, the size scales employed for the polyacrylamide gels were in the range of 0.5mm to 1mm. To overcome the size constraint shown by some of these methods and to avoid the use of photochemistry, we decided to employ extrusion-based 3D printing to create self-oscillating polymers. Through this approach, a precise control over shape and size while maintaining chemical integrity at macro-scale dimensions would be possible, with short preparation times and flexibility for the design of shapes. Moreover, the design size for the 3D-printed materials would facilitate the creation of biomimetic actuators that could reproduce wave patterns shown by marine species. Different aquatic organisms present changes in color or morphology in response to environmental stimuli[39]. Such changes can serve as communication tools or as camouflage strategies. Squids, for example, emit flashing and flickering signals[183], fish show dynamic Turing patterns[184-185] and flounder fish conceal themselves through

unique patterns[186]. Understanding such dermal patterns or other dynamic pigmentation

changes is difficult due to the biological diversity of the marine organisms, even among

the same family of species. Therefore, a study for self-oscillating gels that could

replicate dynamic skin patterns on aquatic organisms, while comprising numerous

morphology variations in macro-scaled architectures, is desired. To achieve this, an

assessment on the effect of shape and size on the color patterns and oscillations was

designed based on the starfish. The starfish can present diverse geometries: different

number of points, overall size and angle of the points[187-188]. The number of points or

appendages, for instance, can go from 3 up to 33[189]. In addition to points, starfish have

sizes spanning from 2 mm to 352 mm in diameter[190]. Finally, appendages on starfish

possess varying angles (degree of inner-angle), ranging between 12⁰ (*Linckia*

laevigata)[187] and 90⁰ (*Patiriella exigua*)[191-192]. Hence, the study comprised star-shaped

gels with variations based on the morphology parameters described for starfish (points,

size and angle).

The polymer matrix employed for the fabrication of the starfish architectures was a

composite formed by gelatin, a positively-charged polyaminoacid, and κ-carrageenan, a

negatively-charged polysaccharide[193-196]. The electrostatic interaction between these two

matrices would stabilize the pattern formations. As mentioned earlier in section 1.3, the

available options for polymer matrices in the design of self-oscillating polymers have

mainly been limited to PNIPAM[112, 197]. This synthetic polymer limits the mechanical

robustness of the gels, whereas gelatin permits the post-functionalization of the

composite[107].

Overall, the electrostatic interactions between gelatin and κ-carrageenan along with their feasibility for additive manufacturing makes them a suitable, reinforced gel network to investigate spatiotemporal patterns in the BZ reaction. By linking 3D printing techniques with self-oscillating chemical reactions, precise macro-scaled architectures for studies on the geometry effects on color patterns could be fabricated. Thus, these models can be applied as biomimetic examples of spatio-temporal phenomena observed in nature.

4.2 Experimental

4.2.1. Bioink Fabrication

Ferroin and iron catalyst were employed for the fabrication of inks. Ferroin was used as received in the commercially available bottle and the iron catalyst was synthesized with the same methodology as the one reported in section 2.2 (Catalyst synthesis).

A solution of gelatin (10 wt.%) was prepared by dissolving the desired amount of gelatin (Type A, 300 bloom) into heated deionized water (50˚C) while constantly stirring on a hot plate for about 5 min. Once the gelatin solution was fully transparent, ferroin or iron catalyst was added (~2 mM of iron). The red solution was stirred for additional 5-10 min to ensure full dissolution. Finally, kappa-carrageenan (3 wt.%) was slowly incorporated into the solution and stirred to obtain the hydrogel precursor solution. Prior usage on the 3D printing technique, the solution was stored overnight at 50˚C.

4.2.2. Rheological Characterization

The rheological characterization was carried out with a stress-controlled Discovery Hybrid Rheometer 2 (DHR-2, TA Instruments), utilizing a parallel plate geometry (40 mm diameter). This geometry was equilibrated to 37°C, considering a gap height of 0.25 mm, and a solvent trap was included for all experiments. Rotational shear-rate sweeps were completed between 10^{-2} and 10^4 (s^{-1}) to determine the shear behavior. Herschel-Bulkley (HB) parameter's n (flow behavior index), τ_o (yield stress), and K (consistency index) were calculated applying the TRIOS software (TA instruments) and verified by excel. Rotational time sweeps were performed at three consecutive shear rates (s^{-1}): 3.02 (60 sec.), 23,000 (5 sec.), and 0.01 (120 sec.) to characterize the shear recoverability of the different precursor solutions.

4.2.3. Uniaxial Compression

The uniaxial compression testing of all printed samples was performed with an ADMET MTEST Quattro eXpert 7600 Single Column Testing System, equipped with a 25 lb. load cell. The hydrogels were casted into 2 mm thick sheets and by means of a biopsy punch, the circle samples were stamped (7mm diameter, n=4). The sample's height and diameter were measured with a digital caliper, and variations on the measurements were considered into the moduli calculations. Unconstrained samples were compressed 20% of the measured height and returned to the original position at a strain rate of 1 mm /min. Raw numbers for cyclic compression were processed with Excel, and the compressive

modulus was computed as the slope of the linear region of the data (0 to 20% strain). Compression data was obtained for Gelatin, Kappa, and Gelatin + Kappa gels as well as gels using ferroin and gels using synthesized iron catalyst.

4.2.4. 3D Printing

The printed shapes were designed with Solidworks, exported into STL files, loaded and modified in Slic3r, and exported into G-code instructions for the 3D printer. The printed samples were programmed to have a layer height of 200 μm at a speed of 0.20 mm/s. The precursors were printed at 50˚C employing a 400 μm diameter gauge and an I3 RepRap Printer. Upon printing, the hydrogels were crosslinked through different methods: covalent (glutaraldehyde), ionic (potassium chloride), or combination of ionic and covalent (potassium chloride and glutaraldehyde). The covalently crosslinked hydrogels required to be immersed in a 5mM glutaraldehyde (GA) solution for 24 hours. Alternatively, the ionically crosslinked hydrogels were soaked in a 5 wt.% of potassium chloride (KCl) solution for 30 min. For the combined crosslinked method (ionic and covalent), the hydrogels were exposed to both potassium chloride (KCl) and glutaraldehyde (GA) solutions.

4.2.5. Scanning Electron Microscopy

The microstructure of the hydrogels was analyzed with a scanning electron microscopy (SEM), and the instrument employed was a JEOL NeoScope JCM-5000: Benchtop SEM. The hydrogel samples were lyophilized, frozen in liquid nitrogen and cut with a

razor blade. Once split, the samples were fixed and sputter-coated with gold (21 nm thickness).

4.2.6. BZ Reaction Conditions

The 3D-printed gels were fully immersed in a 16 mL solution of 1,4-cyclohexanedione (0.125 M), HNO_3 (0.950 M), and $NaBrO_3$ (0.100M). The gels were allowed to react and the monitoring of the reaction was performed with the same technique described in Section 2.3 (Monitoring of the BZ reaction).

4.3 Results and Discussion

The 3D printing technique consists of the layer-by-layer deposition of filaments, where each deposited filament ties with previous layers and constructs a compiled structure. Since the inks are in a non-crosslinked, precursor solution during the extrusion stage, it is essential to characterize the flow properties of the ink precursors. Specifically, the ink precursors must be tested under dynamic shear conditions to demonstrate that the printing filament formulation is effective and can prepare geometries with highly viscous, gel-like structures. Therefore, the mechanical properties of the printing precursors employed for the hydrogels were measured through shear-rate sweep, peak hold and compressive moduli testing. Upon printing, the constructed shapes were tested under different crosslinking methods to evaluate the oscillatory response when subjected to the BZ reaction conditions. The crosslinking method that demonstrated stable hydrogels with dynamic color changes and pattern stability was selected. Finally, new hydrogels containing the desired morphologies were fabricated and analyzed for the

effect of the shape on oscillatory frequencies and other kinetic parameters of the BZ reaction.

4.3.1. Bioink Determination

In order to determine the most suitable bioink for printing, the rheological properties of different precursors were analyzed. First, the precursors gelatin (Gelatin), kappa-carrageenan (Kappa) and the combination of both were characterized for shear-thinning properties (figure 21). According to the graph, the rheological flow profile of Gelatin showed a constant low-shear viscosity (~10^{-1} Pa·s), whereas Kappa presented low-shear viscosity around 10^4 Pa·s, that decayed linearly as the shear-rate was increased. Correspondingly, the combination of Gelatin and Kappa proved to conserve the shear-thinning flow behavior of the Kappa component.

	Flow Behavior Index (n)	Consistency Index (K; Pa·s)	Yield Stress (τ_o)	Correlation
Gelatin	0.90	0.056	-0.135	99.99%
Kappa	0.35	28.31	48.43	97.66%
Gelatin + Kappa	0.52	28.37	47.99	98.44%

$$\tau = \tau_o + K(\dot{\gamma})^n$$

n= flow behavior index
K= consistency index
τ_o= yield stress
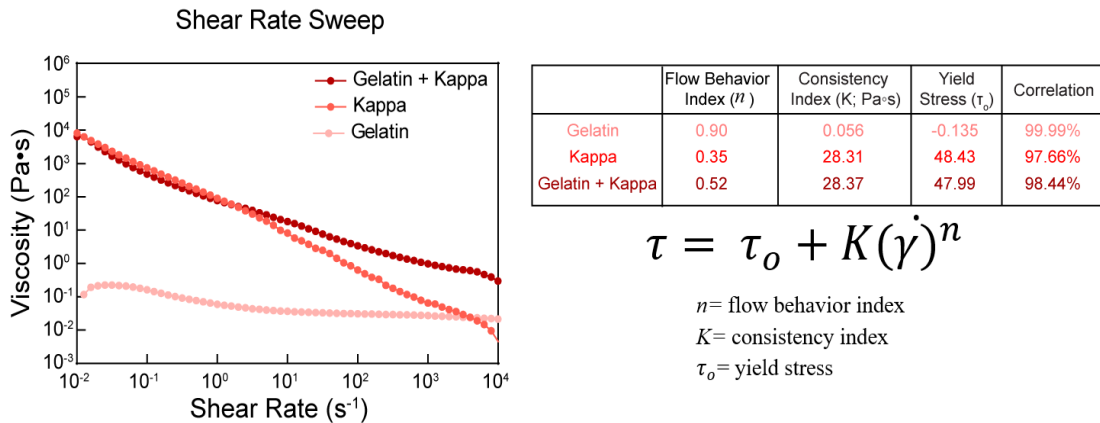
Figure 21. Shear-rate Sweep Measurements of Printing Precursors

The flow behaviors presented by the precursors were additionally modeled as Herschel-Bulkley (HB) fluids (equation in Figure 21). After fitting to this model, it was found that Gelatin had a low consistency index (n), low yield stress (τ_o), and a flow behavior index

(*n*) around 1, with the latter being an indication of a Newtonian-like performance. In contrast, the precursors containing kappa-carrageenan (Kappa, Gelatin + Kappa) exhibited an increased yield stress (~ 48 Pa) and an increased consistency index (~28 Pa·s). Additionally, the flow behavior index for the Kappa-containing precursors indicated behavior of a shear-thinning fluid ($n \leq 1$). Collectively, these results determined that bio-inks with Kappa behave as solids until the shear-stress reaches a yield stress of 48 Pa. Past this stress, Kappa and Gelatin+Kappa presented low-shear viscosity (~28 Pa·s), that decreased quickly at increasing shear-rates (10^1 s^{-1}).

Likewise, the bioink recovering properties were investigated through peak-hold analysis. In the peak-hold test, the bioink is subjected to low and high shear conditions to confirm that the printing materials are resilient to the forces employed in the 3D printing process. During printing, the ink is first placed in a barrel (low-shear conditions), extruded through the printing gauge (high-shear conditions), and finally deposited on the printing bed (low-shear conditions). Correspondingly, the ink must stay highly viscous within the barrel so the volume to extrude is regulated. When subjected to high-shear forces, the ink's viscosity should rapidly decrease so the flow properties are improved and the extrusion onto the printer bed is facilitated. After the high-shear forces are released, the ink must quickly regain its initial, high viscosity to allow the preservation of the printed constructs. Hence, the ink recovery capabilities of the three different precursors (Gelatin, Kappa, Gelatin+Kappa) were obtained (figure 22).
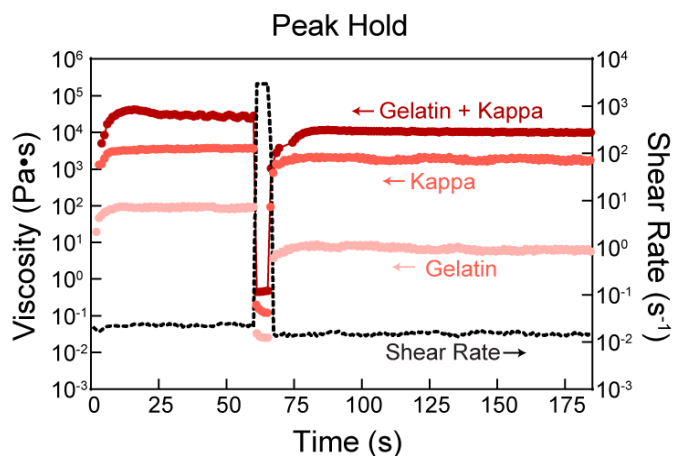
Figure 22. Peak Hold Measurements of Printing Precursors

Gelatin viscosity decreased upon application of the high-shear rate, and it was not able to completely recover to its original state. In contrast, Kappa and Gelatin+Kappa, recovered their initial, low-shear viscosity following the application of high-shear forces. These results, taken together, confirm the viability of Kappa and Gelatin+Kappa complexes to flow and extrude into designed structures.

4.3.2. Crosslinking Methods

Due to the acidic conditions presented in the BZ reaction, the chemical stability and mechanical reinforcement of the 3D printed structures is necessary. For such reinforcement, three different crosslinking methods can be employed: ionic (KCl), covalent (GA) and ionic-covalent (KCl and GA). The ionic crosslinking method works as an electrostatic interaction between kappa-carrageenan and potassium chloride (KCl). Alternatively, the covalent crosslinking method is plausible by the reaction between amino groups in the lysine residues of gelatin and glutaraldehyde (GA). In order to

51

evaluate the mechanically-reinforced structures, the compressive elastic moduli of the

crosslinked 3D prints were tested (figure 23). Covalently-crosslinked Gelatin presented

an elastic modulus around 0.42 ± 0.02 kPa; furthermore, if the precursor is composed of

Gelatin+Kappa, the covalently-crosslinked print increased its modulus to 0.95 ± 0.02

kPa. However, if the Gelatin+Kappa mixture is only crosslinked via ionic interactions

(KCl), the elastic modulus decreased to 0.79 ± 0.04 kPa. Lastly, a 3D-printed hydrogel

can be made with two precursors (Gelatin+Kappa) and employing the dual, ionic-

covalent crosslinking method. This last modality presented an elastic modulus similar to

the one of covalently crosslinked Gelatin+Kappa (0.96 ± 0.08 kPa). The Gelatin+Kappa

combination was chosen as the suitable precursor formulation, and it was used for any of

the upcoming printings.
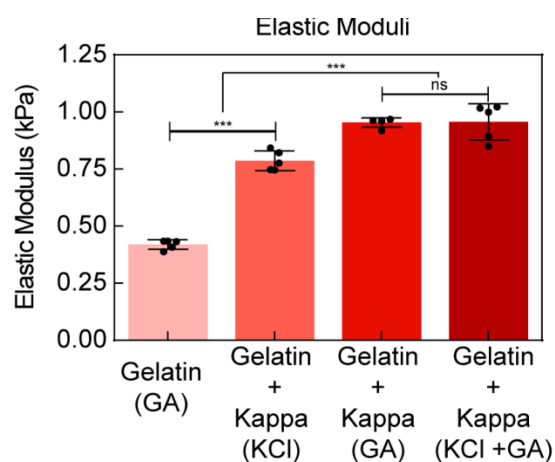
Figure 23. Compressive Elastic Moduli of 3D Printed Hydrogels

Additionally, the different crosslinking methods presented an overall effect on the

morphology of the hydrogels as well as the BZ reaction kinetics. For the morphology

effect, SEM micrographs were utilized to analyze the pore structure of the polymeric

networks (figure 24c). The ionic crosslinking produced macro-sized pores on the

Gelatin+Kappa hydrogels (top). The covalent crosslinking generated smaller, micro-

sized pores (middle). Furthermore, the combination of ionic and covalent crosslinking

mechanisms demonstrated macro-sized pores with small, micro-sized pores within them

(bottom).
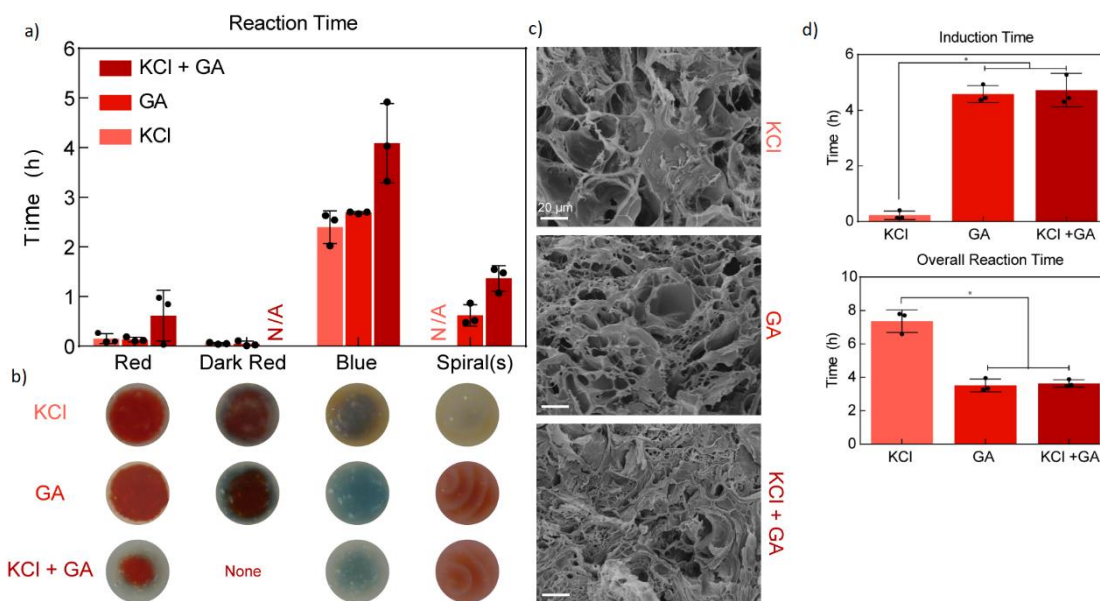
Figure 24. Crosslinked Hydrogels Morphology and Oscillatory Response

The microstructures observed for the crosslinking methods greatly influenced the

kinetics of the hydrogels performing the BZ reaction (figure 24d). Specifically, ionically

crosslinked hydrogels (KCl) presented the shortest induction time (0.23 ± 0.15 h) and the

longest reaction time (7.37 ± 0.68 h). In contrast, covalently crosslinked gels (GA)

showed a substantial increase in induction time (4.58 ± 0.30 h) and the reaction time was

greatly decreased (3.52 ± 0.38 h). In addition, the hydrogels with a dual crosslinking

method (KCl + GA) exhibited values similar to those observed for the covalent crosslinking (induction time: 4.72 ± 0.61 h; overall reaction time: 3.63 ± 0.22 h). The morphology of the polymeric network has also shown to affect oscillatory colors, formation of wave patterns and stability of the chemical waves (figure 24a, b). At typical conditions, the BZ reaction passes through three different phases: excitation, refractory and responsive[36, 198]. The ionically crosslinked hydrogels mainly exhibited blue color and did not form any spirals, which suggests that the reaction only reached the excitation phase[150]. The excitation phase occurs by the oxidation of the catalyst and the catalyst (iron complex) changes from red to blue color; therefore, the catalyst was not able to return to the reduced state (red) to create dynamic color changes that would result in oscillatory response and stable chemical waves. Alternatively, the covalent and ionic-covalent hydrogels reached all of the phases, since they both presented the blue stage, followed a red stage, and ultimately the formation of spirals for extended times. Among these two crosslinking methods, the dual, ionic-covalent one was the most appropriate for pattern formation since the spiral waves proved to be stable for more time than the covalent method.

Altogether, it can be concluded that the type of crosslinking method affects the morphology of the network, the chemical, oscillatory response of the hydrogels and the stability of the wave patterns. For the dynamics of the BZ reaction, it was found that the reactants in the BZ system took a longer time to diffuse into the hydrogel as the pore sizes were decreased, as a response, the reaction was delayed (induction time). Similarly, the reaction times were reduced for the crosslinking methods with covalent interactions

(GA, KCl + GA). However, these two methods had the advantage of presenting stable spiral formations, which are crucial for the purpose of this study. It is hypothesized that the macro-sized pores in the ionically crosslinked hydrogels prevented a continuous feeding of reactants within the network. This uncontrolled diffusion would restrict the exchange of electrons that facilitate the cyclic redox process of the iron, which is responsible for the constant changes of color. Correspondingly, the decrease in pore size affected the permeability of the system by prolonging the diffusion of reactants within the composite, hence the reaction patterns occurred at a slower rate but with stable presence of spirals. Overall, the pore sizes and crosslinking density demonstrated to play a key role in the diffusion of chemicals and reactivity of the BZ systems; consequently, the Gelatin+Kappa matrix reinforced with ionic-covalent crosslinking method was determined as the adequate formulation for pattern-rich phenomena.

Even though the polymeric components and crosslinking methods modify the mechanical properties of the 3D printed hydrogels, the type of iron catalyst can also produce an overall effect on their compressive modulus. The incorporation of iron catalyst into the hydrogels is possible with two different chemical compounds: free ferroin and iron-based catalyst. The use of free ferroin into the 3D printed hydrogels does not result in strong interactions, thus the term "free". The iron-based catalyst, on the other hand, creates new chemical linkages between the bromine groups on the phenanthroline ligands and the amino groups in the gelatin chains. Thus, the elastic modulus is further reinforced (figure 25). The incorporation of iron with the iron-based

Ferroin Catalyst ICE Reinforcement
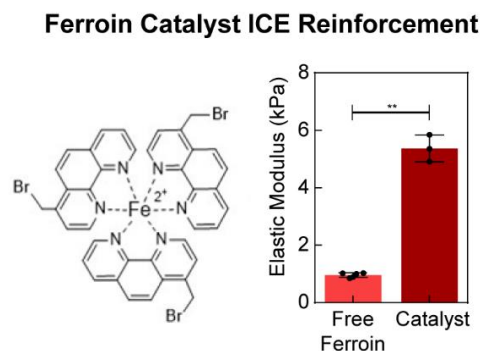
Figure 25. Catalyst Effect on Elastic Moduli of 3D Printed Hydrogels

catalyst, instead of the free ferroin, also has the potential to improve the transduction of electrons along the network, and consequently influence the dynamic change of colors. Hence, the iron-based catalyst was incorporated for any of the following 3D printed hydrogels due to the enhanced mechanical stability.

To investigate the effect of morphology variations on wave patterns and color oscillations, a study was designed utilizing starfish as the Nature model. This platform would allow the creation of 3D printed hydrogels that mimic natural, oscillatory phenomena under variable parameters: number of points, overall size and angle of the points.

4.3.3. Effect of Number of Star Points

Starfish have numerous appendages, herein referred as points, spanning from 3 to 33 points. Thus, 3-point, 5-point and 7-point stars were programmed and printed (figure 26a top, middle). The printed stars were allowed to react under BZ conditions and they successfully demonstrated oscillatory phenomena. By analyzing the beginning and end point of the oscillations present in the hydrogels, it was found that there was no

significant trend in induction or reaction times among the number of points (3, 5 and 7 appendages). Nonetheless, a spiral was formed at each of the appendages (figure 26a, bottom). In other words, the 3-point stars showed 3 different spirals, appearing at each point of the construct. Such behavior was replicated with the 5-point stars and 7-point stars since they formed 5 and 7 spirals, respectively (figure 26b top, middle). Therefore, an increase in the number of points resulted in an increase in the number of spirals. In addition, the time required for the spiral formation at each point (equilibrium spiral formation, figure 26b bottom) reduced as the number of points was incremented.
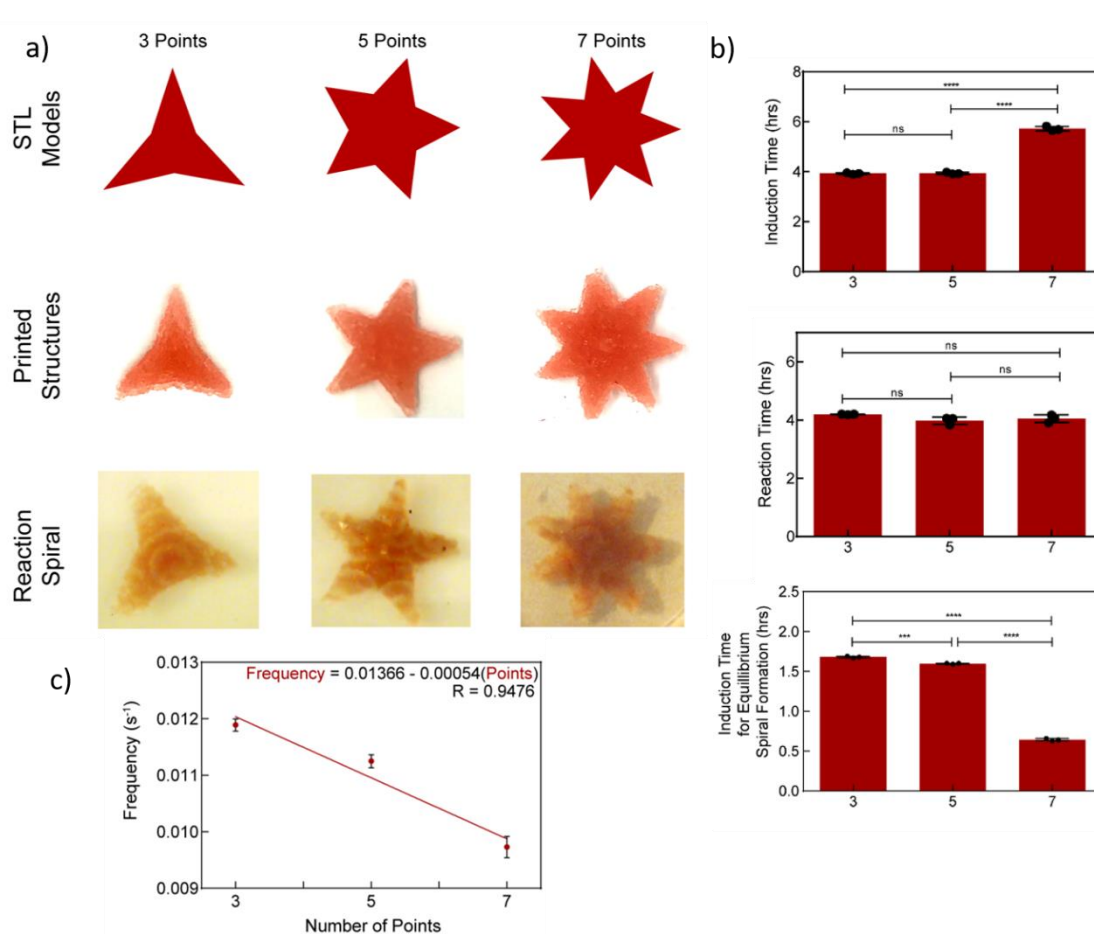
Figure 26. Effect of Number of Star Points on Oscillations

57

Explicitly, 3-pointed stars required 1.68 ± 0.01 h to present a spiral in each point. This

equilibrium time for spiral formation was reduced to 1.60 ± 0.01 h for the case of 5-

pointed stars and further reduced to 0.64 ± 0.02 h for 7-pointed stars. These results

suggest that the formation of spirals is correlated to diffusion kinetics at each appendage.

Lastly, the frequency of oscillations was computed for each of the printed hydrogels (3-,

5- and 7-point stars, appendix C). The oscillatory frequency was analyzed given the

colorful, dynamic shift of oxidation state of iron ($2^+ \rightleftharpoons 3^+$) in each of the cases. A

decreasing linear trend (R: 0.9476) was obtained when frequency values were plotted

against the number of points (figure 26c). Hence, the rate at which the color fluctuations

occurred decreased as the number of points were increased. These results, altogether,

support that the number of points (or appendages) possess an effect on pattern formation

and rate of oscillations.

4.3.4. Effect of Star Size

Starfish can also vary in size, fluctuating from 2 mm to 352 mm in diameter. Therefore,

the assessment of size effect required the fabrication of 5-pointed stars with diameters

ranging from 10 mm (small) to 30 mm (large), changing by increments of 10 mm (figure

27a). The formation of diverse wave patterns and color changes was positively observed

for the small, medium and large stars. As depicted in figure 27b (top, middle) ¸ the

variations of size did not result in a substantial effect on induction time for the waves;

however, there was a significant correlation between reaction time and star size, with

larger stars presenting oscillations for longer periods of time. It can be theorized that the

increased volume in the star hydrogels resulted in a higher amount of iron, causing a prolonged, enhanced response for color changes within the system. Similarly, an increase in the size of the printed hydrogels required a larger volume of printing filament for the constructs (figure 27b, bottom). This increased volume permitted the waves to propagate on an increased surface area and to create a high number of linear,
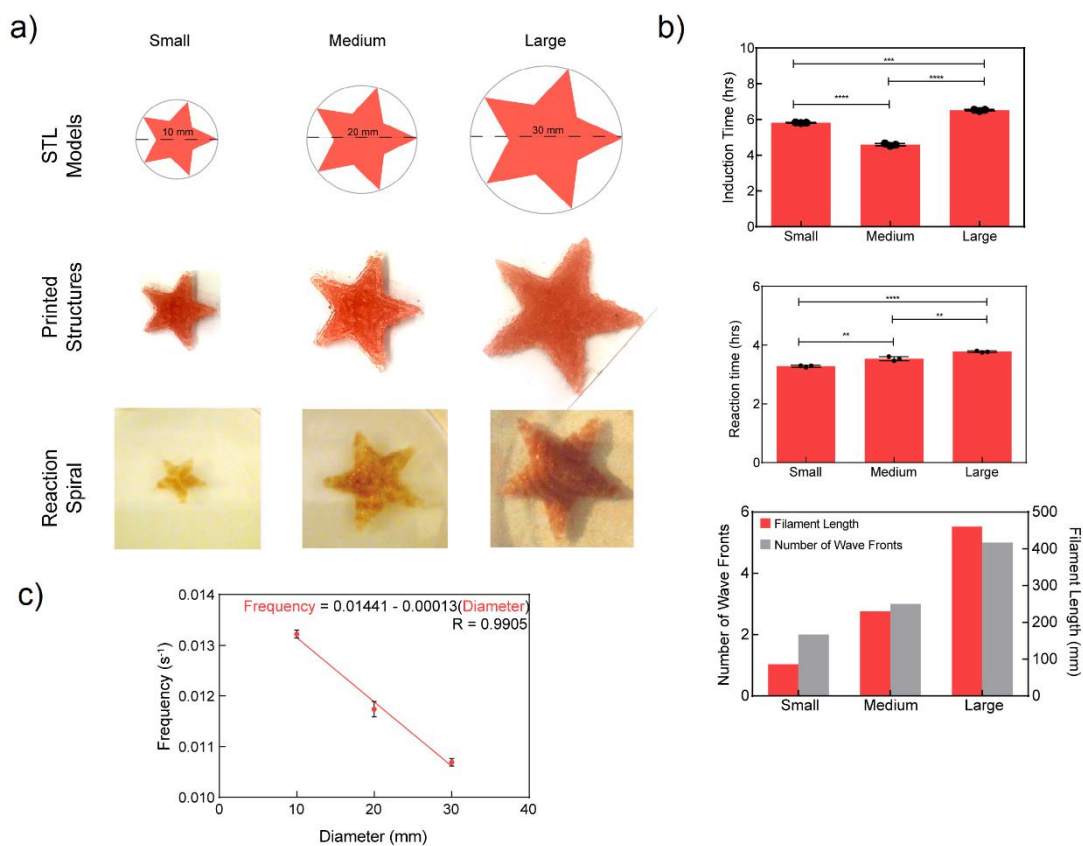
Figure 27. Effect of Star Size on Oscillations

wave fronts within the hydrogels. As an example, the small stars showed about 2 wave fronts whereas the large stars generated about 5 wave fronts, due to an increased area and volume. Furthermore, oscillatory frequency and star size were inversely correlated, with the small star presenting higher frequency than the medium and large stars (R:

0.9905, figure 27c). Taken together, an increase in the star size (or star volume) affected the oscillatory response of the system, which resulted in extended wave patterns and a decreased rate for color fluctuations.

4.3.5. Effect of Inner Angle of the Star

In addition to number of points and size, appendages on starfish have variable angles (degree of inner-angle) depending on the biological species. This morphological diversity allowed the creation of acute (18º), normal (36º), and obtuse (72º) starfish models (figure 28a).
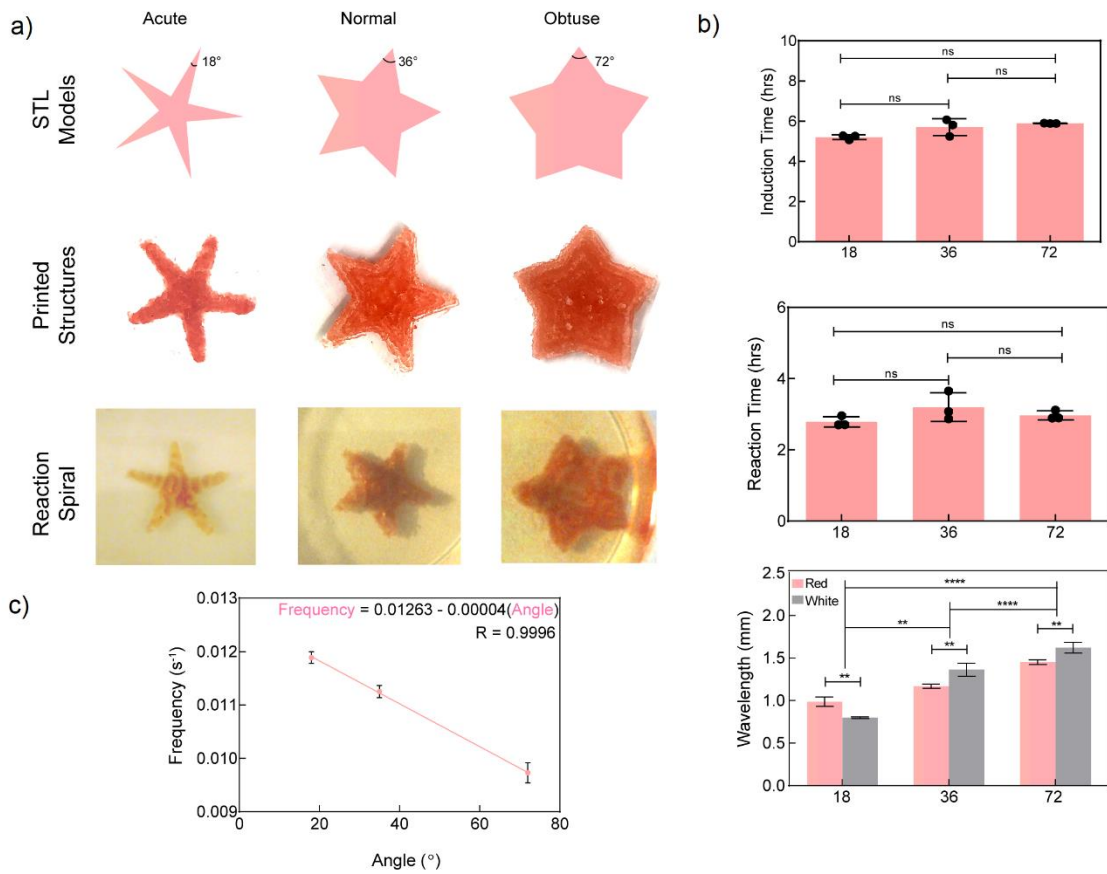
Figure 28. Effect of Inner Angle of the Star on Oscillations

The alteration of the appendage's angle did not cause a significant effect on the time occurrence of waves, which was evaluated with the observed induction and reaction times (figure 28b top, middle). Nonetheless, the width of the colored waves changed as the angle was increased. Explicitly, the wavelengths of the observed red wave (2^+ state of iron) and transparent wave (3^+ state of iron) increased as the angle on the appendage was increased (figure 28b, bottom). Moreover, normal and obtuse stars depicted red waves with larger dimensions than the transparent waves. Conversely, the acute stars illustrated an increased wavelength on the oxidized state (3^+), rather than the reduced state (2^+). For a final evaluation on the oscillatory frequencies, the acute, normal and obtuse stars were analyzed and they also revealed a decreasing linear trend as the inner angle increased (R: 0.9996, figure 28c). Altogether, these results demonstrated that the alterations on the angle of appendage had an effect on the reaction dynamics and patterns, mainly through changes in the wave dimensions and rate of color oscillations.

4.4 Conclusions

The employment of a 3D printing technique proved to be efficient for the creation of new self-oscillating polymers. In contrast to other scientific approaches, the use of this engineering technique allowed a facile production of varied constructs, with pre-programmed sizes and morphologies. Likewise, the dimensions of the polymers were controllable and in the centimeter scale, which permitted the macro visualization of wave patterns and color changes. Therefore, this type of printed macrostructures can be

applied as models that replicate oscillatory phenomena found in Nature, and specifically, in aquatic organisms.

The fabrication of the 3D printed models required the evaluation of suitable printing precursors (bioinks) and crosslinking methods. Previously, Gelatin was used as a polymer matrix to design self-oscillating hydrogels. However, Gelatin presented limited mechanical strength and recoverability under the high shear forces employed in extrusion-based printing. To overcome this challenge, kappa was incorporated to strengthen the Gelatin network and reinforced Gelatin + Kappa hydrogels were obtained. Post-fabricated hydrogels required a crosslinking method to maintain shape integrity and chemical stability under the BZ reaction conditions. Therefore, crosslinking density was a determinant factor in the microstructure of the hydrogels, that either promoted or inhibited oscillatory responses. The three crosslinking methods employed were ionic, covalent and ionic-covalent, with the ionic-covalent being the best option for a dynamic color change and stable wave patterns.

Upon determining precursors and crosslinking conditions, self-oscillating hydrogels with morphology variations were designed. Inspired by the biological diversity found in the starfish, different stars were fabricated to assess the oscillatory behavior given the geometrical settings. The variations in volume and shape features of the stars included number of points (or appendages), size and inner angle of the appendages. These parameters, altogether, considerably influenced the patterns, wave formation and duration of oscillations. Furthermore, the stars displayed a linear correlation on the rate of oscillations with each of the parameters used for the geometrical deviations.

62

Overall, the coupling of self-oscillating reactions with 3D printing methodology proved to be an appropriate approach for the fabrication of models that study and mimic spatio-temporal patterns. Due to the facile and short preparation times, it can also be used to explore oscillatory behavior under greater dimensions or other complex, biological architectures such as heart valves or neural networks. Such advances would benefit the development of novel biomimetic models and would expand the applications of engineered biological oscillators.

CHAPTER V

STUDY OF GELATIN-BASED HYDROGELS FOR AUTONOMOUS MOTION

5.1 Introduction

This chapter describes the study of the hydrogels that presented autonomous motion depending on the surrounding conditions and wave pattern originated within the material. The design and preparation of the hydrogels was based on the methodology described in chapter II, which utilized gelatin as the biopolymer matrix.

5.1.1. Background

Autonomous motion of diverse soft matter structures has been an attractive research field as it leads to the creation of self-propelled objects and soft robots. Some hydrogels with self-motion are designed based on thermal, electrical, magnetic, pressure driven and chemical responses[199-203], whereas some other self-propelled objects are able to convert chemical energy to mechanical energy by the action of surface tension, contact angle and chemical reactions[204].

Self-propelled materials that rely on the surface tension dynamics can be achieved by altering the force symmetry generated at the interface (air-liquid, liquid-liquid, and solid-liquid). This disruption can be produced via previously set gradients or by spontaneous symmetry breaking. For example, a silicon surface with pre-arranged polarity gradients can drive a water droplet from the hydrophobic region to the hydrophilic side[205]. In a similar manner, the gradient (or asymmetry) can be previously introduced to the system by designing asymmetrical objects that move in homogeneous fields[206]. Asymmetrical shapes of camphor particles, for instance, have presented lower surface tension on one

side than the other when placed in water; thus, creating a driving force for their motion[207]. Therefore, gradients in chemical concentration, light intensity and temperature can also be employed to drive motion in droplets[208-210]. On the other hand, spontaneously self-propelled objects appear when the force symmetry at the interface breaks due to surfactants and simple chemical reactions. To give an example, the molecular structure of the surfactant will alter the contact angle of an organic droplet and accelerate its speed as the carbon chain length is increased[211]. Similarly, surfactants can cause the motion of liquid droplets while they undergo simple chemical reactions: hydrolysis[212], acidic dissociation[213] or bromination[214]. Yet, the self-propelled objects described so far present linear, continuous motion that neglect to further change with time. Therefore, the design of self-propelled materials with oscillatory behavior would present fluctuating modes of motion.

Self-propelled objects presenting oscillatory, nonlinear behavior are conceivable through the coupling to complex reactions and nonlinear reactions[215]. Some examples of complex reactions that propel non-linear motion in micro-objects are: acid-base reaction of camphoric acid[216], complex formation of 1,10-phenathroline with iron[217], redox reaction between benzoquinone and ascorbic acid[218-219], and hydrogen peroxide with catalase enzymes[220]. Furthermore, the most representative reaction for non-linear motion is the Belousov-Zhabotinsky (BZ) reaction.

The coupling of the BZ reaction with polymeric matrices, as described in section 1.3, has served as the platform to design self-oscillating materials with rhythmic response and, in many cases, rhythmic motion[74, 90, 92-93, 95-96, 98-101, 125]. The chemical waves generated

65

during the course of the BZ reaction have been identified as the driving force for the propulsion of BZ-based soft materials. To mention some examples, the self-propelled materials reported so far have been employed as artificial cilia, conveyer for mass transport and actuators with peristaltic motion. However, these results mainly demonstrate motion in 1D, with free or fixed gels that generated planar waves in the micrometer and millimeter scales. To translate those results into 2D while presenting other type of wave patterns, we decided to explore the motion of gelatin-based hydrogels on the centimeter scale and with a free possible path. To analyze the motion feasibility and influence on oscillatory frequency of the hydrogels, different surrounding conditions were employed: illumination gradients, light intensity and type of surface at the bottom of the reaction vessel. In addition, the type of wave pattern, generated during the course of the oscillatory response, was considered for the studies due to its influence on the motion profiles of the hydrogels.

5.2 Experimental

5.2.1. Sample Preparation and Experimental Setup

The procedure reported in section 2.2 for the preparation of gelatin-based hydrogels was

employed for the hydrogels described in this chapter. The circle-shaped hydrogels were

prepared with a diameter of 1 cm and height of 0.25 cm. To maintain consistency on the

sample dimensions, the gelatin solution was casted in a Petri dish at a fixed volume and

once gelled the material was cut into four equal parts with the aid of a biopsy puncher

(appendix D). Once cut, the hydrogels were left to react in a solution with 1,4-

cyclohexanedione, nitric acid and sodium bromate at variable concentrations.

Correspondingly, the reaction vessel was placed on a leveled metal stand, and the

monitoring technique employed was the same as the one reported in section 2.3.

The lighting conditions were controlled via a portable microscope, digital camera

equipped with white light (Dino-Lite, model AD4113TL-M40, 640mW, 8 LED light

bulbs, and wavelength range of 500nm - 700nm with a peak intensity at 460nm). The

majority of the experiments were carried out with the digital camera, with the exception

of other experiments mediated by UV light (UVP Blak-Ray B-100 Series, 400 nm), blue

LED light (450-455nm, one bulb connected to a power source, 3V) and purple LED light

(395-400 nm, one bulb connected to a power source, 3V). The commercially available

desk lamp uses a 40 W light bulb at 120 V.

A MATLAB code (appendix D) was created for the tracking of the self-moving gelatin

samples; therefore, the code analyzed the center of the circle and tracked its trajectory

over time.

5.3 Results and Discussion

The oscillatory responses of self-actuators based on the BZ reaction have been controlled via diverse stimuli: temperature[221], force[222], organic substrate[223], light[224-225] and pH[226]. Motivated by computational modeling of gels demonstrating autonomous rotational and translational motion when a force is applied, we decided to use the light as one type of stimuli to control the behavior of the hydrogels. We aimed to observe motion of the gelatin-based samples in a free, 2D possible path.

First, the conditions for self-moving hydrogels were achieved. Circle-shaped hydrogel presented the highest frequency from the assessment described in chapter II. For the sample preparation, it was determined that the samples required to be individually crosslinked at room temperature, the thickness could not be higher than 0.3 cm, and an increase in the type of organic acid (CHD) had a concentration limit of 0.150M. For the experimental setup, the light source required to be placed on the rim of the petri dish and a loosened lid placed on the dish generated a pseudo-closed system. The circle-shaped hydrogel demonstrated motion and a maximum frequency of $(12 \pm 0.6) \times 10^{-3}$ s^{-1}. From these results, the concentration of the BZ reaction substrates as well as the hydrogel dimensions and experimental setup were established. The external stimuli were, then, tested given variable conditions.

5.3.1. Light Sources

Some experiments were carried out under different types of light. First, a UV light (400 nm) was employed but the results were not favorable as the temperature of the reaction vessel increased and the UV energy can produce radicals in the system. An additional

variation in the wavelength was done through the use of blue (450-455 nmm) and purple (395-400nm) light bulbs. The blue light had some indication of higher frequency than the frequency of the gel under white light; however, the type of light was not at the same intensity as the one used for all of the other experiments, and the motion of the gel was not achieved. From these results, it was concluded that the experimental setup required conditions with equal light intensities and equal camera position regardless of the light source.

5.3.2. Masks

Previous modeling of motion directionality under light gradients[227] suggested the study of hydrogels while subjected to different lighting patterns. The lighting patterns were created with the masks shown in Figure 29. The hydrogels did not present any significant motion. In addition, some difficulties were encountered for frequency calculations due to hidden bodies and blurry conditions, which were inappropriate for visualization and quantification of color changes.
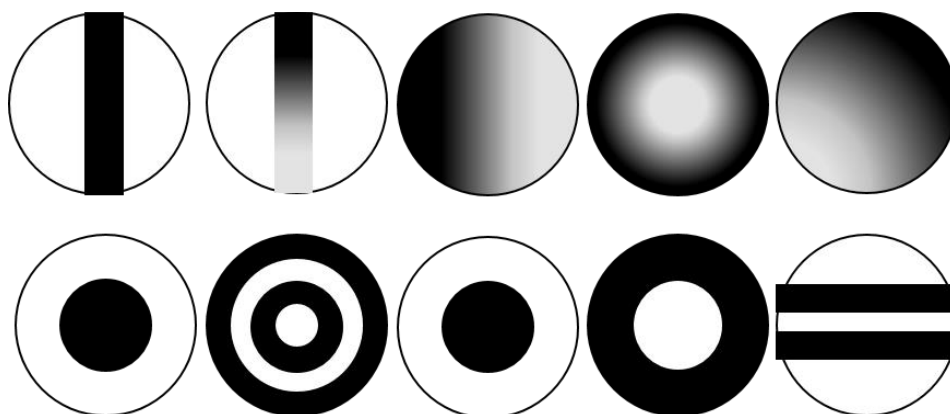
Figure 29. Masks for Lighting Pattern on Self-Moving Gelatin

5.3.3. Substrate

Given previous reports that discuss an enhancement of motion through changes in the surface roughness[99], different coatings or type of surfaces were tested: sandpaper (grit size 80, 150, 220, 240, 320, 400 and 600), fabrics (82 and 120 mesh size), metallic mesh, and a hydrophobic coating with silanes. The silane-coated reaction vessel was the only surface under which the hydrogel presented a slight motion; however, the displacement and speed were negligible compared to the non-coated, previous ones. It was possible that the hydrophilicity of the gelatin matrix increased the interactions with the surfaces and restricted the motion. It can be proposed that an ideal surface would be composed of hydrophobic coating but with certain roughness to allow traction.

5.3.4. Light Distance

The digital camera (white LED included) was clamped to a metal stand and the position of the camera was varied for three distances: short, medium and long. The camera was placed respectively at 9", 14" and 19" from the petri dish containing the gel and substrate solution.

The hydrogel under light situated at a long distance (figure 30) moved and the MATLAB analysis served to obtain the coordinates for the position of the centroid in x and y coordinates (figure 30a and b, respectively). The gel moved away from the light and in the y direction only. Given the y position data, it was estimated that the average speed was 5.0×10^{-4} cm/s (figure 30c).
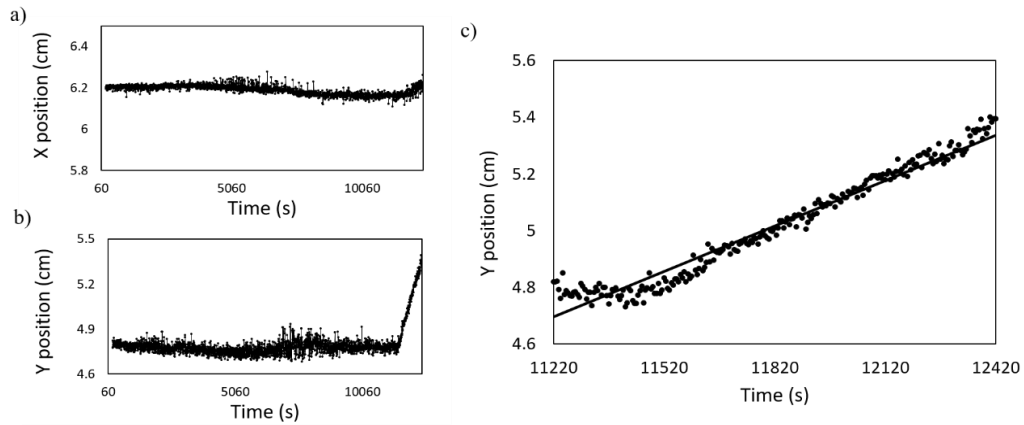
a) Position of hydrogel in x axis, b) position of hydrogel in y axis and c) speed analysis using the y position

Figure 30. Trajectory Analysis for Light Effect at Long Distance

The hydrogel under light placed at a medium distance moved in x and y coordinates (figure 31a and b, respectively), and the traveling direction was towards and away from the light. From the x and y position data (figure 31c and d), it was estimated that the average speeds were 7.0×10^{-5} cm/s and 8.0×10^{-5} cm/s respectively, which combined generated a net speed of 7.5×10^{-5} cm/s.
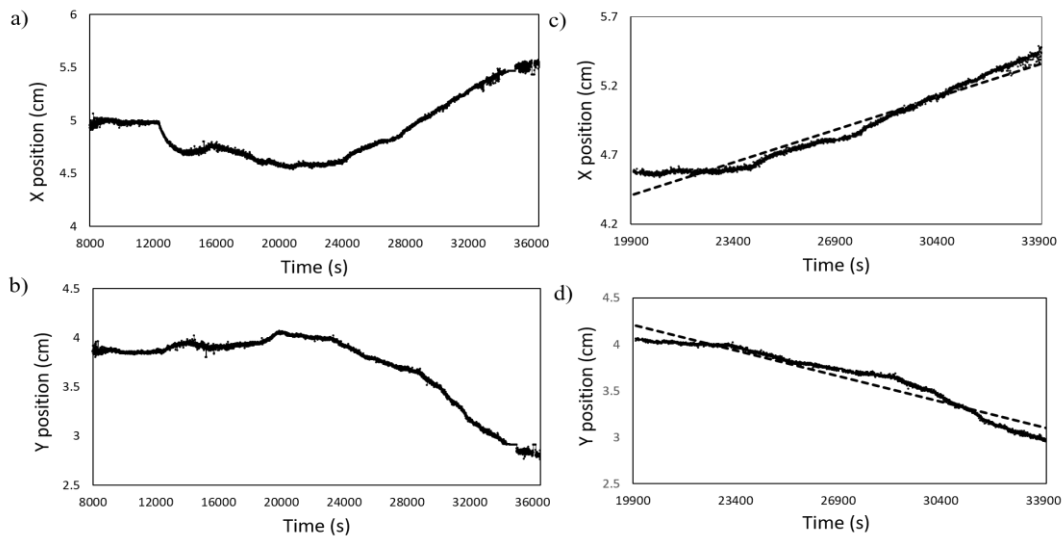
a) Position of hydrogel in x axis and the respective speed analysis in graph c), and b) position of hydrogel in y axis and the respective speed analysis in graph d).

Figure 31. Trajectory Analysis for Light Effect at Medium Distance

71

Lastly, the hydrogel under light placed at a short distance moved away from the light, generating values in x and y coordinates (figure 32a and b, respectively). The slopes for the varying position data in x and y (figure 32c and d) provided an estimated speed of 4.0×10^{-4} cm/s and 3.0×10^{-6} cm/s respectively, which produced a net speed of 4.0×10^{-4} cm/s.
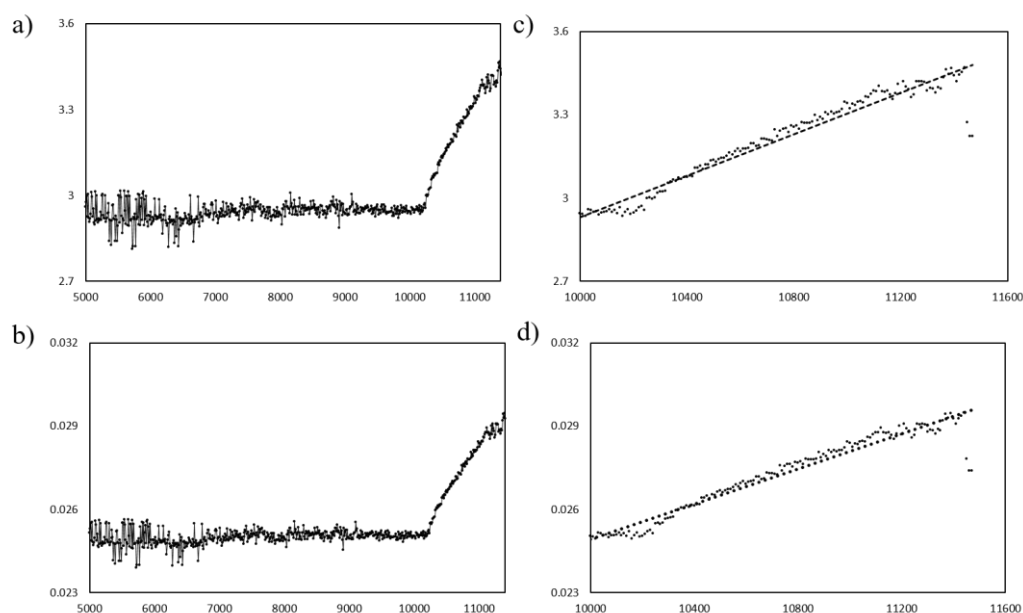
a) Position of hydrogel in x axis and the respective speed analysis in graph c), and b) position of hydrogel in y axis and the respective speed analysis in graph d).

Figure 32. Trajectory Analysis for Light Effect at Short Distance

Interestingly, the type of waves that generated within these hydrogels were variable. For the hydrogel with the slowest speed (medium light distance), two front waves were generated and traveled against each other, which can be hypothesized as a competition of driving forces. In contrast, the other two hydrogels showed wave fronts propagating in one direction for some periods of time. In addition to such effect from the wave pattern, it has also been reported that light is able to photoinhibit the BZ reaction by formation of

72

radicals that generate a photoexcited state of the catalyst[228]. Simultaneously, photoinduction occurs by the production of $HBrO_2$ which is an activator species in the mechanism[229].

Diverse research has proved the effect of light on self-oscillating gels based on ruthenium catalysts, indicating the ability of hydrogels to travel away from the light, with photophobic behavior [225, 230-232]. Specifically, the illumination with blue light produces Br^- ions that inhibit BZ reaction[233]; therefore, it can be exploited to control the wave propagation and to direct motion.

5.3.5. Spiral-Mediated Locomotion

In efforts to set a successful light gradient, the type of lighting was changed and the gelatin hydrogel was tested under household lighting (desk lamp) in a less illuminated area of the room, therefore the light gradient was smaller than the previous ones. The disk-shaped gelatin was immersed in 40 mL of a solution with 0.090 M HNO_3, 0.125M CHD, 0.100 M $NaBrO_3$. As a result, the gelatin sample successfully reacted and generated a unique spiral wave within its structure. Moreover, the gelatin sample presented superior autonomous locomotion, which was governed by the dynamics of the spiral formation. In figure 33, an analysis for the trajectory of the spiral tip is presented. The x and y coordinates of the spiral tip during the locomotive period were obtained from beginning (green point) to start (red point). The motion of the gel occurred in a diagonal line, traveling from the center of the reaction vessel (petri dish) to the rim. The gel presented retrograde wave locomotion[234] as the spiral wave became asymmetric in

relation to the center of the gel. Once the gel reached the rim, the spiral wave ceased and target waves originated.
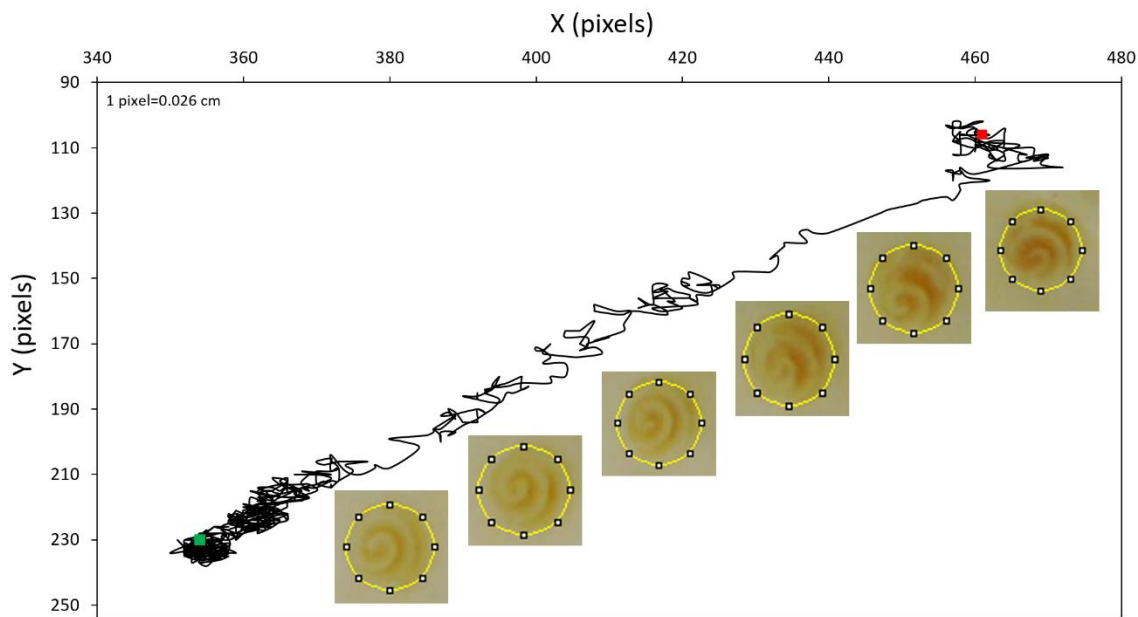
Figure 33. Position of Spiral Tip in (x, y) Coordinates

The oscillatory frequencies for the two types of wave patterns differed; the spiral wave changed colors at a higher pace (frequency: $(1.24 \pm 0.01) \times 10^{-2} \text{ s}^{-1}$) than the target waves (frequency: $(1.06 \pm 0.02) \times 10^{-2} \text{ s}^{-1}$). The corresponding graphs for the obtained frequencies are depicted in figure 34. This observation agrees with a previous publication reporting that for solution-based BZ reactions, the wave with the highest frequency will prevail over the other. In this case, the spiral wave dominated over target waves[235]. This publication also discussed the pattern selection in BZ reaction systems, for which the occurrence of spiral waves is typically diminished by the presence of target waves.
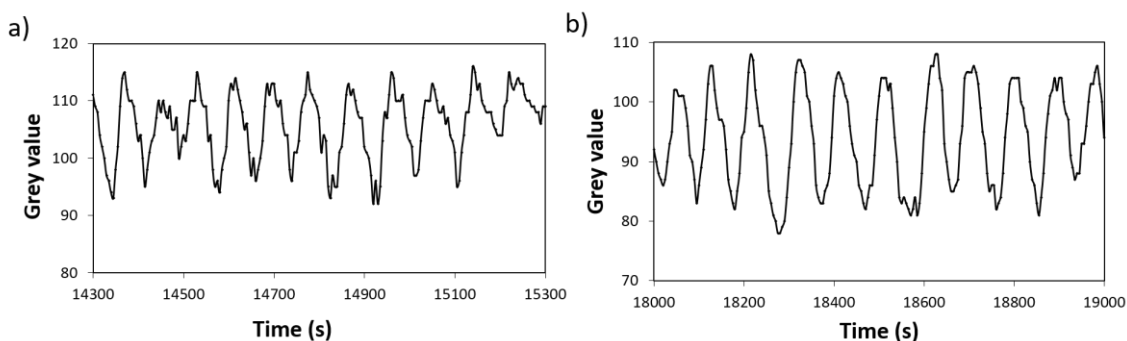
Figure 34. Frequencies for Spiral (a) and Target (b) Waves in Spiral-driven Gelatin

Subsequently, the geometrical features of the spiral wave formation were analyzed; specifically, the wavelength (λ). According to Kheowan et. al.[236], the wavelength in a spiral wave can be calculated as the average length of the normal vector connecting two consecutive waves; therefore, such distance was obtained in the direction of the traveling wave (black arrow, figure 35a). The measured wavelength corresponds to the width of the white (light blue) wave as indicated by the grey line in figure 35a.
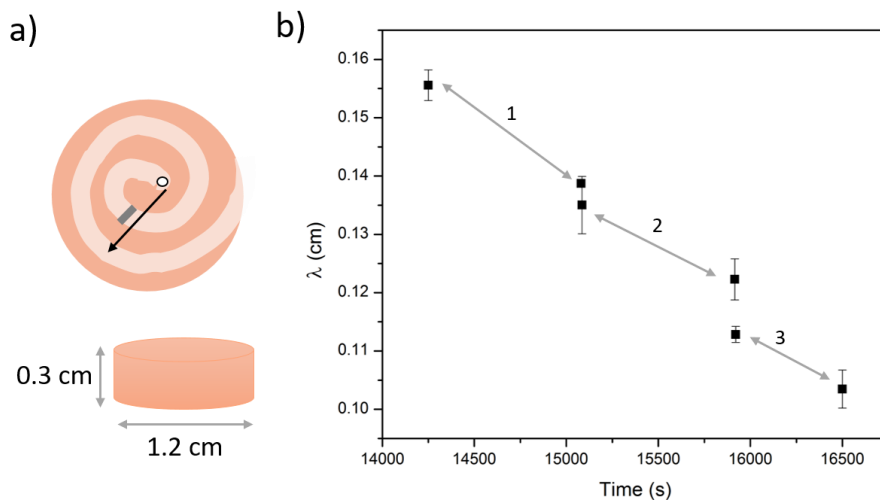
a) Top and side view of gelatin sample. Top view shows the spiral wave. The arrow indicates the direction of the traveling wave and the grey line marks the distance set as the wavelength.
b) Graph for the wavelength changes over the course of the reaction

Figure 35. Wavelength Analysis for Spiral Wave

75

The motion period for the gel was divided in three segments (labeled as 1, 2, and 3 in figure 35b) and the corresponding wavelength values were plotted versus time. It was found that as the reaction progressed, the wavelength produced by Fe^{3+} decreased. The wave vector ($\vec{K}$) relates to the wavelength (λ) with the formula below:

$$\vec{K} = \frac{2\pi}{\lambda}$$

Thus, the inverse relationship between the wave vector and wavelength was demonstrated with an increase in the wave vector as the reaction progressed (figure 36a). Furthermore, a proportional relationship was found between the speed of the gel and wave vector. This relationship was found by analyzing the speed of the gel motion at the three regions and plotting those values versus their corresponding wave vectors (figure 36b).
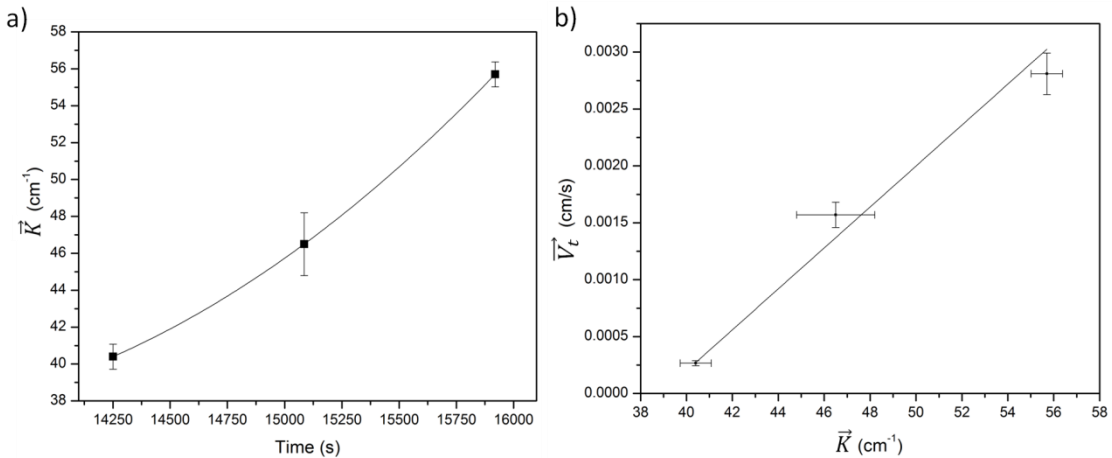
a) Graph for changes on wave vector in the spiral wave over the course of the reaction
b) Graph for correlation between speed of motion and wave vector

Figure 36. Speed Dependence on Wave Vector

This relationship agrees with the computation model on spiral-mediated locomotion developed by Epstein et. al.[237], which expresses that the wave vector ($\vec{K}$) and speed of

the gel ($\vec{V_t}$) are directly proportional to each other given the formula below, where D is a dynamic parameter, independent of position, that characterizes the driving effect of the chemical wave.

$$-D\vec{K} = \vec{V_t}$$

Overall, it can be determined that this system was light sensitive under such light gradient, creating a gel that can freely move in a plane at a remarkable speed. The speed was proportional to the wave vector; therefore, the asymmetry generated by the spiral wave was a key factor to generate motion. The motion of the gel was mainly driven by the type of wave generated within the structure, and the prevalence of one type of wave (spiral) over the other wave (target) was determined by the oscillatory frequencies. Furthermore, the presence of a light gradient affected the direction of the gel and, in this case, instigated a gel moving with retrograde waves (motion away from the light).

5.4 Conclusions

The results presented in this last chapter exemplify an advance for self-locomotive materials mediated by light. Compared to previous reports based on fixed, micro-scaled actuators, these hydrogels were constructed in the centimeter scale and they were allowed to react in a free path. Similarly, past reports mainly demonstrated hydrogels with linear waves traveling in one direction (1D). By increasing the dimensions of the sample, the type of wave patterns generated in the current hydrogels were expanded to spiral or target (2D) waves; as a result, the wave dynamics were altered. The incidence of light on the hydrogels proved to influence the wave pattern and, in consequence, the

motion property; however, there was no correlation between light distance and motion speed. These results could indicate that the competition between wave diffusion and formation of the 2D waves caused different speeds in the self-moving hydrogels. Although the wave pattern turned complex, the use of a photometer to precisely control and quantify the light gradient could enhance future studies of locomotive hydrogels subjected to changes in light intensity or light gradients.

A decrease in the light gradient allowed us to achieve the first spiral-mediated locomotion in soft gels driven by the BZ reaction. Previously, computational modeling analyzed the motion of self-oscillating gel in 1D under light gradients[234]; instead, we studied such phenomenon in a three-dimensional system. This freely-moving actuator achieved motion at a high speed. The spiral wave proved to be essential for motion in large oscillating polymers. Further strategies to direct the 2D motion of hydrogels could include structural anisotropy and the inclusion of light-responsive components within the hydrogel such as spiropyran[238], azobenzene[239] or chromophores[240]. The investigation of biomimetic locomotive materials can aid to understand active organisms, especially those that migrate due to changing light conditions[234].

CHAPTER VI

CONCLUSIONS

The incorporation of the iron-mediated Belousov-Zhabotinsky reaction into polymeric matrices for the creation of new self-oscillating materials has been investigated in the present dissertation. Variations in the microstructure and type of polymeric matrix, concentration of reactants, hydrogel dimensions and geometrical features, and external stimuli allowed us to explore and better understand the dynamics of the BZ reaction given different settings. Chemically, all the wave patterns and motion described herein were driven by the redox oscillations between the reduced and oxidized form of iron, $Fe^{2+} \leftrightarrow Fe^{3+}$, respectively. Through the findings, these polymeric materials served as models to replicate the oscillatory phenomena under biomimetic conditions.

In Chapter II, the creation of self-oscillating polymers with the incorporation of iron complexes into a gelatin matrix was achieved. The reaction conditions were first explored for an adequate oscillatory response given the change of catalyst from the widely used ruthenium complexes to iron complexes. The iron complex was designed based on a structure similar to ferroin (catalyst for solution-based BZ reactions), and upon synthesis, the iron complex was incorporated into the biopolymer gelatin. The change of catalyst mainly required a change in the concentration of reaction substrates in order to obtain visible, long-lasting oscillations that generated clear wave patterns within the gelatin-based hydrogels. For that purpose, a new organic substrate (1,4-cyclohexanedione) was employed to replace the one that most of the literature reports employ (malonic acid). Exploring the tuning of the BZ reaction through different

79

concentrations substrates not only allowed new patterns in 2D materials such as spiral and target waves, it also produced oscillations at different frequencies. Given these varying frequencies, the options for natural oscillators to model with self-oscillating hydrogels can be widened in the future. In addition, the monitoring technique for the analysis of the reacting hydrogels was developed and it allowed for the proper visualization and image processing. This technique was utilized for any of the experiments carried out in the following chapters.

For Chapter III, we studied the effect of phase changing, liquid crystalline materials on the dynamics of oscillations and type of generated wave patterns within PNIPAM-based hydrogels. Discotic particles composed of zirconium phosphate (ZrP) were synthesized and incorporated into the hydrogels. Through an increase in the concentration of ZrP nanoparticles, a reorganization in the microstructure occurred and the ZrP nanoparticles assembled from isotropic to nematic phases. As a result, the phase change altered the formation of wave patterns and, in a similar way, the oscillatory frequencies varied. Specifically, low concentrations of nanoparticles generated disordered wave patterns at low oscillatory frequencies; in contrast, high concentration of nanoparticles produced ordered, long-lasting spiral and target waves with high oscillatory frequencies. With these results, the exploration of oscillatory phenomena under the effect of micro self-organized matter was possible. The ZrP nanoparticles served as biomimetic active media that allowed us to study the BZ reaction considering the dynamic profile of nature structures, such as biological, nematic tissue that reorganizes and behaves as liquid crystals. These findings also provided insight on how to possibly disrupt the spiral

formation by introducing disorganized muscle or other isotropic cells, which are key

contributions for models that study tachycardia and irregular heart muscle beating.

Chapter IV described the use of 3D printing as a new engineering tool for the design and

fabrication of self-oscillating hydrogels. First, the type of polymer matrix, gelatin and k-

carrageenan, required to be determined based on mechanical properties that were

adequate for the extrusion process during printing. Similarly, the crosslinking conditions

played an essential role in the matrix microstructure and diffusion of the reactants that

either inhibited or facilitated the propagation of chemical waves. Due to the precise

settings in the manufacturing technique, the hydrogels shape and geometrical features

were easily varied, which allowed us to systematically assess the effect of shape and size

on the dynamics of the BZ reaction. Precisely, the number of points, construct size, and

appendage angle in star-shaped hydrogels correlated to changes in the oscillatory

responses and dynamic spiral and target wave patterns. The dynamic skin patterns and

camouflage behavior found in aquatic organisms (cephalopods) inspired us to fabricate

star-shaped hydrogels; however, the type of architectures constructed with the 3D

printing technique are not restricted to this shape and could be, in fact, expanded to

complex structures found in other biological oscillators.

Lastly, chapter V presented the creation of locomotive hydrogels driven by the chemical

energy generated during the BZ reaction and under the effect of external stimuli. It is

relevant to note that the polymers developed in chapter III and IV did not present

locomotive properties. This limitation arose from the type of polymer matrix that

generated a robust material with steady spiral and target waves, thus compromising the

flexibility of the hydrogels. In contrast, hydrogels with a polymer matrix constituted only from gelatin had the possibility to present motion. A future improvement in these advances would be to obtain a matrix composition suitable for 3D printing that permits spiral patterns without comprising the elasticity of the material. For the gelatin-based hydrogels in the last chapter, the external conditions (light intensity, illumination gradients and type of surface at the bottom of the reaction vessel) were varied to achieve motion in a free possible path. By modifying the lighting conditions, we confirmed that the BZ reaction is a photosensitive system; however, the type of wave pattern demonstrated to be a crucial parameter to propel the hydrogel, and in our case, the single spiral wave directed the motion of the disk-shaped hydrogel. These results enhance the creation of novel soft robots with photophobic and phototropic responses.

Concluding remarks & future research directions

Overall, the use of catalysts based on iron for the creation of gels that model oscillatory behavior was possible. Not only did the iron complexes represent a new, viable alternative to ruthenium-based catalysts, they also enhanced the biomimetic conditions of the BZ reaction systems through the employment of biologically available polymer matrices, such as gelatin and k-carrageenan. In addition, the contrast of wave formation was enhanced with color oscillations between red and light blue, in distinction to dark yellow and light yellow presented for the ruthenium. The obtained results showed rich wave patterns and adequate oscillatory response at centimeter-sized hydrogels, which contrasts reports on smaller dimensions[241]. Moreover, the frequency of oscillations was

able to be tuned via concentration of reactants, ordering of the microstructure and geometry of the hydrogels.

In the future, these iron-based hydrogels can be enhanced through changes in the chemical structure of the polymer[242]. For example, the oxidizing agent and the inorganic acid are two water-soluble substrates required for the hydrogels to oscillate when immersed in the BZ solution; thus, the incorporation of these chemical moieties into the backbone of the polymer would create a material with activating sites capable of tuning the reaction. By achieving this multifunctionality, the hydrogels could fully be self-actuators that only need to be immersed in water. The hydrogels that we studied contained a homogeneous matrix structure; however, layered hydrogels could be created and arranged in architecture with each layer containing one of the components from the BZ reaction system.

To the best of our knowledge, 2D patterns in chemomechanical hydrogels are not so widely reported and difficult to achieve. Therefore, the waves obtained herein could be expanded to hydrogels with higher dimensions in the z direction that could even open the possibility for locomotive materials in 3D. Furthermore, the introduction of chemical structures with reversible response under light, such as spiropyran[238], can be incorporated in BZ hydrogels and serve as an alternative for a controlled response of the motion and oscillations. The development of hydrogels with light-induced motion represents new directions for phototropic and photophobic capabilities in soft robots. By achieving a higher control on the motion of hydrogels, novel drug delivery devices with oscillating release can be designed as well[243].

The ordering and phase transition of the surrounding structures added directionality to the BZ system, as described in Chapter III; therefore, utilizing layered materials to incorporate anisotropy could boost the creation of hydrogels with directed motion or peristaltic crawling[244-245]. Oscillating, anisotropic hydrogels can then be designed through the incorporation of concentration gradients or by structural variations that result in frequency gradients as presented in Chapters III and IV, respectively.

Furthermore, the creation of new, complex structures for self-oscillating hydrogels with the employment of 3D printing will be essential. This processing technique requires short times and facile preparation and could bring versatility and novel applications to the BZ reaction system. For instance, artificial muscles or heart valves could replicate spiral-mediated arrhythmias, a 3D-printed network of coupled oscillators could serve as a model for synchronized pulses between dendrites in the neurons, or a 3D printed tissue could mimic the environment in which the BZ reaction system is studied.

Finally, other potential applications of the BZ reaction systems include analytical tools such as: chemical computers that classify cancer cells as malignant or benign[198, 246], sensors that quantify organic compounds such as ethanol, vitamin C, drugs and proteins[247-248], and as intelligent devices that navigate complex labyrinths[249].

REFERENCES

1.   Tyson, J. J. In *What Everyone Should Know About the Belousov-Zhabotinsky Reaction*, Frontiers in Mathematical Biology, Berlin, Heidelberg, 1994//; Levin, S. A., Ed. Springer Berlin Heidelberg: Berlin, Heidelberg, 1994; pp 569-587.

2.   De Kepper, P.; Epstein, I. R., Mechanistic study of oscillations and bistability in the Briggs-Rauscher reaction. *Journal of the American Chemical Society* **1982,** *104* (1), 49-55.

3.   Alyea, H. N., The Old Nassau reaction. *Journal of Chemical Education* **1977,** *54* (3), 167.

4.   Epstein, I. R.; Showalter, K., Nonlinear Chemical Dynamics: Oscillations, Patterns, and Chaos. *The Journal of Physical Chemistry* **1996,** *100* (31), 13132-13147.

5.   Vanag, V. K., Waves and patterns in reaction–diffusion systems. Belousov–Zhabotinsky reaction in water-in-oil microemulsions. *Physics-Uspekhi* **2004,** *47* (9), 923-941.

6.   Grzybowski, B. A.; Bishop, K. J. M.; Campbell, C. J.; Fialkowski, M.; Smoukov, S. K., Micro- and nanotechnology via reaction–diffusion. *Soft Matter* **2005,** *1* (2), 114-128.

7.   Merkin, J. H.; Poole, A. J.; Scott, S. K.; Smith, J. D. B.; Thompson, B. W., Analysis of the bromate-ferroin clock reaction. *Journal of Mathematical Chemistry* **1996,** *19* (1), 15-32.

8.   Mikhailov, A. S.; Ertl, G., *Engineering of chemical complexity. II. editors, Alexander S Mikhailov, Gerhard Ertl*. World Scientific: 2015.

9.   Buskohl, P. R.; Vaia, R. A., Belousov-Zhabotinsky autonomic hydrogel composites: Regulating waves via asymmetry. *Sci Adv* **2016,** *2* (9), e1600813-e1600813.

10.   Huang, X.; Troy, W.; Yang, Q.; Ma, H.; Laing, C.; Schiff, S.; Wu, J.-y., Spiral Waves in Disinhibited Mammalian Neocortex. *The Journal of neuroscience : the official journal of the Society for Neuroscience* **2004,** *24*, 9897-902.

11.   Qian, Y.; Zhang, Z., The Fundamental Structure and the Reproduction of Spiral Wave in a Two-Dimensional Excitable Lattice. *PLOS ONE* **2016,** *11* (2), e0149842.

12.   Epstein, I., Predicting complex biology with simple chemistry. *Proceedings of the National Academy of Sciences of the United States of America* **2006,** *103*, 15727-8.

13.   Wang, G.; Wang, Q.; He, P.; Pullela, S.; Marquez, M.; Cheng, Z., Target-wave to spiral-wave pattern transition in a discrete Belousov-Zhabotinsky reaction driven by inactive resin beads. *Physical Review E* **2010,** *82* (4), 045201.

14.   Gyorgyi, L.; Turanyi, T.; Field, R. J., Mechanistic details of the oscillatory Belousov-Zhabotinskii reaction. *The Journal of Physical Chemistry* **1990,** *94* (18), 7162-7170.

15.   Field, R. J.; Koros, E.; Noyes, R. M., Oscillations in chemical systems. II. Thorough analysis of temporal oscillation in the bromate-cerium-malonic acid system. *Journal of the American Chemical Society* **1972,** *94* (25), 8649-8664.

16.   Scott, S. K., *Oscillations, waves, and chaos in chemical kinetics*. Oxford University Press Oxford: 1994.

17.   Zaikin, A. N.; Zhabotinsky, A. M., Concentration Wave Propagation in Two-dimensional Liquid-phase Self-oscillating System. *Nature* **1970,** *225* (5232), 535-537.

18.   Zhabotinsky, A. M.; Buchholtz, F.; Kiyatkin, A. B.; Epstein, I. R., Oscillations and waves in metal-ion-catalyzed bromate oscillating reactions in highly oxidized states. *The Journal of Physical Chemistry* **1993,** *97* (29), 7578-7584.

19.   Biosa, G.; Masia, M.; Marchettini, N.; Rustici, M., A ternary nonequilibrium phase diagram for a closed unstirred Belousov–Zhabotinsky system. *Chemical Physics* **2005,** *308* (1), 7-12.

20.   AM TURING, F., The chemical basis of morphogenesis. *Sciences-cecm. usp. br* **1952**.

21.   Tompkins, N.; Li, N.; Girabawe, C.; Heymann, M.; Ermentrout, G. B.; Epstein, I. R.; Fraden, S., Testing Turing's theory of morphogenesis in chemical cells. *Proceedings of the National Academy of Sciences* **2014,** *111* (12), 4397.

22.   Berding, C.; Harbich, T.; Haken, H., A pre-pattern formation mechanism for the spiral-type patterns of the sunflower head. *Journal of Theoretical Biology* **1983,** *104* (1), 53-70.

23.   Ball, P., Forging patterns and making waves from biology to geology: a commentary on Turing (1952) 'The chemical basis of morphogenesis'. *Philos Trans R Soc Lond B Biol Sci* **2015,** *370* (1666), 20140218.

24.   Bard, J. B. L., A model for generating aspects of zebra and other mammalian coat patterns. *Journal of Theoretical Biology* **1981,** *93* (2), 363-385.

25.   Guiu-Souto, J.; Carballido-Landeira, J.; Muñuzuri, A. P., Characterizing topological transitions in a Turing-pattern-forming reaction-diffusion system. *Physical Review E* **2012,** *85* (5), 056205.

26.   Meinhardt, H., Biological Pattern Formation as a Complex Dynamic Phenomenon. *International Journal of Bifurcation and Chaos* **1997,** *07* (01), 1-26.

27.   Glazier, D. B.; Murphy, D. P.; Cummings, K. B.; Morrow, F. A., Liesegang Rings. *Journal of Urology* **1997,** *157* (3), 940-941.

28.   Perrotta, P. L. M. D.; Ginsburg, F. W. M. D.; Siderides, C. I.; Parkash, V. M. D., Liesegang Rings and Endometriosis. *International Journal of Gynecological Pathology* **1998,** *17* (4), 358-362.

29.   Ng, K. H.; Siar, C. H., A clinicopathological and immunohistochemical study of the calcifying epithelial odontogenic tumour (Pindborg tumour) in Malaysians. *The Journal of Laryngology & Otology* **1996,** *110* (8), 757-762.

30.   Jiang, T.-X.; Widelitz, R. B.; Shen, W.-M.; Will, P.; Wu, D.-Y.; Lin, C.-M.; Jung, H.-S.; Chuong, C.-M., Integument pattern formation involves genetic and epigenetic controls: feather arrays simulated by digital hormone models. *The International journal of developmental biology* **2004,** *48*, 117.

31.   Garzón-Alvarado, D. A.; Ramírez Martinez, A. M., A biochemical hypothesis on the formation of fingerprints using a turing patterns approach. *Theoretical Biology and Medical Modelling* **2011,** *8* (1), 24.

32.   Kondo, S.; Asai, R., A reaction–diffusion wave on the skin of the marine angelfish Pomacanthus. *Nature* **1995,** *376* (6543), 765-768.

33.   Kondo, S.; Miura, T., Reaction-Diffusion Model as a Framework for Understanding Biological Pattern Formation. *Science* **2010,** *329* (5999), 1616.

34.   Salmon, P., Non-Linear Pattern Formation in Bone Growth and Architecture. *Frontiers in Endocrinology* **2015,** *5* (239).

35.   Cartwright, J. H. E., Labyrinthine Turing Pattern Formation in the Cerebral Cortex. *Journal of Theoretical Biology* **2002,** *217* (1), 97-103.

36.   Epstein, I. R.; Pojman, J. A., *An Introduction to Nonlinear Chemical Dynamics : Oscillations, Waves, Patterns, and Chaos*. 1998.

37.   Rovinskii, A. B., Turing bifurcation and stationary patterns in the ferroin-catalyzed Belousov-Zhabotinskii reaction. *The Journal of Physical Chemistry* **1987,** *91* (17), 4606-4613.

38.   Tam, W. Y.; Horsthemke, W.; Noszticzius, Z.; Swinney, H. L., Sustained spiral waves in a continuously fed unstirred chemical reactor. *The Journal of Chemical Physics* **1988,** *88* (5), 3395-3396.

39.   How, M. J.; Norman, M. D.; Finn, J.; Chung, W.-S.; Marshall, N. J., Dynamic Skin Patterns in Cephalopods. *Frontiers in Physiology* **2017,** *8* (393).

40.   Hanlon, R., Cephalopod dynamic camouflage. *Current Biology* **2007,** *17* (11), R400-R404.

41.   Siegert, F.; Weijer, C. J., Spiral and concentric waves organize multicellular Dictyostelium mounds. *Current Biology* **1995,** *5* (8), 937-943.

42.   Shanks, N. J. F. o. C., Modeling biological systems: the Belousov–Zhabotinsky reaction. **2001,** *3* (1), 33-53.

43.   Lechleiter, J.; Girard, S.; Peralta, E.; Clapham, D., Spiral calcium wave propagation and annihilation in Xenopus laevis oocytes. *Science* **1991,** *252* (5002), 123.

44.   Davidenko, J. M.; Pertsov, A. V.; Salomonsz, R.; Baxter, W.; Jalife, J., Stationary and drifting spiral waves of excitation in isolated cardiac muscle. *Nature* **1992,** *355* (6358), 349-351.

45.   Tse, G., Mechanisms of cardiac arrhythmias. *J Arrhythm* **2016,** *32* (2), 75-81.

46.   Weise, L. D.; Panfilov, A. V., New Mechanism of Spiral Wave Initiation in a Reaction-Diffusion-Mechanics System. *PLOS ONE* **2011,** *6* (11), e27264.

47.   Gorelova, N. A.; Bures, J., Spiral waves of spreading depression in the isolated chicken retina. *Journal of neurobiology* **1983,** *14* (5), 353-63.

48.   Mendez, V.; Méndez, V.; Llebot, J., Hyperbolic reaction-diffusion equations for a forest fire model. *Physical Review E: Statistical Physics, Plasmas, Fluids, and Related Interdisciplinary Topics* **1997,** *56* (6), 6557-6563.

49.   Smolin, L., Galactic disks as reaction-diffusion systems. *arXiv preprint astro-ph/9612033* **1996**.

50.   Nozakura, T.; Ikeuchi, S., Formation of dissipative structures in galaxies. *The Astrophysical Journal* **1984,** *279*, 40-52.

51.   Schulman, L. S.; Seiden, P. E., Percolation and Galaxies. *Science* **1986,** *233* (4762), 425.

52.   Dzeja, P. P.; Terzic, A., Phosphotransfer networks and cellular energetics. *Journal of Experimental Biology* **2003,** *206* (12), 2039.

53.   Bagyan, S.; Mair, T.; Dulos, E.; Boissonade, J.; De Kepper, P.; Müller, S. C., Glycolytic oscillations and waves in an open spatial reactor: Impact of feedback regulation of phosphofructokinase. *Biophysical Chemistry* **2005,** *116* (1), 67-76.

54.   Sune, D.; Preben Graae, S.; Finn, H., Sustained oscillations in living cells. *Nature* **1999,** (6759), 320.

55.   Tabony, J.; Glade, N.; Demongeot, J.; Papaseit, C., Biological Self-Organization by Way of Microtubule Reaction−Diffusion Processes. *Langmuir* **2002,** *18* (19), 7196-7207.

56.   Heitmann, S.; Boonstra, T.; Breakspear, M., A Dendritic Mechanism for Decoding Traveling Waves: Principles and Applications to Motor Cortex. *PLOS Computational Biology* **2013,** *9* (10), e1003260.

57.   Horch, H. W.; Katz, L. C., BDNF release from single cells elicits local dendritic growth in nearby neurons. *Nature Neuroscience* **2002,** *5* (11), 1177-1184.

58.   Bell-Pedersen, D.; Cassone, V. M.; Earnest, D. J.; Golden, S. S.; Hardin, P. E.; Thomas, T. L.; Zoran, M. J., Circadian rhythms from multiple oscillators: lessons from diverse organisms. *Nature Reviews Genetics* **2005,** *6* (7), 544-556.

59.   Roenneberg, T.; Dragovic, Z.; Merrow, M., Demasking biological oscillators: Properties and principles of entrainment exemplified by the *Neurospora* circadian clock. *Proceedings of the National Academy of Sciences of the United States of America* **2005,** *102* (21), 7742.

60.   Reno, A.; Hunter, A. W.; Li, Y.; Ye, T.; Foley, A. C., Quantification of Cardiomyocyte Beating Frequency Using Fourier Transform Analysis. **2018,** *5* (4), 39.

61.   Berkow, R.; Beers, M.; Bogin, R., The Merck Manual of Medical Information. New Jersey: Merck and Co. Inc: 1997.

62.   Aschoff, J., A Survey on Biological Rhythms. In *Biological Rhythms*, Aschoff, J., Ed. Springer US: Boston, MA, 1981; pp 3-10.

63.   Field, R. J.; Noyes, R. M., Oscillations in chemical systems. IV. Limit cycle behavior in a model of a real chemical reaction. *The Journal of Chemical Physics* **1974,** *60* (5), 1877-1884.

64.   Field, R. J.; Noyes, R. M., A model illustrating amplification of perturbations in an excitable medium. *Faraday Symposia of the Chemical Society* **1974,** *9* (0), 21-27.

65.   Ruoff, P.; Noyes, R. M., Phase response behaviors of different oscillatory states in the Belousov–Zhabotinsky reaction. **1988,** *89* (10), 6247-6254.

66.   Pullela, S. R.; Cristancho, D.; He, P.; Luo, D.; Hall, K. R.; Cheng, Z., Temperature dependence of the Oregonator model for the Belousov-Zhabotinsky reaction. *Physical Chemistry Chemical Physics* **2009,** *11* (21), 4236-4243.

67.   Field, R. J.; Troy, W. C., The Existence of Solitary Traveling Wave Solutions of a Model of the Belousov-Zhabotinskii Reaction. **1979,** *37* (3), 561-587.

68.   Zhou, H.; Zheng, Z.; Wang, Q.; Xu, G.; Li, J.; Ding, X., A modular approach to self-oscillating polymer systems driven by the Belousov–Zhabotinsky reaction. *RSC Advances* **2015,** *5* (18), 13555-13569.

69.   Yashin, V. V.; Balazs, A. C., Pattern Formation and Shape Changes in Self-Oscillating Polymer Gels. *Science* **2006,** *314* (5800), 798.

70.   Yashin, V. V.; Balazs, A. C., Theoretical and computational modeling of self-oscillating polymer gels. *The Journal of Chemical Physics* **2007,** *126* (12), 124707.

71.   Kuksenok, O.; Yashin, V. V.; Balazs, A. C., Three-dimensional model for chemoresponsive polymer gels undergoing the Belousov-Zhabotinsky reaction. *Physical Review E* **2008,** *78* (4), 041406.

72.   Yoshida, R.; Ichijo, H.; Hakuta, T.; Yamaguchi, T., Self-oscillating swelling and deswelling of polymer gels. *Macromolecular Rapid Communications* **1995,** *16* (4), 305-310.

73.   Yoshida, R.; Yamaguchi, T.; Ichijo, H., Novel oscillating swelling-deswelling dynamic behaviour for pH-sensitive polymer gels. *Materials Science and Engineering: C* **1996,** *4* (2), 107-113.

74.   Yoshida, R.; Takahashi, T.; Yamaguchi, T.; Ichijo, H., Self-Oscillating Gel. *Journal of the American Chemical Society* **1996,** *118* (21), 5134-5135.

75.   Yoshida, R.; Takahashi, T.; Yamaguchi, T.; Ichijo, H., Self-oscillating gels. *Advanced Materials* **1997,** *9* (2), 175-178.

76.   Yoshida, R.; Ueki, T., Evolution of self-oscillating polymer gels as autonomous polymer systems. *NPG Asia Materials* **2014,** *6* (6), e107-e107.

77.   Yoshida, R.; Sakai, T.; Ito, S.; Yamaguchi, T., Self-Oscillation of Polymer Chains with Rhythmical Soluble-Insoluble Changes. *Journal of the American Chemical Society* **2002,** *124* (27), 8095-8098.

78.   Suzuki, D.; Kobayashi, T.; Yoshida, R.; Hirai, T., Soft actuators of organized self-oscillating microgels. *Soft Matter* **2012,** *8* (45), 11447-11449.

79.   Suzuki, D.; Sakai, T.; Yoshida, R., Self-Flocculating/Self-Dispersing Oscillation of Microgels. *Angewandte Chemie International Edition* **2008,** *47* (5), 917-920.

80.   Suzuki, D.; Yoshida, R., Temporal Control of Self-Oscillation for Microgels by Cross-Linking Network Structure. *Macromolecules* **2008,** *41* (15), 5830-5838.

81.   Suzuki, D.; Yoshida, R., Effect of Initial Substrate Concentration of the Belousov−Zhabotinsky Reaction on Self-Oscillation for Microgel System. *The Journal of Physical Chemistry B* **2008,** *112* (40), 12618-12624.

82.   Suzuki, D.; Yoshida, R., Self-oscillating core/shell microgels: effect of a crosslinked nanoshell on autonomous oscillation of the core. *Polymer Journal* **2010,** *42* (6), 501-508.

83.   Hara, Y.; Yoshida, R., A viscosity self-oscillation of polymer solution induced by the Belousov–Zhabotinsky reaction under acid-free condition. *The Journal of Chemical Physics* **2008,** *128* (22), 224904.

84.   Suzuki, D.; Taniguchi, H.; Yoshida, R., Autonomously Oscillating Viscosity in Microgel Dispersions. *Journal of the American Chemical Society* **2009,** *131* (34), 12058-12059.

85.   Taniguchi, H.; Suzuki, D.; Yoshida, R., Characterization of Autonomously Oscillating Viscosity Induced by Swelling/Deswelling Oscillation of the Microgels. *The Journal of Physical Chemistry B* **2010,** *114* (7), 2405-2410.

86.   Mitsunaga, R.; Okeyoshi, K.; Yoshida, R., Design of a comb-type self-oscillating gel. *Chemical Communications* **2013,** *49* (43), 4935-4937.

87.   Zhou, H.; Wang, Y.; Zheng, Z.; Ding, X.; Peng, Y., Periodic auto-active gels with topologically "polyrotaxane-interlocked" structures. *Chemical Communications* **2014,** *50* (48), 6372-6374.

88.   Masuda, T.; Hidaka, M.; Murase, Y.; Akimoto, A. M.; Nagase, K.; Okano, T.; Yoshida, R., Self-Oscillating Polymer Brushes. *Angewandte Chemie International Edition* **2013,** *52* (29), 7468-7471.

89.   Ueki, T.; Shibayama, M.; Yoshida, R., Self-oscillating micelles. *Chemical Communications* **2013,** *49* (62), 6947-6949.

90.   Kuksenok, O.; Yashin, V. V.; Kinoshita, M.; Sakai, T.; Yoshida, R.; Balazs, A. C., Exploiting gradients in cross-link density to control the bending and self-propelled motion of active gels. *Journal of Materials Chemistry* **2011,** *21* (23), 8360-8371.

91.   Kim, Y. S.; Tamate, R.; Akimoto, A. M.; Yoshida, R., Recent developments in self-oscillating polymeric systems as smart materials: from polymers to bulk hydrogels. *Materials Horizons* **2017,** *4* (1), 38-54.

92.   Maeda, S.; Hara, Y.; Yoshida, R.; Hashimoto, S., Peristaltic Motion of Polymer Gels. *Angewandte Chemie International Edition* **2008,** *47* (35), 6690-6693.

93.   Shiraki, Y.; Yoshida, R., Autonomous Intestine-Like Motion of Tubular Self-Oscillating Gel. *Angewandte Chemie International Edition* **2012,** *51* (25), 6112-6116.

94.   Shiraki, Y.; Akimoto, A. M.; Miyata, T.; Yoshida, R., Autonomous Pulsatile Flow by Peristaltic Motion of Tubular Self-Oscillating Gels. *Chemistry of Materials* **2014,** *26* (19), 5441-5443.

95.   Tabata, O.; Hirasawa, H.; Aoki, S.; Yoshida, R.; Kokufuta, E., Ciliary motion actuator using self-oscillating gel. *Sensors and Actuators A: Physical* **2002,** *95* (2), 234-238.

96.   Tabata, O.; Kojima, H.; Kasatani, T.; Isono, Y.; Yoshida, R. In *Chemo-mechanical actuator using self-oscillating gel for artificial cilia*, The Sixteenth Annual International Conference on Micro Electro Mechanical Systems, 2003. MEMS-03 Kyoto. IEEE, IEEE: 2003; pp 12-15.

97.   Murase, Y.; Hidaka, M.; Yoshida, R., Self-driven gel conveyer: Autonomous transportation by peristaltic motion of self-oscillating gel. *Sensors and Actuators B: Chemical* **2010,** *149* (1), 272-283.

98.   Murase, Y.; Takeshima, R.; Yoshida, R., Self-Driven Gel Conveyer: Effect of Interactions Between Loaded Cargo and Self-Oscillating Gel Surface. *Macromolecular Bioscience* **2011,** *11* (12), 1713-1721.

99.   Yoshida, R.; Murase, Y., Self-oscillating surface of gel for autonomous mass transport. *Colloids and Surfaces B: Biointerfaces* **2012,** *99*, 60-66.

100.   Murase, Y.; Maeda, S.; Hashimoto, S.; Yoshida, R., Design of a Mass Transport Surface Utilizing Peristaltic Motion of a Self-Oscillating Gel. *Langmuir* **2009,** *25* (1), 483-489.

101.   Maeda, S.; Hara, Y.; Sakai, T.; Yoshida, R.; Hashimoto, S., Self-Walking Gel. *Advanced Materials* **2007,** *19* (21), 3480-3484.

102.   Hara, Y.; Yoshida, R., Self-Oscillating Polymer Fueled by Organic Acid. *The Journal of Physical Chemistry B* **2008,** *112* (29), 8427-8429.

103.	Ueki, T.; Takasaki, Y.; Bundo, K.; Ueno, T.; Sakai, T.; Akagi, Y.; Yoshida, R., Autonomous viscosity oscillation via metallo-supramolecular terpyridine chemistry of branched poly(ethylene glycol) driven by the Belousov–Zhabotinsky reaction. *Soft Matter* **2014,** *10* (9), 1349-1355.

104.	Ueno, T.; Bundo, K.; Akagi, Y.; Sakai, T.; Yoshida, R., Autonomous viscosity oscillation by reversible complex formation of terpyridine-terminated poly(ethylene glycol) in the BZ reaction. *Soft Matter* **2010,** *6* (24), 6072-6074.

105.	Hidaka, M.; Yoshida, R., Self-oscillating gel composed of thermosensitive polymer exhibiting higher LCST. *Journal of Controlled Release* **2011,** *150* (2), 171-176.

106.	Nakamaru, S.; Maeda, S.; Hara, Y.; Hashimoto, S., Control of Autonomous Swelling−Deswelling Behavior for a Polymer Gel. *The Journal of Physical Chemistry B* **2009,** *113* (14), 4609-4613.

107.	Smith, M. L.; Heitfeld, K.; Slone, C.; Vaia, R. A., Autonomic Hydrogels through Postfunctionalization of Gelatin. *Chemistry of Materials* **2012,** *24* (15), 3074-3080.

108.	Zhou, H.; Ding, X.; Zheng, Z.; Peng, Y., Self-regulated intelligent systems: where adaptive entities meet chemical oscillators. *Soft Matter* **2013,** *9* (20), 4956-4968.

109.	Codazzi, F.; Pelizzoni, I.; Zacchetti, D.; Grohovaz, F., Iron entry in neurons and astrocytes: a link with synaptic activity. *Frontiers in molecular neuroscience* **2015,** *8*, 18.

110.	Moreb, J.; Hershko, C.; Hasin, Y., Effects of acute iron loading on contractility and spontaneous beating rate of cultured rat myocardial cells. *Basic research in cardiology* **1988,** *83* (4), 360-368.

111.	Muñoz, P.; Humeres, A.; Elgueta, C.; Kirkwood, A.; Hidalgo, C.; Núñez, M. T., Iron mediates N-methyl-D-aspartate receptor-dependent stimulation of calcium-induced pathways and hippocampal synaptic plasticity. *J Biol Chem* **2011,** *286* (15), 13382-13392.

112.	Yoshida, R., Self-oscillating gels driven by the Belousov-Zhabotinsky reaction as novel smart materials. *Advanced materials (Deerfield Beach, Fla.)* **2010,** *22* (31), 3463-83.

113.	Delgado, J.; Zhang, Y.; Xu, B.; Epstein, I. R., Terpyridine- and Bipyridine-Based Ruthenium Complexes as Catalysts for the Belousov−Zhabotinsky Reaction. *The Journal of Physical Chemistry A* **2011,** *115* (11), 2208-2215.

114.   Hara, Y.; Fujimoto, K.; Mayama, H., Self-Oscillation of Polymer Chains with an Fe(bpy)3 Catalyst Induced by the Belousov–Zhabotinsky Reaction. *The Journal of Physical Chemistry B* **2014,** *118* (2), 608-612.

115.   Arimura, T.; Mukai, M., A self-oscillating gel actuator driven by ferroin. *Chemical Communications* **2014,** *50* (44), 5861-5863.

116.   Braterman, P. S.; Song, J. I.; Peacock, R. D., Electronic absorption spectra of the iron(II) complexes of 2,2'-bipyridine, 2,2'-bipyrimidine, 1,10-phenanthroline, and 2,2':6',2''-terpyridine and their reduction products. *Inorganic Chemistry* **1992,** *31* (4), 555-559.

117.   Nord, G.; Wernberg, O., Reduction of tris(2,2′-bipyridyl) and tris(1,10-phenanthroline) complexes of iron(III) and osmium(III) by hydroxide ion. *Journal of the Chemical Society, Dalton Transactions* **1975,** (10), 845-849.

118.   Ren, J.; Zhang, A.; Gu, J.; Tao, L.; He, J.; Yang, W., Autonomous oscillating microgels involving Fe(phen)3 catalyst synchronized with the Belousov–Zhabotinsky reaction. *Soft Materials* **2018,** *16* (2), 134-140.

119.   Ren, J.; Yao, M.; Zhang, G.; Yang, X.; Gu, J.; Yang, W., Effect of initial substrate concentrations of the BZ reaction on self-oscillating of polymer chains with Fe(phen)3 catalyst. *Journal of Polymer Research* **2015,** *22* (10), 197.

120.   Ren, J.; Yao, M.; Zhang, G.; Yang, X.; Gu, J.; Yang, W., Self-oscillating soluble-insoluble changes of polymer chain induced by the BZ reaction with Fe(phen)3 catalyst. *Journal of Polymer Research* **2015,** *22* (4), 44.

121.   Chen, I. C.; Kuksenok, O.; Yashin, V. V.; Moslin, R. M.; Balazs, A. C.; Van Vliet, K. J., Shape- and size-dependent patterns in self-oscillating polymer gels. *Soft Matter* **2011,** *7* (7), 3141-3146.

122.   Konotop, I. Y.; Nasimova, I.; Rambidi, N.; Khokhlov, A. J. P. S. S. B., Chemomechanical oscillations in polymer gels: Effect of the size of samples. **2011,** *53* (1-2), 26-30.

123.   Konotop, I. Y.; Nasimova, I. R.; Rambidi, N. G.; Khokhlov, A. R., Self-oscillatory systems based on polymer gels. *Polymer Science Series B* **2009,** *51* (9), 383.

124.   Hara, Y.; Mayama, H.; Yamaguchi, Y.; Fujimoto, K., Activation Energy of the Belousov–Zhabotinsky Reaction in a Gel with [Fe(bpy)3] Catalyst. *Chemistry Letters* **2014,** *43* (5), 673-675.

125.   Smith, M. L.; Slone, C.; Heitfeld, K.; Vaia, R. A., Designed Autonomic Motion in Heterogeneous Belousov–Zhabotinsky (BZ)-Gelatin Composites by Synchronicity. *Advanced Functional Materials* **2013,** *23* (22), 2835-2842.

126.   Yersin, H., Czerwieniec, R., Monkowius, U. Kupfer(i)-komplexe für opto-elektronische vorrichtungen 2015.

127.   Ueda, M.; Hara, Y.; Sakai, T.; Yoshida, R.; Takai, M.; Ito, Y., Characterization of a self-oscillating polymer with periodic soluble-insoluble changes. *Journal of Polymer Science Part B: Polymer Physics* **2007,** *45* (13), 1578-1588.

128.   Masuda, T.; Hidaka, M.; Murase, Y.; Akimoto, A.; Nagase, K.; Okano, T.; Yoshida, R., Self-Oscillating Polymer Brushes. *Angewandte Chemie International Edition* **2013,** *52* (29), 7468-7471.

129.   Zhang, Y.; Zhou, N.; Akella, S.; Kuang, Y.; Kim, D.; Schwartz, A.; Bezpalko, M.; Foxman, B.; Fraden, S.; Epstein, I.; Xu, B., Active Cross-Linkers that Lead to Active Gels. *Angewandte Chemie International Edition* **2013,** *52* (44), 11494-11498.

130.   Ito, Y.; Hara, Y.; Uetsuka, H.; Hasuda, H.; Onishi, H.; Arakawa, H.; Ikai, A.; Yoshida, R., AFM Observation of Immobilized Self-Oscillating Polymer. *The Journal of Physical Chemistry B* **2006,** *110* (11), 5170-5173.

131.   Yoshimoto, M.; Shirahama, H.; Kurosawa, S.; Naito, M., Periodic change of viscosity and density in an oscillating chemical reaction. *The Journal of Chemical Physics* **2004,** *120* (15), 7067-7070.

132.   Hara, Y.; Mayama, H.; Morishima, K., Generative Force of Self-Oscillating Gel. *The Journal of Physical Chemistry B* **2014,** *118* (9), 2576-2581.

133.   Agreda, J.; Ágreda, J.; Barragán, D.; Gómez, A., Calorimetric study of the component steps of oscillating chemical reactions. *Journal of Thermal Analysis and Calorimetry* **2003,** *74* (3), 875-881.

134.   Maćešić, S.; Čupić, Ž.; Blagojević, S.; Pejic, N.; Anić, S.; Kolar-Anić, L., Current rates and reaction rates in the Stoichiometric Network Analysis (SNA). *Open Chemistry* **2015,** *13*, 591-599.

135.   Onel, L.; Bourceanu, G.; Bitter, I.; Wittmann, M.; Noszticzius, Z., Uncatalyzed Reactions in the Classical Belousov−Zhabotinsky System. 2. The Malonic Acid−Bromate Reaction in Acidic Media. *The Journal of Physical Chemistry A* **2006,** *110* (3), 990-996.

136.   Dähmlow, P.; Almeida, J.; Müller, S. C., Patterns in the bubble-free Belousov-Zhabotinsky reaction dissolved in a microemulsion. *EPL (Europhysics Letters)* **2016,** *116* (6), 60016.

137.   Szalai, I.; Kurin-Csörgei, K.; Epstein, I. R.; Orbán, M., Dynamics and Mechanism of Bromate Oscillators with 1,4-Cyclohexanedione. *The Journal of Physical Chemistry A* **2003,** *107* (47), 10074-10081.

138.   Egorova, K. S.; Ananikov, V. P., Toxicity of Metal Compounds: Knowledge and Myths. *Organometallics* **2017,** *36* (21), 4071-4090.

139.   Pornprompanya, M.; Müller, S. C.; Ševčíková, H., Pulse waves under an electric field in the Belousov–Zhabotinsky reaction with pyrogallol as substrate. *Physical Chemistry Chemical Physics* **2002,** *4* (14), 3370-3375.

140.   Agladze, K. I.; De Kepper, P., Influence of electric field on rotating spiral waves in the Belousov-Zhabotinskii reaction. *The Journal of Physical Chemistry* **1992,** *96* (13), 5239-5242.

141.   Nishikiori, R.; Morimoto, S.; Fujiwara, Y.; Katsuki, A.; Morgunov, R.; Tanimoto, Y., Magnetic Field Effect on Chemical Wave Propagation from the Belousov–Zhabotinsky Reaction. *The Journal of Physical Chemistry A* **2011,** *115* (18), 4592-4597.

142.   Vanag, V. K.; Zhabotinsky, A. M.; Epstein, I. R., Oscillatory Clusters in the Periodically Illuminated, Spatially Extended Belousov-Zhabotinsky Reaction. *Physical Review Letters* **2001,** *86* (3), 552-555.

143.   Ueki, T.; Watanabe, M.; Yoshida, R., Belousov–Zhabotinsky Reaction in Protic Ionic Liquids. *Angewandte Chemie International Edition* **2012,** *51* (48), 11991-11994.

144.   Amemiya, T.; Nakaiwa, M.; Ohmori, T.; Yamaguchi, T., Chemical waves in mesoporous media. *Physica D: Nonlinear Phenomena* **1995,** *84* (1), 103-111.

145.   Dähmlow, P.; Vanag, V. K.; Müller, S. C., Effect of solvents on the pattern formation in a Belousov-Zhabotinsky reaction embedded into a microemulsion. *Physical Review E* **2014,** *89* (1), 010902.

146.   Vanag, V. K., Dissipative structures in systems of diffusion-bonded chemical nano- and micro oscillators. *Russian Journal of General Chemistry* **2011,** *81* (1), 181-190.

147.   Paul, A., Observations of the Effect of Anionic, Cationic, Neutral, and Zwitterionic Surfactants on the Belousov−Zhabotinsky Reaction. *The Journal of Physical Chemistry B* **2005,** *109* (19), 9639-9644.

148.   Rossi, F.; Lombardo, R.; Sciascia, L.; Sbriziolo, C.; Liveri, M. L. T., Spatio-Temporal Perturbation of the Dynamics of the Ferroin Catalyzed Belousov−Zhabotinsky Reaction in a Batch Reactor Caused by Sodium Dodecyl Sulfate Micelles. *The Journal of Physical Chemistry B* **2008,** *112* (24), 7244-7250.

149.   Magnani, A.; Marchettini, N.; Ristori, S.; Rossi, C.; Rossi, F.; Rustici, M.; Spalla, O.; Tiezzi, E., Chemical Waves and Pattern Formation in the 1,2-Dipalmitoyl-sn-glycero-3-phosphocholine/Water Lamellar System. *Journal of the American Chemical Society* **2004,** *126* (37), 11406-11407.

150.   Marchettini, N.; Ristori, S.; Rossi, F.; Rustici, M., An Experimental Model for Mimicking Biological Systems: The Belousov–Zhabotinsky Reaction in Lipid Membranes. *International Journal of Design & Nature and Ecodynamics* **2013,** *1*, 55-63.

151.   Torbensen, K.; Rossi, F.; Pantani, O. L.; Ristori, S.; Abou-Hassan, A., Interaction of the Belousov–Zhabotinsky Reaction with Phospholipid Engineered Membranes. *The Journal of Physical Chemistry B* **2015,** *119* (32), 10224-10230.

152.   Rey, A. D., Liquid crystal models of biological materials and processes. *Soft Matter* **2010,** *6* (15), 3402-3429.

153.   Kemkemer, R.; Teichgräber, V.; Schrank-Kaufmann, S.; Kaufmann, D.; Gruler, H., Nematic order-disorder state transition in a liquid crystal analogue formed by oriented and migrating amoeboid cells. *The European Physical Journal E* **2000,** *3* (2), 101-110.

154.   Hague, J.; Mieczkowski, P.; O'Rourke, C.; Loughlin, A.; Phillips, J., A minimal model for nematic cell ordering in tissue. *arXiv preprint arXiv:1902.02768* **2019**.

155.   Gupta, M.; Sarangi, B. R.; Deschamps, J.; Nematbakhsh, Y.; Callan-Jones, A.; Margadant, F.; Mège, R.-M.; Lim, C. T.; Voituriez, R.; Ladoux, B., Adaptive rheology and ordering of cell cytoskeleton govern matrix rigidity sensing. *Nature Communications* **2015,** *6* (1), 7525.

156.   Saw, T. B.; Xi, W.; Ladoux, B.; Lim, C. T., Biological Tissues as Active Nematic Liquid Crystals. *Advanced Materials* **2018,** *30* (47), 1802579.

157.   Kawaguchi, K.; Kageyama, R.; Sano, M., Topological defects control collective dynamics in neural progenitor cell cultures. *Nature* **2017,** *545* (7654), 327-331.

158.   Shintate, M.; Inadomi, T.; Yamamoto, S.; Kuboyama, Y.; Ohsedo, Y.; Arimura, T.; Nakazumi, T.; Hara, Y.; Miyamoto, N., Anisotropic Self-Oscillating Reaction in Liquid Crystalline Nanosheet Hydrogels. *The Journal of Physical Chemistry B* **2018,** *122* (11), 2957-2961.

159.   Zhou, Y.; Huang, R.; Ding, F.; Brittain, A. D.; Liu, J.; Zhang, M.; Xiao, M.; Meng, Y.; Sun, L., Sulfonic Acid-Functionalized α-Zirconium Phosphate Single-Layer Nanosheets as a Strong Solid Acid for Heterogeneous Catalysis Applications. *ACS Applied Materials & Interfaces* **2014,** *6* (10), 7417-7425.

160.   Pica, M.; Donnadio, A.; Casciola, M.; Cojocaru, P.; Merlo, L., Short side chain perfluorosulfonic acid membranes and their composites with nanosized zirconium phosphate: hydration, mechanical properties and proton conductivity. *Journal of Materials Chemistry* **2012,** *22* (47), 24902-24908.

161.   Pica, M.; Donnadio, A.; Bianchi, V.; Fop, S.; Casciola, M., Aminoalcohol functionalized zirconium phosphate as versatile filler for starch-based composite membranes. *Carbohydrate polymers* **2013,** *97* (1), 210-6.

162.   Mejia, A. F.; Diaz, A.; Pullela, S.; Chang, Y.-W.; Simonetty, M.; Carpenter, C.; Batteas, J. D.; Mannan, M. S.; Clearfield, A.; Cheng, Z., Pickering emulsions stabilized by amphiphilic nano-sheets. *Soft Matter* **2012,** *8* (40), 10245-10253.

163.   Díaz, A.; González, M. L.; Pérez, R. J.; David, A.; Mukherjee, A.; Báez, A.; Clearfield, A.; Colón, J. L., Direct intercalation of cisplatin into zirconium phosphate nanoplatelets for potential cancer nanotherapy. *Nanoscale* **2013,** *5* (23), 11456-11463.

164.   Sun, L.; Boo, W. J.; Sun, D.; Clearfield, A.; Sue, H.-J., Preparation of Exfoliated Epoxy/α-Zirconium Phosphate Nanocomposites Containing High Aspect Ratio Nanoplatelets. *Chemistry of Materials* **2007,** *19* (7), 1749-1754.

165.   Díaz, A.; Mosby, B. M.; Bakhmutov, V. I.; Martí, A. A.; Batteas, J. D.; Clearfield, A., Self-Assembled Monolayers Based Upon a Zirconium Phosphate Platform. *Chemistry of Materials* **2013,** *25* (5), 723-728.

166.   Au - Yu, Y.-H.; Au - Wang, X.; Au - Shinde, A.; Au - Cheng, Z., Synthesis and Exfoliation of Discotic Zirconium Phosphates to Obtain Colloidal Liquid Crystals. *JoVE* **2016,** (111), e53511.

167.   Shuai, M.; Mejia, A. F.; Chang, Y.-W.; Cheng, Z., Hydrothermal synthesis of layered α-zirconium phosphate disks: control of aspect ratio and polydispersity for nano-architecture. *CrystEngComm* **2013,** *15* (10), 1970-1977.

168.   Mejia, A. F.; Chang, Y.-W.; Ng, R.; Shuai, M.; Mannan, M. S.; Cheng, Z., Aspect ratio and polydispersity dependence of isotropic-nematic transition in discotic suspensions. *Physical Review E* **2012,** *85* (6), 061708.

169.   Bauman, D., The Study of the Guest Effect on the Nematic Phase Stabilization. *Molecular Crystals and Liquid Crystals Incorporating Nonlinear Optics* **1988,** *159* (1), 197-218.

170.   van der Kooij, F. M.; Vogel, M.; Lekkerkerker, H. N. W., Phase behavior of a mixture of platelike colloids and nonadsorbing polymer. *Physical Review E* **2000,** *62* (4), 5397-5402.

171.   Prasanna Kumar, D. J.; Verma, S.; Jasuja, K.; Dayal, P., Tuning the oscillatory dynamics of the Belousov–Zhabotinsky reaction using ruthenium nanoparticle decorated graphene. *Physical Chemistry Chemical Physics* **2019,** *21* (6), 3164-3173.

172.   Ren, J.; Zhao, L.; Zhang, A.; Zhang, L.; Li, Y.; Yang, W., Designing multifunctional gels with electrical conductivity, mechanical toughness and self-oscillating performance. *New Journal of Chemistry* **2020**.

173.   Sung, B.; Kim, M.-H., Liquid-crystalline nanoarchitectures for tissue engineering. *Beilstein J Nanotechnol* **2018,** *9*, 205-215.

174.   Biosa, G.; Ristori, S.; Spalla, O.; Rustici, M.; Hauser, M. J. B., Macroscopic Dynamics as Reporter of Mesoscopic Organization: The Belousov−Zhabotinsky Reaction in Aqueous Layers of DPPC Lamellar Phases. *The Journal of Physical Chemistry A* **2011,** *115* (15), 3227-3232.

175.   Mejia, A. F.; Ng, R.; Nguyen, P.; Shuai, M.; Acosta, H. Y.; Mannan, M. S.; Cheng, Z., Thermo-responsive discotic nematic hydrogels. *Soft Matter* **2013,** *9* (43), 10257-10264.

176.   Israel, C. W., Mechanisms of sudden cardiac death. *Indian Heart J* **2014,** *66 Suppl 1* (Suppl 1), S10-S17.

177.   Fenton, F.; Karma, A.; Hastings, H.; Evans, S., *Transition from ventricular tachycardia to ventricular fibrillation as function of tissue characteristics computer model*. 2000; Vol. 1, p 391-394 vol.1.

178.   Zhang, Y.; Zhou, N.; Li, N.; Sun, M.; Kim, D.; Fraden, S.; Epstein, I. R.; Xu, B., Giant Volume Change of Active Gels under Continuous Flow. *Journal of the American Chemical Society* **2014,** *136* (20), 7341-7347.

179.   Torbensen, K.; Rossi, F.; Ristori, S.; Abou-Hassan, A., Chemical communication and dynamics of droplet emulsions in networks of Belousov–Zhabotinsky micro-oscillators produced by microfluidics. *Lab on a Chip* **2017,** *17* (7), 1179-1189.

180.   Gorecki, J.; Gizynski, K.; Guzowski, J.; Gorecka, J. N.; Garstecki, P.; Gruenert, G.; Dittrich, P., Chemical computing with reaction-diffusion processes. *Philosophical Transactions of the Royal Society A: Mathematical, Physical and Engineering Sciences* **2015,** *373* (2046), 20140219.

181.   Kramb, R. C.; Buskohl, P. R.; Slone, C.; Smith, M. L.; Vaia, R. A., Autonomic composite hydrogels by reactive printing: materials and oscillatory response. *Soft Matter* **2014,** *10* (9), 1329-1336.

182.   Yuan, P.; Kuksenok, O.; Gross, D. E.; Balazs, A. C.; Moore, J. S.; Nuzzo, R. G., UV patternable thin film chemistry for shape and functionally versatile self-oscillating gels. *Soft Matter* **2013,** *9* (4), 1231-1243.

183.   Rosen, H.; Gilly, W.; Bell, L.; Abernathy, K.; Marshall, G., Chromogenic behaviors of the Humboldt squid (Dosidicus gigas) studied in situ with an animal-borne video package. *Journal of Experimental Biology* **2015,** *218* (2), 265-275.

184.   Watanabe, M.; Kondo, S., Is pigment patterning in fish skin determined by the Turing mechanism? *Trends in Genetics* **2015,** *31* (2), 88-96.

185.   Nakamasu, A.; Takahashi, G.; Kanbe, A.; Kondo, S., Interactions between zebrafish pigment cells responsible for the generation of Turing patterns. *Proceedings of the National Academy of Sciences* **2009,** *106* (21), 8429.

186.   Akkaynak, D.; Siemann, L. A.; Barbosa, A.; Mäthger, L. M., Changeable camouflage: how well can flounder resemble the colour and spatial scale of substrates in their natural habitats? *R Soc Open Sci* **2017,** *4* (3), 160824-160824.

187.   VandenSpiegel, D.; Lane, D. J.; Stampanato, S.; Jangoux, M., The asteroid fauna (Echinodermata) of Singapore, with a distribution table and an illustrated identification to the species. *Raffles Bulletin of Zoology* **1998,** *46*, 431-470.

188.   Wu, L.; Ji, C.; Wang, S.; Lv, J., The advantages of the pentameral symmetry of the starfish. *arXiv preprint arXiv:1202.2219* **2012**.

189.   Wintz, W.; Döbereiner, H. G.; Seifert, U., Starfish vesicles. *Europhysics Letters (EPL)* **1996,** *33* (5), 403-408.

190.   Hotchkiss, F. H. C., On the Number of Rays in Starfish1. *Integrative and Comparative Biology* **2015,** *40* (3), 340-354.

191.   Byrne, M.; Anderson, M. J., Hybridization of Sympatric Patiriella Species (Echinodermata: Asteroidea) in New South Wales. *Evolution* **1994,** *48* (3), 564-576.

192.   Jackson, A. C.; Murphy, R.; Underwood, A. J., Patiriella exigua: Grazing by a starfish in an overgrazed intertidal system. *Marine Ecology-progress Series - MAR ECOL-PROGR SER* **2009,** *376*, 153-163.

193.   Voron'ko, N. G.; Derkach, S. R.; Vovk, M. A.; Tolstoy, P. M., Formation of κ-carrageenan–gelatin polyelectrolyte complexes studied by 1H NMR, UV spectroscopy and kinematic viscosity measurements. *Carbohydrate polymers* **2016,** *151*, 1152-1161.

194.   Cao, Y.; Fang, Y.; Nishinari, K.; Phillips, G., Effects of conformational ordering on protein/polyelectrolyte electrostatic complexation: Ionic binding and chain stiffening. *Scientific Reports* **2016,** *6*, 23739.

195.   Cao, Y.; Wang, L.; Zhang, K.; Fang, Y.; Nishinari, K.; Phillips, G. O., Mapping the Complex Phase Behaviors of Aqueous Mixtures of κ-Carrageenan and Type B Gelatin. *The Journal of Physical Chemistry B* **2015,** *119* (30), 9982-9992.

196.   Meka, V. S.; Sing, M. K. G.; Pichika, M. R.; Nali, S. R.; Kolapalli, V. R. M.; Kesharwani, P., A comprehensive review on polyelectrolyte complexes. *Drug Discovery Today* **2017,** *22* (11), 1697-1706.

197.   Chen, I. C.; Kuksenok, O.; Yashin, V. V.; Balazs, A. C.; Van Vliet, K. J., Mechanical Resuscitation of Chemical Oscillations in Belousov–Zhabotinsky Gels. *Advanced Functional Materials* **2012,** *22* (12), 2535-2541.

198.   Gizynski, K.; Gruenert, G.; Dittrich, P.; Gorecki, J., Evolutionary design of classifiers made of droplets containing a nonlinear chemical medium. *Evol. Comput.* **2017,** *25* (4), 643–671.

199.   Hines, L.; Petersen, K.; Lum, G. Z.; Sitti, M., Soft Actuators for Small-Scale Robotics. *Advanced Materials* **2017,** *29* (13), 1603483.

200.   Morales, D.; Palleau, E.; Dickey, M. D.; Velev, O. D., Electro-actuated hydrogel walkers with dual responsive legs. *Soft Matter* **2014,** *10* (9), 1337-1348.

201.   Lim, H. L.; Chuang, J. C.; Tran, T.; Aung, A.; Arya, G.; Varghese, S., Dynamic Electromechanical Hydrogel Matrices for Stem Cell Culture. *Advanced Functional Materials* **2011,** *21* (1), 55-63.

202.   Tanaka, T.; Nishio, I.; Sun, S.-T.; Ueno-Nishio, S., Collapse of Gels in an Electric Field. *Science* **1982,** *218* (4571), 467.

203.   Yu, L.; Yu, H., Light-Powered Tumbler Movement of Graphene Oxide/Polymer Nanocomposites. *ACS Applied Materials & Interfaces* **2015,** *7* (6), 3834-3839.

204.   Suematsu, N. J.; Nakata, S., Evolution of Self-Propelled Objects: From the Viewpoint of Nonlinear Science. *Chemistry – A European Journal* **2018,** *24* (24), 6308-6324.

205. Chaudhury, M. K.; Whitesides, G. M., How to Make Water Run Uphill. *Science* **1992,** *256* (5063), 1539.

206. Sharma, R.; Chang, S. T.; Velev, O. D., Gel-Based Self-Propelling Particles Get Programmed To Dance. *Langmuir* **2012,** *28* (26), 10128-10135.

207. Nakata, S.; Iguchi, Y.; Ose, S.; Kuboyama, M.; Ishii, T.; Yoshikawa, K., Self-Rotation of a Camphor Scraping on Water: New Insight into the Old Problem. *Langmuir* **1997,** *13* (16), 4454-4458.

208. Yao, X.; Bai, H.; Ju, J.; Zhou, D.; Li, J.; Zhang, H.; Yang, B.; Jiang, L., Running droplet of interfacial chemical reaction flow. *Soft Matter* **2012,** *8* (22), 5988-5991.

209. Brzoska, J. B.; Brochard-Wyart, F.; Rondelez, F., Motions of droplets on hydrophobic model surfaces induced by thermal gradients. *Langmuir* **1993,** *9* (8), 2220-2224.

210. Ichimura, K.; Oh, S. K.; Nakagawa, M., Light-driven motion of liquids on a photoresponsive surface. *Science* **2000,** *288* (5471), 1624-6.

211. Nanzai, B.; Kato, M.; Igawa, M., Spontaneous motion of various oil droplets in aqueous solution of trimethyl alkyl ammonium with different carbon chain lengths. *Colloids and Surfaces A: Physicochemical and Engineering Aspects* **2016,** *504*, 154-160.

212. Hanczyc, M. M.; Toyota, T.; Ikegami, T.; Packard, N.; Sugawara, T., Fatty Acid Chemistry at the Oil−Water Interface: Self-Propelled Oil Droplets. *Journal of the American Chemical Society* **2007,** *129* (30), 9386-9391.

213. Banno, T.; Kuroha, R.; Toyota, T., pH-Sensitive Self-Propelled Motion of Oil Droplets in the Presence of Cationic Surfactants Containing Hydrolyzable Ester Linkages. *Langmuir* **2012,** *28* (2), 1190-1195.

214. Thutupalli, S.; Seemann, R.; Herminghaus, S., Swarming behavior of simple model squirmers. *New Journal of Physics* **2011,** *13* (7), 073021.

215. Nakata, S.; Nagayama, M.; Kitahata, H.; Suematsu, N. J.; Hasegawa, T., Physicochemical design and analysis of self-propelled objects that are characteristically sensitive to environments. *Physical Chemistry Chemical Physics* **2015,** *17* (16), 10326-10338.

216. Nagayama, M.; Yadome, M.; Murakami, M.; Kato, N.; Kirisaka, J.; Nakata, S., Bifurcation of self-motion depending on the reaction order. *Physical Chemistry Chemical Physics* **2009,** *11* (7), 1085-1090.

217.   Iida, K.; Suematsu, N. J.; Miyahara, Y.; Kitahata, H.; Nagayama, M.; Nakata, S., Experimental and theoretical studies on the self-motion of a phenanthroline disk coupled with complex formation. *Physical Chemistry Chemical Physics* **2010,** *12* (7), 1557-1563.

218.   Matsuda, Y.; Suematsu, N. J.; Nakata, S., Photo-sensitive self-motion of a BQ disk. *Physical chemistry chemical physics : PCCP* **2012,** *14* (17), 5988-91.

219.   Suematsu, N. J.; Miyahara, Y.; Matsuda, Y.; Nakata, S., Self-Motion of a Benzoquinone Disk Coupled with a Redox Reaction. *The Journal of Physical Chemistry C* **2010,** *114* (31), 13340-13343.

220.   Nakata, S.; Nomura, M.; Yamamoto, H.; Izumi, S.; Suematsu, N.; Ikura, Y.; Amemiya, T., Periodic Oscillatory Motion of a Self-Propelled Motor Driven by Decomposition of H 2 O 2 by Catalase. *Angewandte Chemie International Edition* **2016,** *56*.

221.   Ito, Y.; Nogawa, M.; Yoshida, R., Temperature Control of the Belousov−Zhabotinsky Reaction Using a Thermoresponsive Polymer. *Langmuir* **2003,** *19* (23), 9577-9579.

222.   Yashin, V.; Kuksenok, O.; Balazs, A., Modeling autonomously ocillating chemo-responsive gels. *Progress in Polymer Science* **2010,** *35*, 155-173.

223.   Yoshida, R.; Takei, K.; Yamaguchi, T., Self-Beating Motion of Gels and Modulation of Oscillation Rhythm Synchronized with Organic Acid. *Macromolecules* **2003,** *36* (6), 1759-1761.

224.   Shinohara, S.-i.; Seki, T.; Sakai, T.; Yoshida, R.; Takeoka, Y., Chemical and optical control of peristaltic actuator based on self-oscillating porous gel. *Chemical Communications* **2008,** (39), 4735-4737.

225.   Dayal, P.; Kuksenok, O.; Balazs, A. C., Using Light to Guide the Self-Sustained Motion of Active Gels. *Langmuir* **2009,** *25* (8), 4298-4301.

226.   Hara, Y.; Yoshida, R., Control of Oscillating Behavior for the Self-Oscillating Polymer with pH-Control Site. *Langmuir* **2005,** *21* (21), 9773-9776.

227.   Dayal, P.; Kuksenok, O.; Balazs, A. C., Directing the Behavior of Active, Self-Oscillating Gels with Light. *Macromolecules* **2014,** *47* (10), 3231-3242.

228.   Kádár, S.; Wang, J.; Showalter, K., Noise-supported travelling waves in sub-excitable media. *Nature* **1998,** *391* (6669), 770-772.

229. Toth, R.; Taylor, A., The Tris(2,2'-Bipyridyl)Ruthenium-Catalysed Belousov–Zhabotinsky Reaction. *Progress in Reaction Kinetics and Mechanism* **2006,** *31* (2), 59-115.

230. Dayal, P.; Kuksenok, O.; Balazs, A. C., Designing autonomously motile gels that follow complex paths. *Soft Matter* **2010,** *6* (4), 768-773.

231. Lu, X.; Ren, L.; Gao, Q.; Zhao, Y.; Wang, S.; Yang, J.; Epstein, I. R., Photophobic and phototropic movement of a self-oscillating gel. *Chemical Communications* **2013,** *49* (70), 7690-7692.

232. Dayal, P.; Kuksenok, O.; Balazs, A. C., Reconfigurable assemblies of active, autochemotactic gels. *Proceedings of the National Academy of Sciences* **2013,** *110* (2), 431-436.

233. Sekiguchi, T.; Mori, Y.; Okazaki, N.; Hanazaki, I., Photoinduction and photoinhibition of chemical oscillations in the tris(2,2′-bipyridine) ruthenium (II)-catalyzed minimal bromate oscillator. *Chemical Physics Letters* **1994,** *219* (1), 81-85.

234. Ren, L.; Wang, M.; Pan, C.; Gao, Q.; Liu, Y.; Epstein, I. R., Autonomous reciprocating migration of an active material. *Proceedings of the National Academy of Sciences* **2017**, 201704094.

235. Zhang, C. X.; Liao, H. M.; Zhou, L. Q.; Ouyang, Q., Pattern Selection in the Belousov−Zhabotinsky Reaction with the Addition of an Activating Reactant. *The Journal of Physical Chemistry B* **2004,** *108* (43), 16990-16994.

236. Kheowan, O.-U.; Gáspár, V.; Zykov, V. S.; Müller, S. C., Measurements of kinematical parameters of spiral waves in media of low excitability. *Physical Chemistry Chemical Physics* **2001,** *3* (21), 4747-4752.

237. Ren, L.; Wang, L.; Gao, Q.; Teng, R.; Xu, Z.; Wang, J.; Pan, C.; Epstein, I. R., Programmed Locomotion of an Active Gel Driven by Spiral Waves. *Angewandte Chemie International Edition* **2020,** *59* (18), 7106-7112.

238. Kuksenok, O.; Singh, A.; Balazs, A. C., Designing polymer gels and composites that undergo bio-inspired phototactic reconfiguration and motion. *Bioinspiration & Biomimetics* **2018,** *13* (3), 035004.

239. Cheng, Z.; Ma, S.; Zhang, Y.; Huang, S.; Chen, Y.; Yu, H., Photomechanical Motion of Liquid-Crystalline Fibers Bending Away from a Light Source. *Macromolecules* **2017,** *50* (21), 8317-8324.

240.   Yu, H., Recent advances in photoresponsive liquid-crystalline polymers containing azobenzene chromophores. *Journal of Materials Chemistry C* **2014,** *2* (17), 3047-3054.

241.   Epstein, I.; Huang, J., Reaction-diffusion processes at the nano- and microscales. *Nature nanotechnology* **2016,** *11*, 312-319.

242.   Yoshizawa, T.; Onoda, M.; Ueki, T.; Tamate, R.; Akimoto, A. M.; Yoshida, R., Fabrication of Self-Oscillating Micelles with a Built-In Oxidizing Agent. *Angewandte Chemie International Edition* **2020,** *59* (10), 3871-3875.

243.   Isakova, A.; Novakovic, K., Oscillatory chemical reactions in the quest for rhythmic motion of smart materials. *European Polymer Journal* **2017,** *95*, 430-439.

244.   Sano, K.; Ishida, Y.; Aida, T., Synthesis of Anisotropic Hydrogels and Their Applications. *Angewandte Chemie International Edition* **2018,** *57* (10), 2532-2543.

245.   Sun, Z.; Yamauchi, Y.; Araoka, F.; Kim, Y. S.; Bergueiro, J.; Ishida, Y.; Ebina, Y.; Sasaki, T.; Hikima, T.; Aida, T., An Anisotropic Hydrogel Actuator Enabling Earthworm-Like Directed Peristaltic Crawling. *Angewandte Chemie International Edition* **2018,** *57* (48), 15772-15776.

246.   Gizynski, K.; Gorecki, J., Cancer classification with a network of chemical oscillators. *Physical Chemistry Chemical Physics* **2017,** *19* (42), 28808-28819.

247.   Sansuk, S.; Juntarakod, P.; Tongphoothorn, W.; Sirimungkala, A.; Somboon, T., Visual chemo-chronometric assay for quantifying ethanol in alcoholic drinks by the colorimetric Belousov-Zhabotinsky oscillator. *Food Control* **2020,** *110*, 107042.

248.   Ren, J.; Zhang, X.; Gao, J.; Yang, W., The application of oscillating chemical reactions to analytical determinations. *Central European Journal of Chemistry* **2013,** *11* (7), 1023-1031.

249.   Steinbock, O.; Tóth, Á.; Showalter, K., Navigating Complex Labyrinths: Optimal Paths from Chemical Waves. *Science* **1995,** *267* (5199), 868-871.

APPENDIX A- CHAPTER II

This appendix for chapter II includes supporting information for the synthesis and

performance of self-oscillating gelatin materials catalyzed by iron.

Brominated Phenanthroline Characterization

The ligand used for the anchoring of the iron catalyst to the gelatin polymer matrix was a

brominated phenanthroline. The spectra below correspond to the nuclear magnetic

resonance (NMR) data obtained for the starting material and crude product.
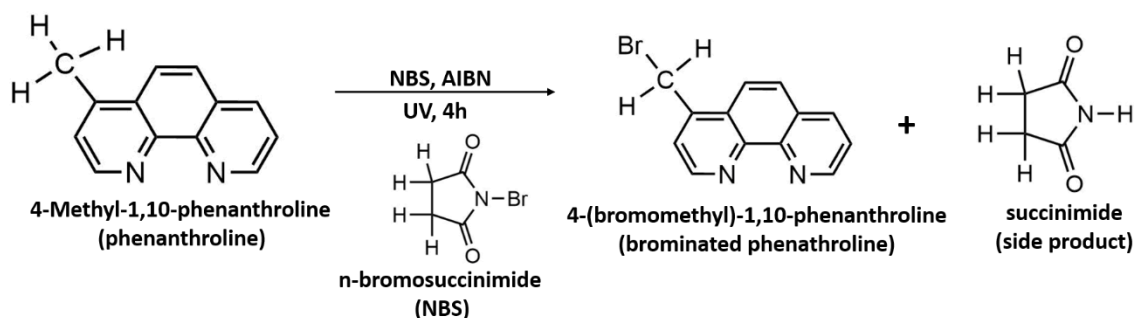
Figure 37. Reaction Scheme for the Synthesis of Brominated Phenanthroline
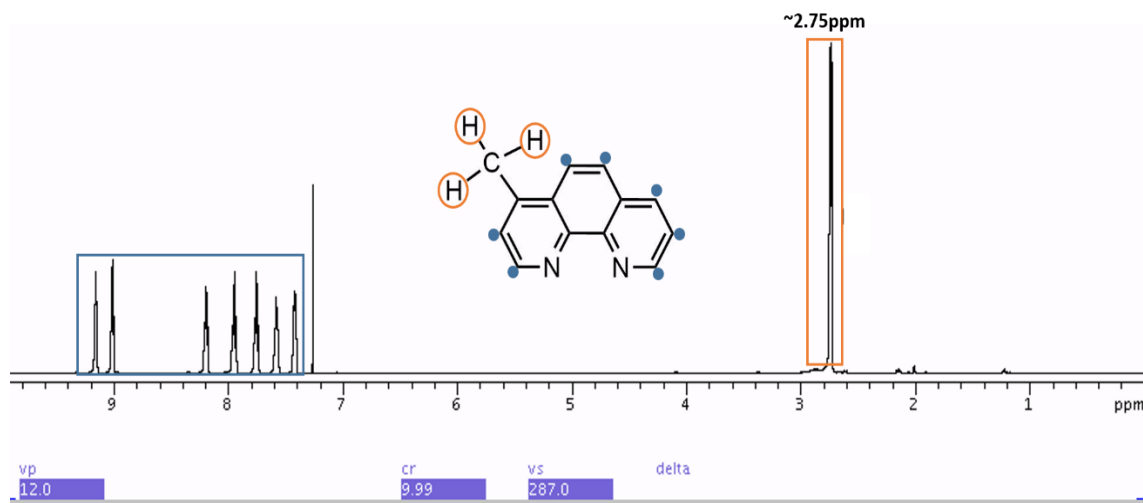
Figure 38. NMR Spectrum of Phenanthroline
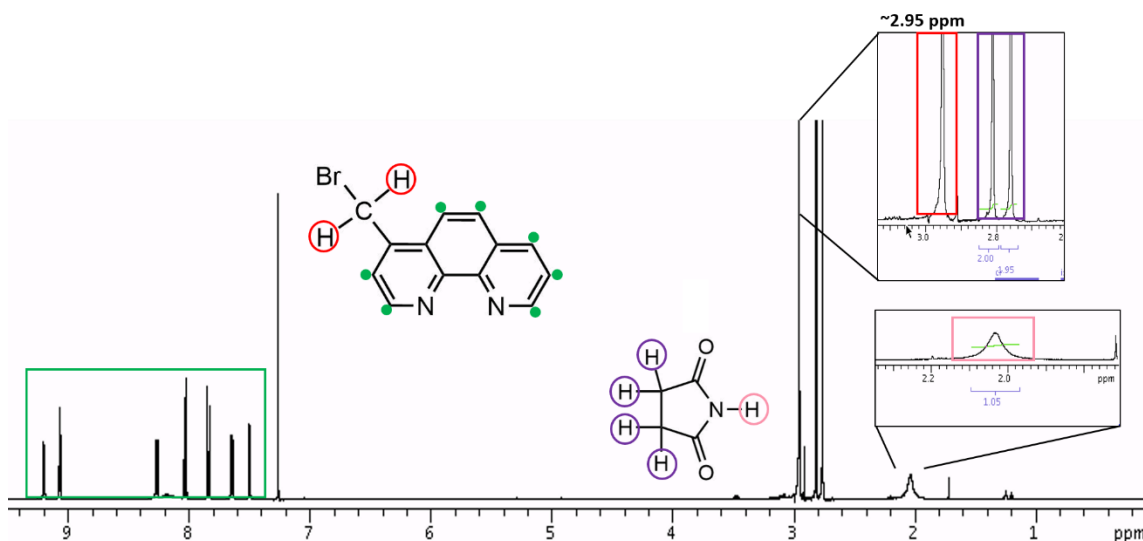
Figure 39. NMR Spectrum of Brominated Phenanthroline and Side Product

Effect of Substrate Concentration on BZ Reaction Dynamics

Different concentrations of reactants were used to test the effect on the oscillations of the

synthesized hydrogels. Only the reaction and induction times were assessed given that

the wave patterns were not clearly visible (limited by the use of malonic acid).

Concentration of reactants			
	1X	1.25 X	1.5X
Malonic acid (M)	0.02	0.025	0.03
Nitric acid (M)	0.72	0.9	1.08
Sodium bromate (M)	0.08	0.1	0.12
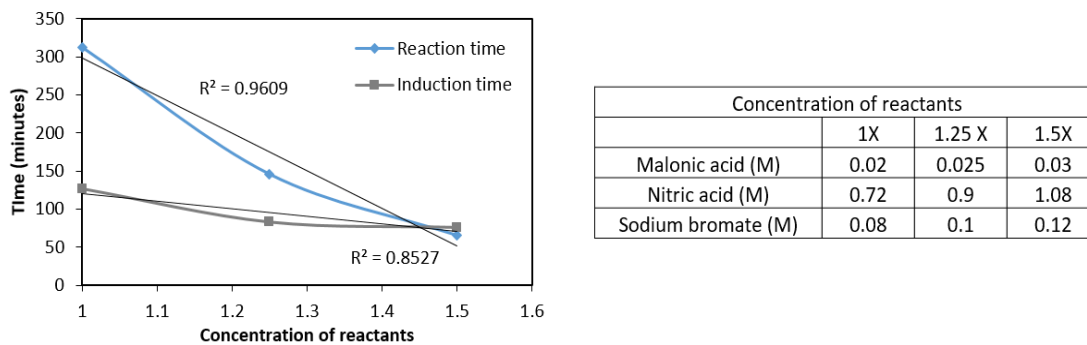
**Figure 40. Effect of BZ Substrate Concentration on Reaction Dynamics of
Iron-based Gelatin**

Adjusting Shape, Dimensions and Chemicals for Oscillatory Response

Table 2 presents additional experiments for gelatin-based hydrogels employing malonic acid (organic substrate) in the BZ reaction. The frequency values did not result in significant trends, and the type of observed waves were mainly planar waves.

Table 2. Frequency Values for Gelatin-based Hydrogels at Varying Dimensions and Shapes

Shape	Dimensions (cm)	NA (M)	MA (M)	SB (M)	Frequency (s^{-1})
	0.40*0.80* 0.60	0.720	0.020	0.080	$0.00147 \pm 1.88E\text{-}04$
	0.25*0.80*0.50	0.720	0.020	0.080	$0.00392 \pm 4.13E\text{-}05$
	0.50*1.00*0.70	0.720	0.020	0.080	$0.00257 \pm 3.46E\text{-}05$
	1.00 dia., 0.25 thickness	0.720	0.020	0.080	$0.00486 \pm 1.18E\text{-}03$
	0.80 dia., 0.30 thickness	0.720	0.020	0.080	$0.00438 \pm 1.01E\text{-}04$
	0.80 dia., 0.30 thickness	0.900	0.025	0.100	$0.00847 \pm 8.79E\text{-}04$
	0.40 dia., 1.20 length, 0.30 thickness	0.900	0.025	0.100	$0.00562 \pm 4.64E\text{-}04$
	0.40 dia., 1.20 length, 0.50 thickness	0.720	0.020	0.093	$0.00223 \pm 1.33E\text{-}04$
	0.80 dia., 0.30 thickness	0.720	0.020	0.080	$0.00299 \pm 5.17E\text{-}04$

*NA: nitric acid, MA: malonic acid, SB: sodium bromate, dia.: diameter

ZrP Oscillating Liquid Crystals and ZrP Nanosurfactants
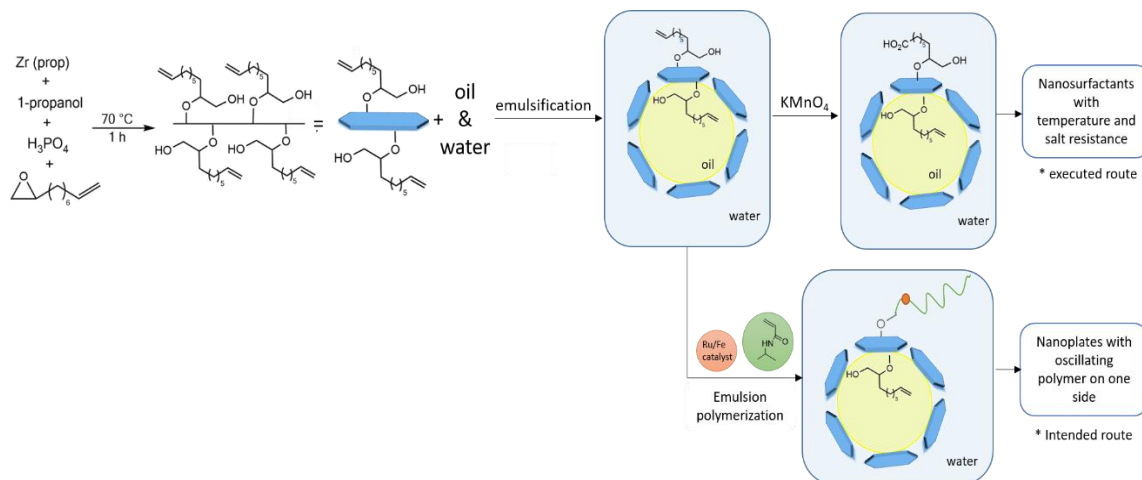
Figure 41. Scheme for the Synthesis of Oscillating Liquid Crystals

Figure 41 depicts the intended route for the design of oscillating liquid crystals, which were based on ZrP nanoparticles synthesized via microwave. The obtained nanoparticles did not meet the desired qualities for liquid crystals formation and, instead, they were used as nanosurfactants with high temperature resistance and salt resistance.
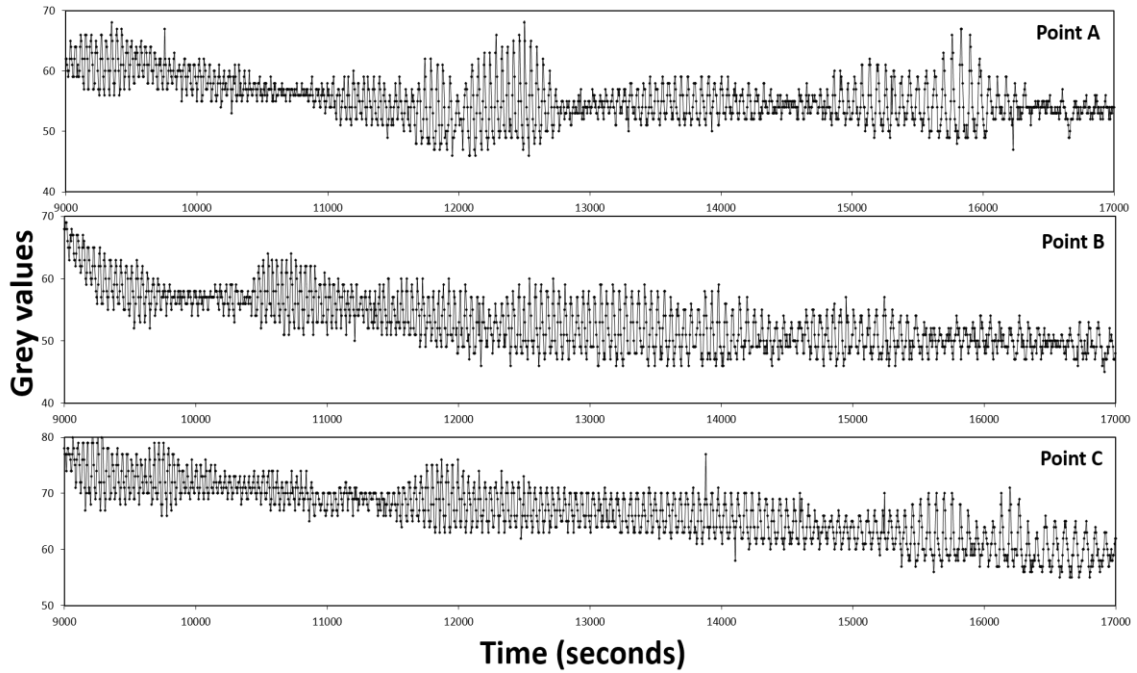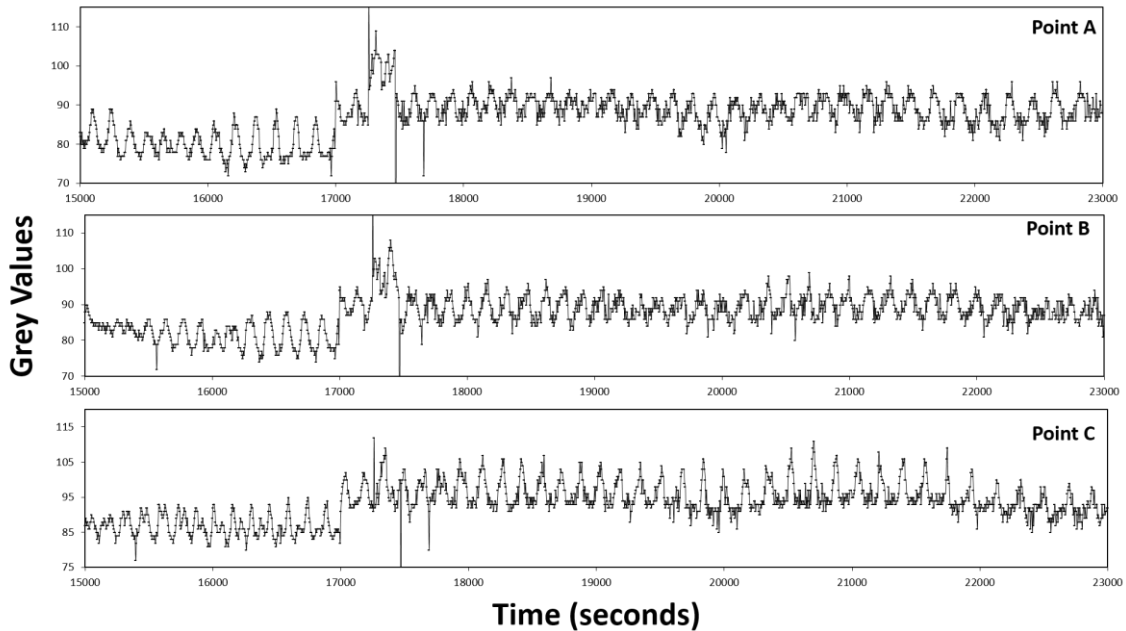
Size of Exfoliated ZrP Nanoplates
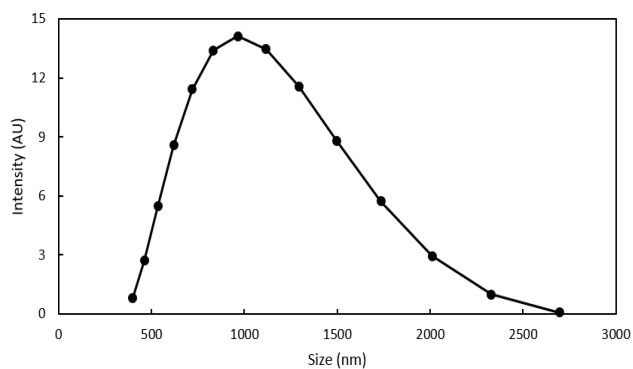
Figure 42. Dynamic Light Scattering (DLS) Data for Exfoliated ZrP Nanoplates

The hydrogels with different concentrations of ZrP reacted and the grey values were

extracted from three equally distributed points (points A, B and C).

Figure 43. Oscillations in Hydrogel with ϕ= 0.000%

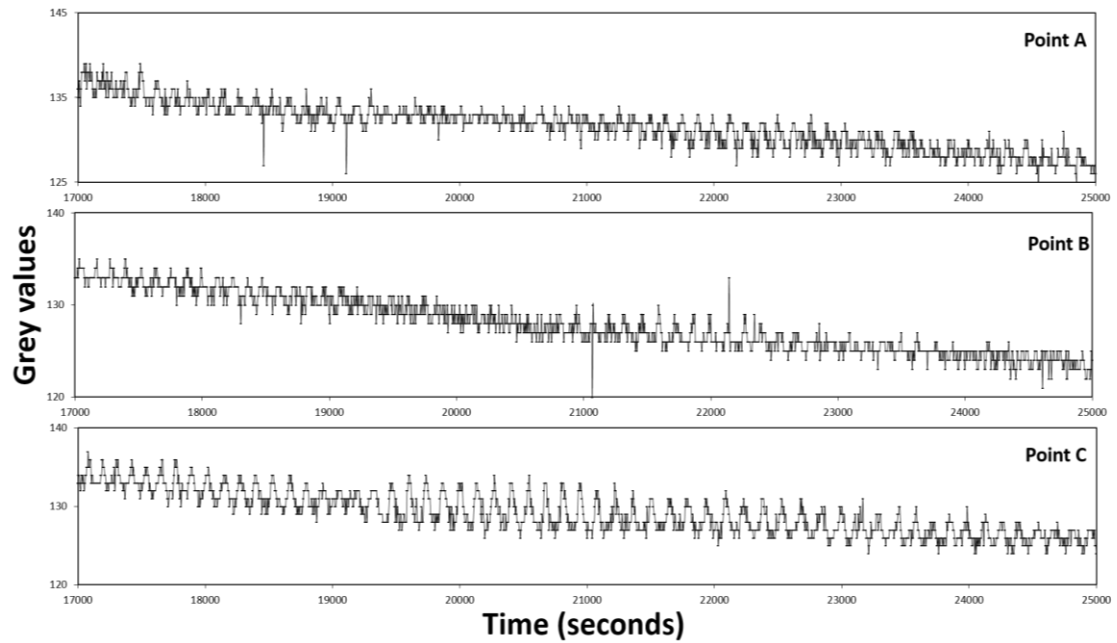**Figure 44. Oscillations in Hydrogel with ϕ= 0.034%**

110
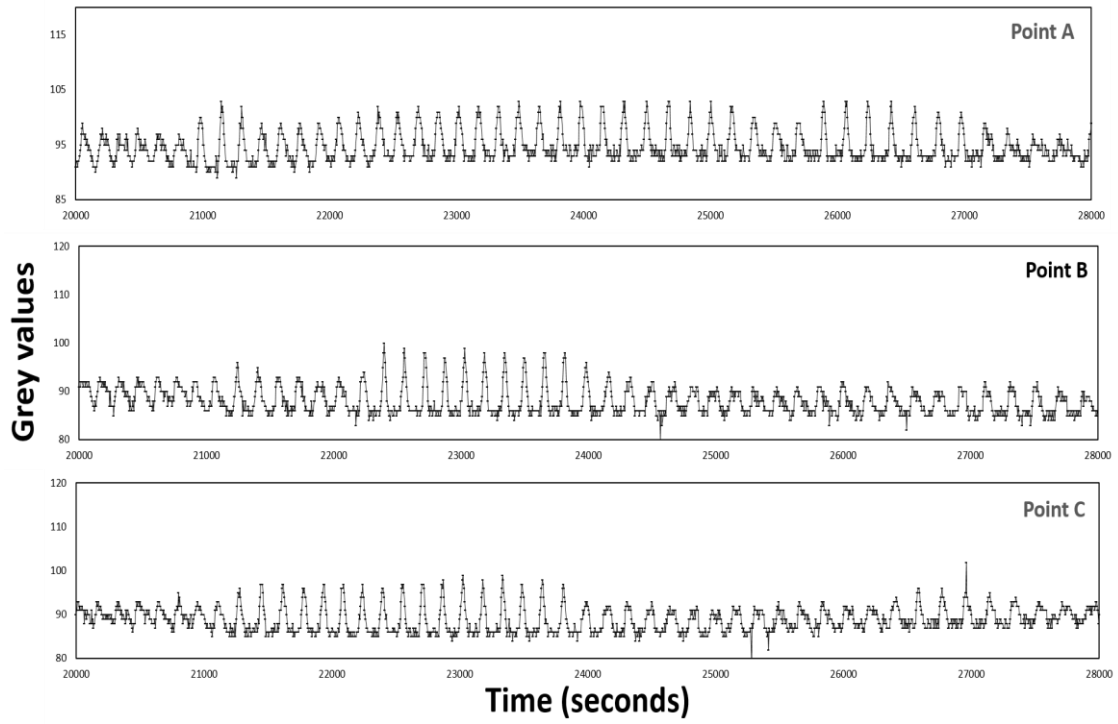
Figure 45. Oscillations in Hydrogel with ϕ= 0.085%
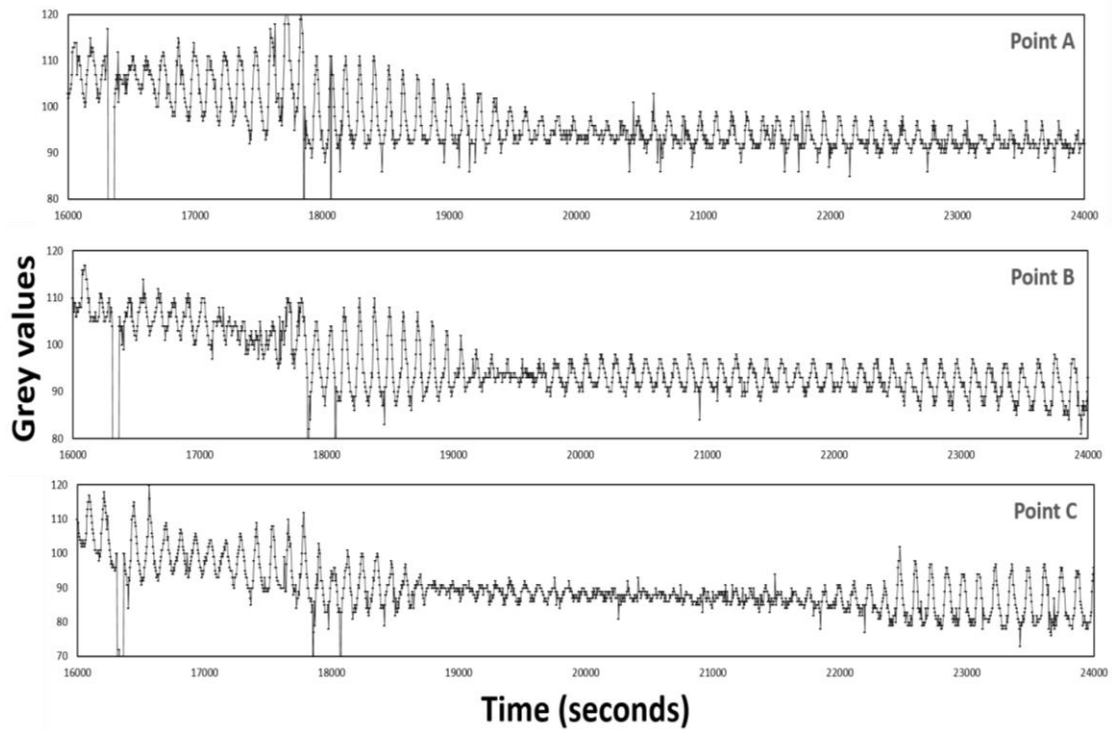
Figure 46. Oscillations in Hydrogel with ϕ= 0.170%

111
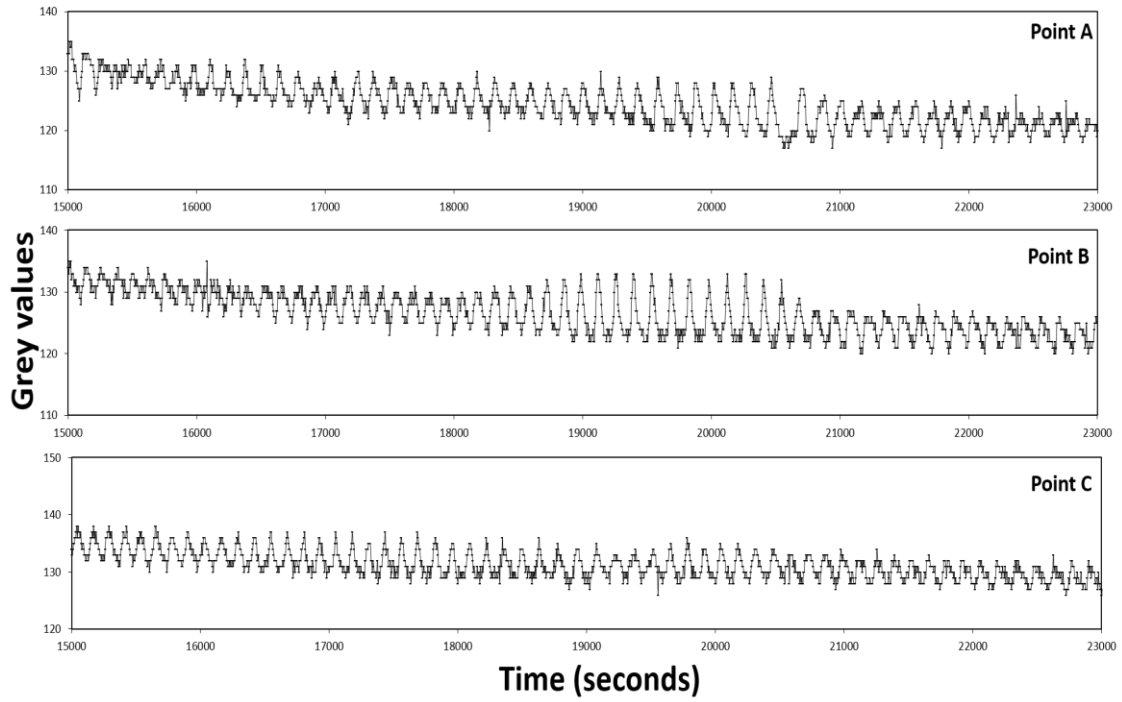
Figure 47. Oscillations in Hydrogel with $\phi = 0.260\%$

Figure 48. Oscillations in Hydrogel with $\phi = 0.340\%$

The frequency of oscillations was obtained for all three points ($\tau = \frac{1}{2}$ to $\frac{3}{4}$) in each of the

hydrogels. The frequency value with the most defined signal was used for later graphing.

Table 3. Frequency Values for Hydrogels at Varying ZrP Volume Fractions

| ZrP (ϕ, %)	Point A	Point B	Point C
0.000	0.01843 ± 0.5629	0.01979 ± 0.00185	0.01924 ± 0.32379
0.034	0.00565 ± 6.616E-04	0.0061 ± 7.366E-05	0.00584 ±2.785E-04
0.085	0.00621 ± 3.42E-04	0.00625 ± 5.31 E-05	0.00629± 2.02 E-04
0.170	0.00683 ± 4.79E-04	0.00696 ± 1.91E-04	0.0075 ± 8.68E-04
0.260	0.00655 ± 0.00101	0.00701 ± 4.69E-05	0.007 ± 1.47E-04
0.340	0.00648 ± 4.02E-04	0.00727 ± 4.59E-05	0.00727 ± 4.59E-05

*highlighted cells indicate the frequency values used for phase transition curves
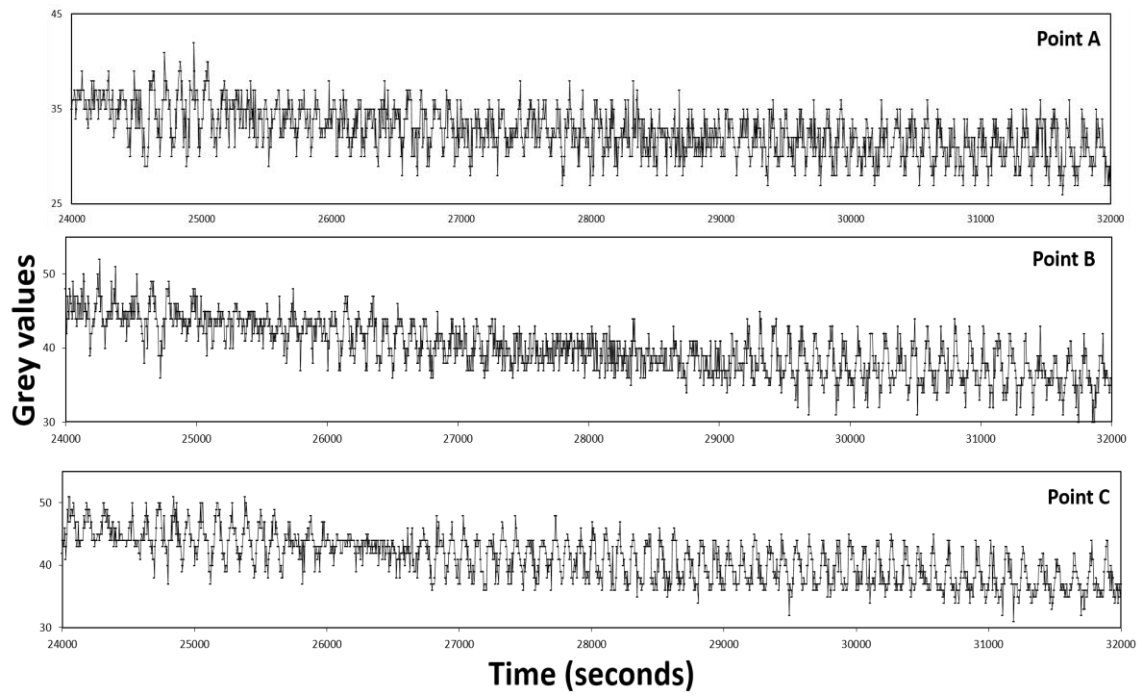
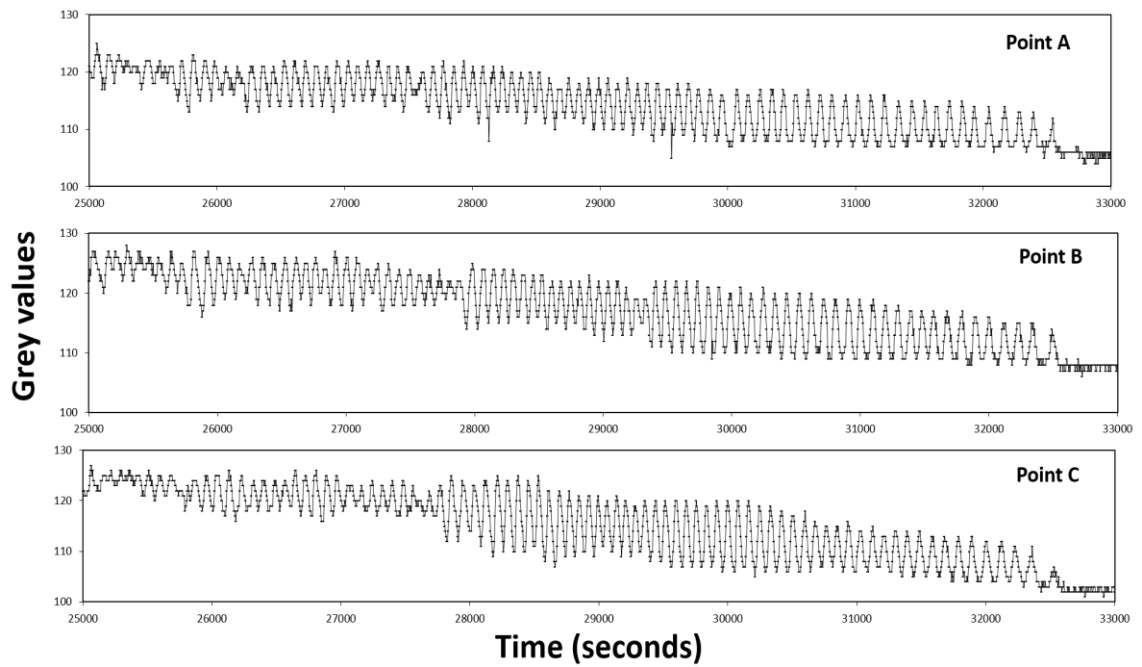*Oscillatory Graphs for the 3D-Printed Stars*
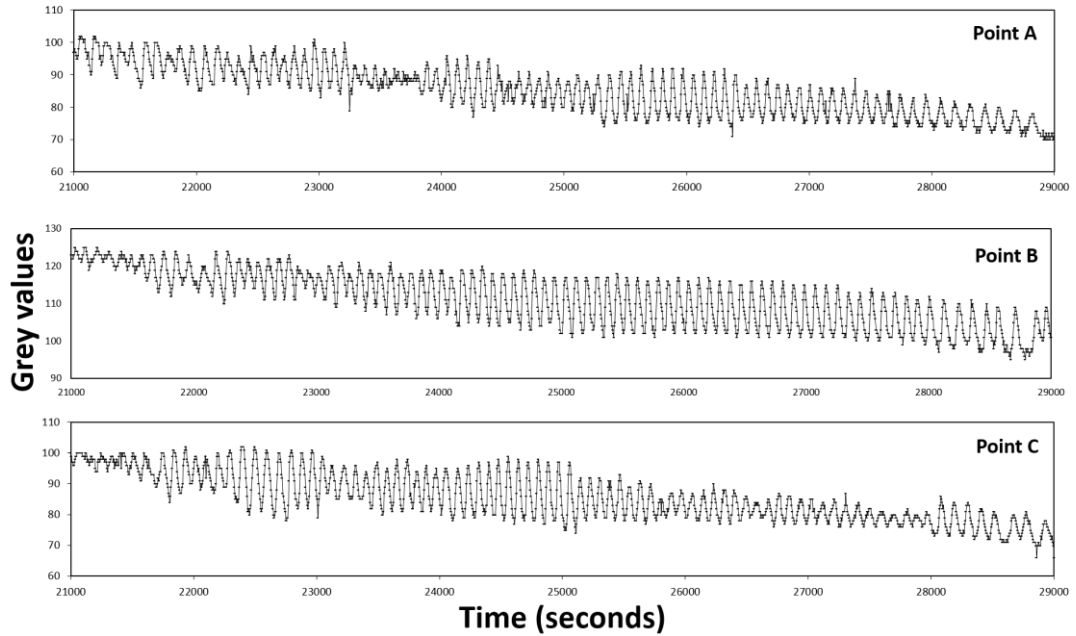
Figure 49. Oscillations in 3-Point Star
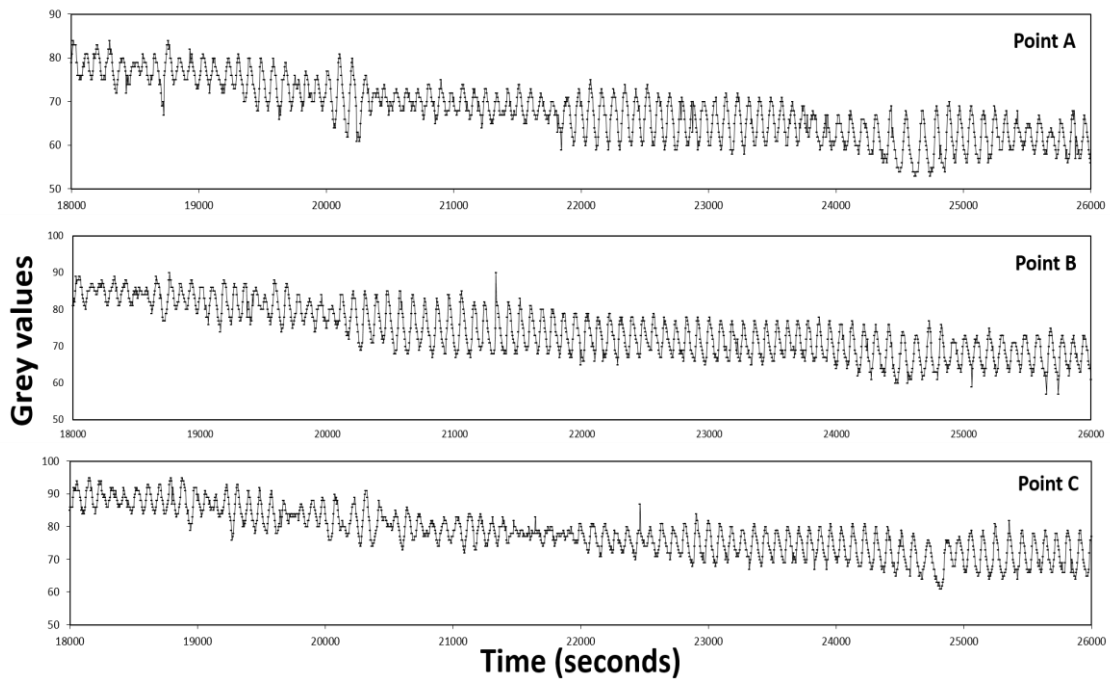
Figure 50. Oscillations in 5-Point Star

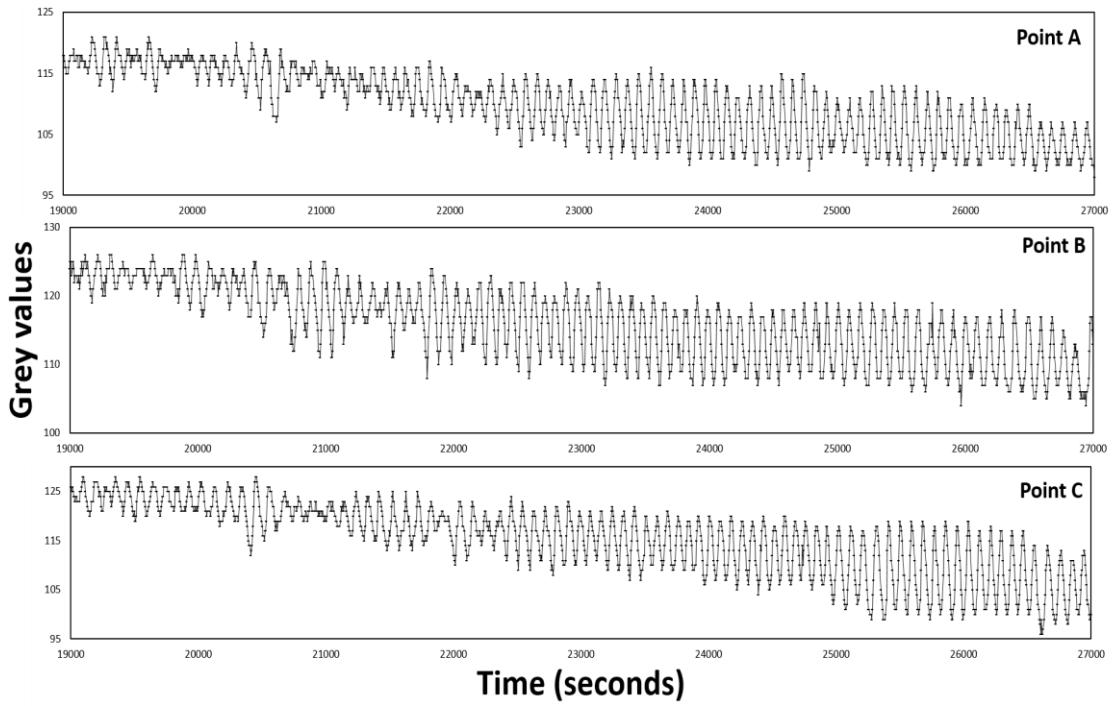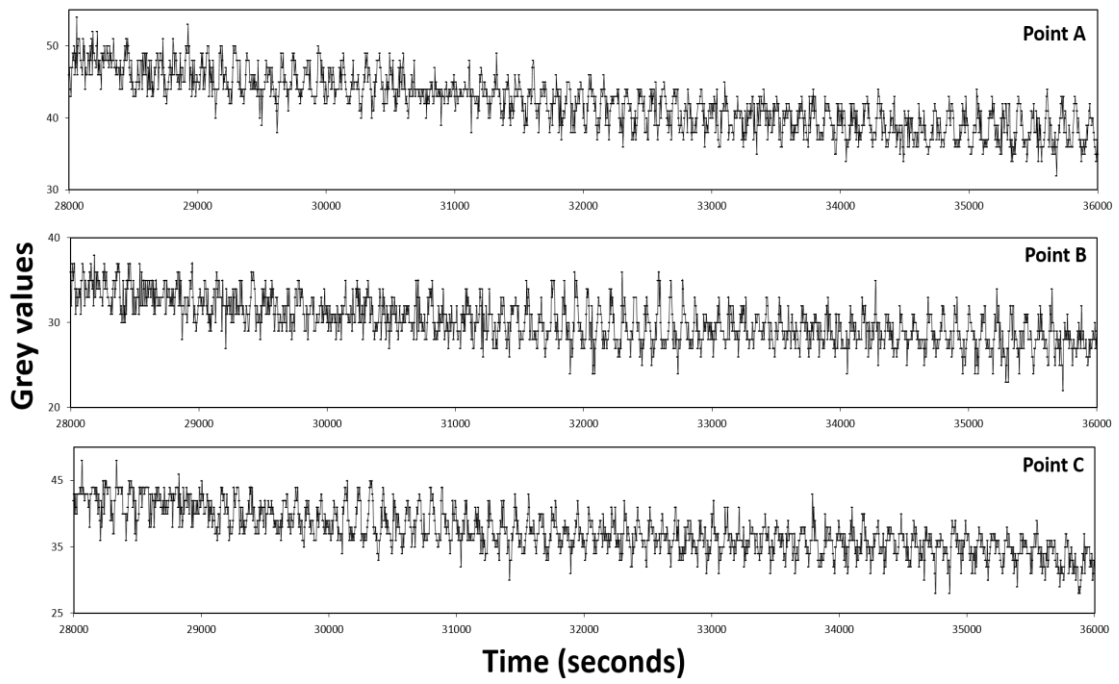**Figure 51. Oscillations in 7-Point Star**

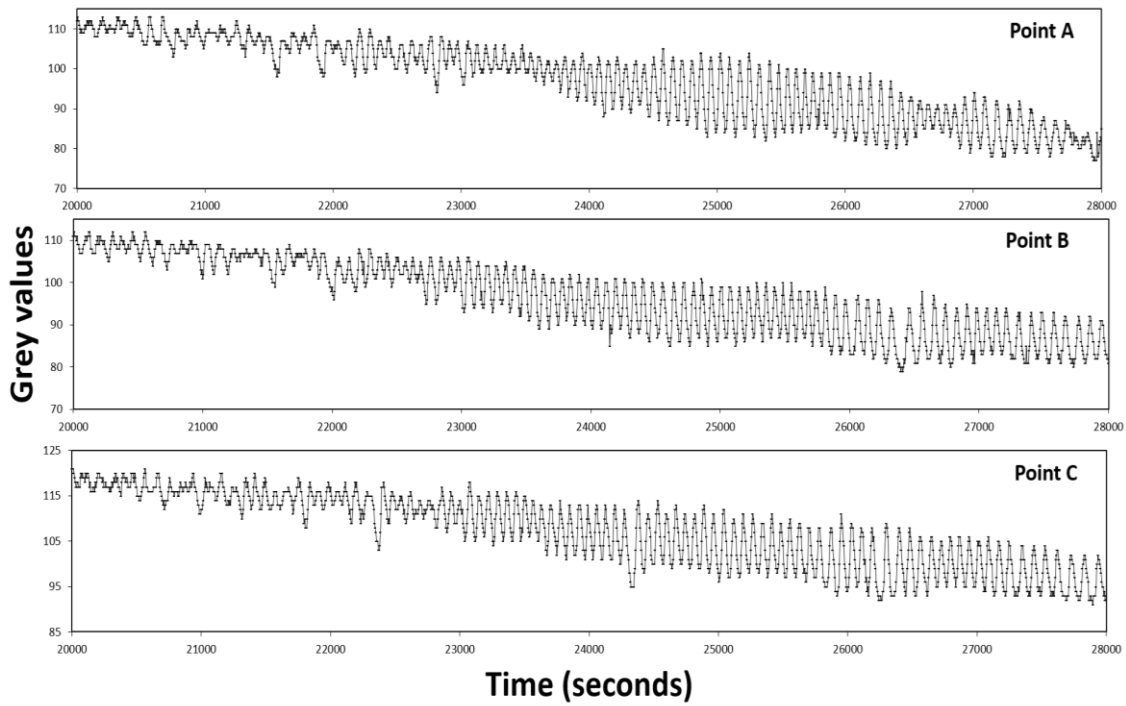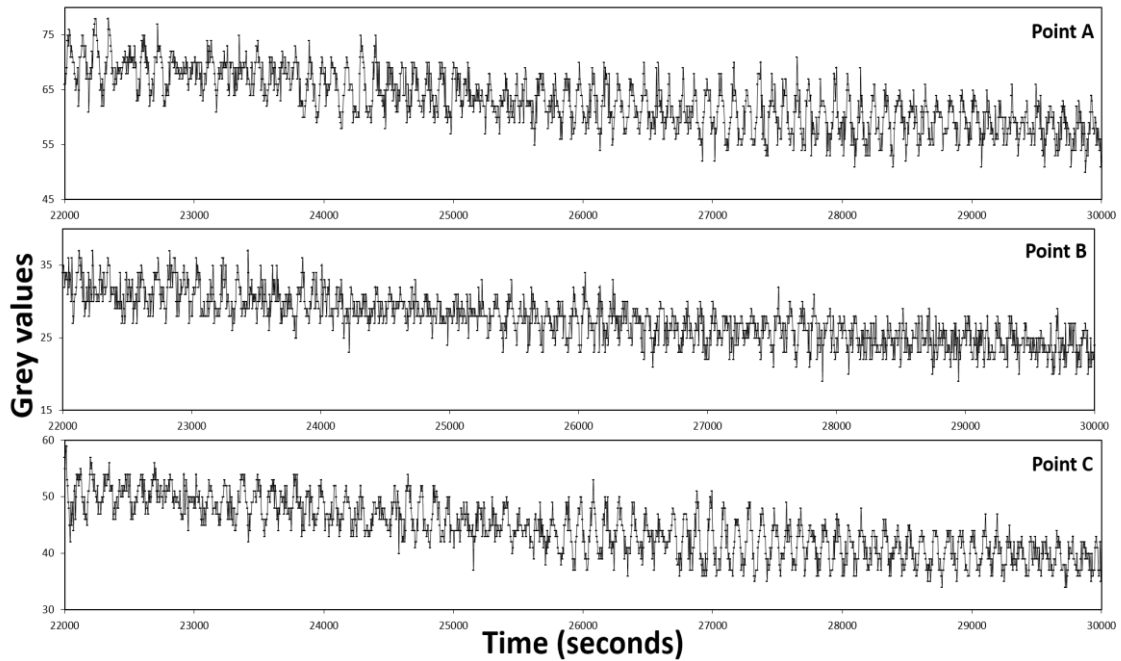**Figure 52. Oscillations in Small Star**

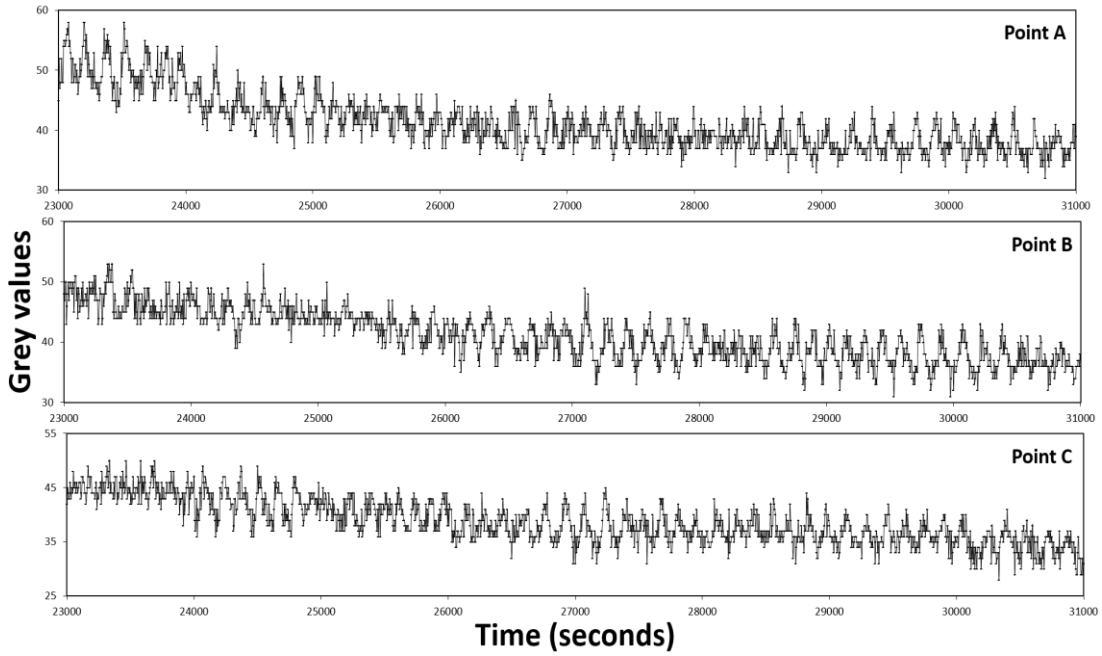**Figure 53. Oscillations in Medium Star**

Figure 54. Oscillations in Big Star

Figure 55. Oscillations in Acute Star

Figure 56. Oscillations in Normal Star

Figure 57. Oscillations in Obtuse Star

Table 4. Frequency Values for Stars (Number of Points, Size and Angle)

Star type	Point A	Point B	Point C
3-point	0.01206 ± 1.14E-04	0.01189 ± 1.07E-04	0.01203 ± 3.04E-04
5-point	0.01123 ± 2.54E-04	0.01112 ± 7.24E-02	0.01125 ± 1.15E-04
7-point	0.00945 ± 2.91E-04	0.00932 ± 4.18E-05	0.00973 ± 1.89E-04
Small	0.01284 ± 5.67E-04	0.01247 ± 1.91E-01	0.01322 ± 7.68E-05
Medium	0.01156 ± 3.78E-04	0.01174 ± 1.52E-04	0.01180 ± 1.78E-04
Large	0.01078 ± 8.31E-05	0.01069 ± 7.49E-05	0.01044 ± 1.88E-04
Acute	0.01445 ± 4.20E-05	0.01416 ± 8.88E-04	0.01451 ± 8.98E-05
Normal	0.01014 ± 7.71E-05	0.01011 ± 1.75E-04	0.01023 ± 1.89E-03
Obtuse	0.00728 ± 1.28E-03	0.00640 ± 2.18E-04	0.00682 ± 1.37E-03

*highlighted cells indicate the frequency values used for frequency trends

118

Rheological Characterization for Different Types of Gelatin

An initial assessment included the rheological characterization of gelatin type A 100

Bloom, G (100), as the one used in Chapter II. The extrusion-based printing technique

required a type of gelatin with robust properties that would allow flow and

recoverability. The type A 300 Bloom gelatin, G (300), had a higher compressive

modulus than the 100-Bloom gelatin, therefore it was employed for all the printed

structures.
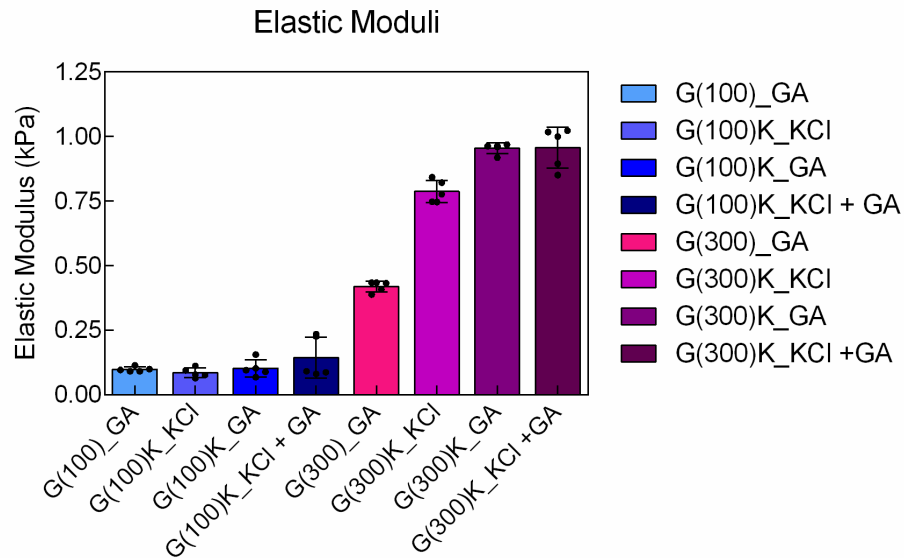
Figure 58. Effect of Gelatin Type and Crosslinking Methods on Elastic Moduli

APPENDIX D-CHAPTER V

Code for MATLAB Analysis

```
function [x,y,image_number]  = Track_v4_working_commented
% look through a directory
d = dir;
% get all the file names
names=cell(3000,1);
names = {d.name}';
names (1:2)=[];
% pick out the jpg images, picks only the files that are images in
the
% folder
for t = 1:numel(names)
    picornot(t,1) = isequal(names{t}(end-3:end),'.jpg');
end
names={names{picornot}}';% keep those images in the names array


%%%Initiliaze variables- YOU CAN CHANGE THESE VALUES
start=3000; %first image Number you want to look at
last=5000;  %last image Number you want to look at
NTH=1;     %tell code to look at every Nth image (if 1 it looks at
all; if 2 looks at every other image; etc.)


%%%Initializing variables
counter=1;
ENTRIES=floor((last-start)/NTH);
y=zeros(1,ENTRIES);%array that stores x position
x=zeros(1,ENTRIES);%array that stores y position
radius=zeros(1,ENTRIES);%array that stores radius found

% create a mask of the image to only view the area that the gelatin
is in
roi_2 = drawrectangle('Position',[10,50,500,350]);
bwm = createMask(roi_2,imread(names{start}));


% run through the rest of the images in the folder every NTH image
for t=start:NTH:last
    %initialize variables
    radii=[];

    difference=[];
    actual_dif=[];
    K=0;
    K2=0;
    %Gets the current image
    rgb = imread(names{t});
    rgb = bsxfun(@times, rgb, cast(bwm, class(rgb)));

    %%Processing the
image%%%%%%%%%%%%%%%%%%%%%%%%%%%%%%%%%%%%%%%%%%%%%%%%%%%%%%%%%%%%%
```

120

```
    I = rgb2gray(rgb);                       %image into grayscale image

    %two image processing techniques to refine grayscale image
    %J = histeq(I);
    J3 = adapthisteq(I);

    J2=
imbinarize(J3,'adaptive','ForegroundPolarity','dark','Sensitivity',
0.58);       %turn image into Black and White image %%%YOU CAN CHANGE
THE LAST NUMBER %this number corresponds to how dark grey has to be
to be turned black
    J2(~bwm)=0;
    J2= bwareaopen(J2,50);
    %FINDING THE CIRCLE
    [centers,radii] = imfindcircles(J2,[50
70],'ObjectPolarity','dark',
'Sensitivity',0.93,'Method','TwoStage');
    %imshow(J2)
    %h = viscircles(centers,radii);
%return
    if size(centers,1)==0 || size(centers,1)>=2
            %if the code found zero circles the sensitivity is
increased
            [centers,radii] = imfindcircles(J2,[40
65],'ObjectPolarity','dark',
'Sensitivity',0.96,'Method','TwoStage');
            %imshow(J3)
            %h = viscircles(centers,radii);

            if size(centers,1)==0
                [centers,radii] = imfindcircles(J2,[40
65],'ObjectPolarity','dark',
'Sensitivity',0.975,'Method','TwoStage');
            end
    end
    %Choosing the right Circle
    if size(radii,1)>=2

        %if there are two circles we choose the one that is
closssest in
        %position to the old circle
        for i=1:(size(radii,1))
            difference(i,2)=abs(centers(i,2)-y(counter-1));
%difference in x pos
            difference(i,1)=abs(centers(i,1)-x(counter-1)); %diff
in y postiotions
        end
        [M,K]=min(difference(:,2)); %finds circle closest in y
        [M2,K2]=min(difference(:,1)); %finds circle closest in x
```

```matlab
        if K~=K2 %if this method failed we go by absolute
difference to a known location
            for i=1:(size(radii,1))
                actual_dif(i,1)=sqrt((centers(i,2)-y(1))^2
+(centers(i,1)-x(1))^2);
            end
            [M,K]=min(actual_dif(:,1));

        end
        %Stores information on position and radius
        x(counter)=centers(K,1);
        y(counter)=centers(K,2);
        radius(counter)=radii(K);

    else
        %If 1 circle was found we must check to verify that it is
correct
        %circle
        %it is imposible for the gelatin to move at a speed greater
than 9
        %pixels in a frame so if the distance is greater than that
then we
        %can conclude the circle found is not legitamit
    if t>start && sqrt((centers(1,2)-y(counter-1))^2
+(centers(1,1)-x(counter-1))^2)>(700*NTH)
        x(counter)=x(counter-1);
        y(counter)=y(counter-1);
        radius(counter)=radius(counter-1);
    else

    x(counter)=centers(1,1);
    y(counter)=centers(1,2);
    radius(counter)=radii(1);
    end

    end
    %figure
    %imshow(J2)
    %h = viscircles(centers,radii);
    image_number(counter)=t;
    counter=counter+1;

end

%DATA Manipulations
Position=[x;y]; %store x and y in single matrix
time=[start:NTH:last];
    %find Change in position over time and over each frame
for t=1:length(x)-1
    change(t)=sqrt((abs(Position(1,(t+1)) -Position(1,(t)))^2
+(Position(2,(t+1))-Position(2,(t)))^2));
```

122

```
    netchange(t)=sqrt((abs(Position(1,(t+1)) -Position(1,(1)))^2
+(Position(2,(t+1))-Position(2,(1)))^2));
end
    %if changes are extremely large then they must be an error in
the
    %programing
change(change > 10) = 0;
%change(change > 200)=0;
length(change)
%plot the change in position and total change in position over time
figure
plot(time(2:length(time)),change)
xlabel('picture number')
ylabel('distance from previous centroid')
figure
plot(time(2:length(time)),netchange)
xlabel('picture number')
ylabel('distance from first centroid')


A=zeros(ENTRIES,3);
A=[image_number; x ;y]
A=A';

save('MyMatrix_172.txt', 'A', '-ascii', '-double', '-tabs')

end
```
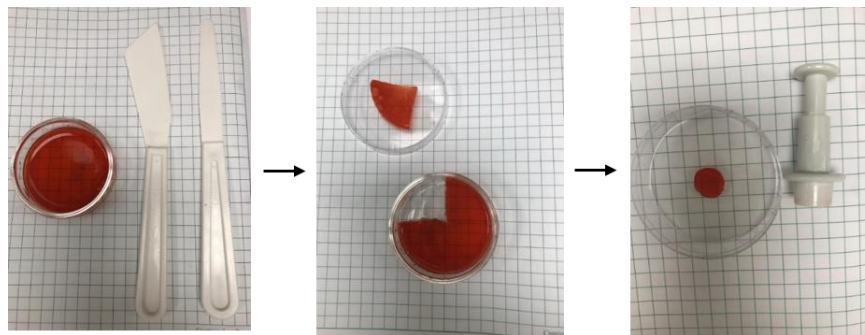
Gelatin Sample Preparation

Figure 59. Sample Preparation for Circle-shaped Hydrogels